Fall 2012

Investigating the effects of internally trapped residuals on the performance of a homogeneous charge compression ignition (HCCI) engine

Aaron David Attebery

Department:

INVESTIGATING THE EFFECTS OF INTERNALLY TRAPPED RESIDUALS ON THE PERFORMANCE OF A HOMOGENEOUS CHARGE COMPRESSION IGNITION (HCCI) ENGINE

by

AARON DAVID ATTEBERY

A THESIS

Presented to the Faculty of the Graduate School of the

MISSOURI UNIVERSITY OF SCIENCE AND TECHNOLOGY

In Partial Fulfillment of the Requirements for the Degree

MASTER OF SCIENCE IN MECHANICAL ENGINEERING

2012

Approved by

James A. Drallmeier, Advisor
Kelly O. Homan
Kakkattukuhy M. Isaac

ABSTRACT

Homogeneous charge compression ignition (HCCI) combustion introduces great opportunity for decreased emissions along with greater engine efficiencies. Implementing an innovative combustion mode such as HCCI presents a great challenge for the engine research community. One such challenge is controlling the innate cyclic variability from this chemical kinetics controlled auto-ignition event when transitioning to or from a SI operating mode. This work includes the study of cycle-to-cycle dynamics that occur within the partial burn regime of an HCCI engine as it approaches the misfire limit. Within this regime there are many successive incomplete combustion events that will impact the next cycle through the fuel/air residual, the chemical kinetics, and the pressure-temperature history of the cylinder during the combustion process. A better understanding of this process will provide information relevant to developing control methods for multi-mode operating strategies. Experiments were conducted using a single cylinder HCCI engine operating in an unstable combustion regime in order to observe cyclic variability using rapid exhaust pressure and temperature measurements to appropriately capture any deterministic behavior of the combustion dynamics. On-board syn-gas strategies were also explored by injecting a reactive species gas, carbon-monoxide, directly into the cylinder in order to perturb the intake charge and study the effects this mass injection had on the onset of combustion in HCCI. This could be utilized as one method of control by an engine control unit in order to push the limits of unstable combustion as well as keep the engine within stable operating regions.

ACKNOWLEDGMENTS

First, I would like to thank my advisor, Dr. James Drallmeier, for his guidance, his encouragement, and his patience throughout the past two years. The opportunities that he presented to me have proven to be invaluable in my development as a young engineer. I am also indebted to my thesis committee, Dr. James Drallmeier, Dr. Kelly Homan, and Dr. Kakkattukuzhy Isaac, for their advice and time commitment in reviewing and criticizing my thesis. I would also like to thanks the National Science Foundation for their financial support, which allowed this research to become a reality.

Secondly, I want to express my appreciation to Dr. Jeff Massey, who I have had the honor to work closely with as a friend and a mentee. His selflessness and willingness to help will never be forgotten. I also want to acknowledge current and previous graduate students of the engines lab, Shawn Wildhaber, Cory Huck, Avinash Singh, and Allen Ernst, who all provided a fun and interactive learning environment during my time here at Missouri S&T. This research could not have been accomplished if it were not for the staff of MAE Department and Machine Shop; Randall Lewis, Joe Boze, and Bob Hribar.

Finally, and most importantly, I want to thank my family, particularly my parents, David and Sherrie Attebery who have been an inspiration to me. Their love and support they have provided my entire life will never be forgotten and have made my accomplishments possible. Thank you for everything, Mom and Dad.

TABLE OF CONTENTS

LIST OF ILLUSTRATIONS

Page

LIST OF TABLES

Page

ABBREVIATIONS

Symbol	Description
HCCI	Homogeneous Charge Compression Ignition
CAI	Controlled Autoignition
LTC	Low Temperature Combustion
NO_x	Nitric Oxides Emissions
uHC	unburned Hydrocarbons
SOC	Start of Combustion
SOI	Start of Injection
SI	Spark Ignition
CI	Compression Ignition
IVC	Intake Valve Close
IVO	Intake Valve Open
EVC	Exhaust Valve Close
EVO	Exhaust Valve Open
TDC	Top Dead Center
BDC	Bottom Dead Center
ATDC	After Top Dead Center
BTDC	Before Top Dead Center
CAD	Crank Angle Degree
EGR	Exhaust Gas Recirculation
PRF	Primary Reference Fuel
RON	Research Octane Number
UTG96	Unleaded Test Gasoline with RON of 96
AFR	Air-to-Fuel Ratio
COV	Coefficient of Variation
IMEP	Indicated Mean Effective Pressure
PRR	Pressure Rise Rate

RHR	Rate of Heat Release
HR	Heat Release
CA10	10% Heat Release Location in CAD
CA50	50% Heat Release Location in CAD
VVA	Variable Valve Actuation
VCR	Variable Compression Ratio
OEM	Original Equipment Manufacturer
RGI	Residual Gas Injector
PFI	Port Fuel Injection
DI	Direct Injection
NVH	Noise, Vibration, and Harshness
LHV	Lower Heating Value
LFE	Laminar Flow Element
OF	Overlap Factor
NN	Neural Network
TC	Thermocouple

1. INTRODUCTION

Homogeneous charge compression ignition (HCCI) is an advanced combustion mode that has been gaining a lot of interest this past decade due to the ever increasing rise in crude oil costs and the stringent government regulations for the automotive industry concerning fuel efficiency for newer automobiles. In HCCI or controlled autoignition (CAI) combustion is achieved when a premixed charge of fuel and air is introduced into the cylinder and compressed until the mixture self-ignites. This type of combustion has been shown to reduce levels of nitrogen oxide emissions (NO_x) while significantly increasing engine efficiency [1]. The most challenging problem with this advanced combustion mode is controlling the ignition timing. Since HCCI relies solely on chemical kinetics in order to occur, the thermodynamic state and the dilution levels of the charge mixture will directly affect the start of the combustion (SOC) process [2]. Cyclic variations in output parameters are influenced by both the thermodynamic state and the dilution levels of the charge mixture. The operating range of an HCCI engine is limited by high pressure rise rates at the most advanced combustion timing and by an instability limit or misfire/partial burn regime at the most retarded timing. At stable combustion, variations in performance parameters are small and the cyclic dynamics are not of concern. However, in the partial burn regime close to the misfire limit, cyclic variations are extremely high and cause unstable combustion. Since the residual gas fraction directly affects the temperature and the concentrations of the newly inducted charge, the characteristics of this residual gas are important parameters when trying to control the SOC. One of the main difficulties in practical utilization of HCCI is controlling

combustion timing and therefore heat release rate in order to avoid the high rate of heat release that is characterized by high pressure rise rates (PRR) and the partial burn regime. The influence of various combustion parameters need to be further analyzed so that control methods can be developed to control the optimum timing of the autoignition process [2]. When HCCI was first introduced it was concluded that the progression of combustion is a chemical kinetic process governed by the temperature, pressure, and composition of the charge in-cylinder [1]. Many studies of this in-cylinder process have been conducted since the discovery of CAI. The result of this research includes progress toward understanding and overcoming the hurdles this advanced combustion mode faces, such as increasing operability at high loads through reduced pressure rise rates, improving low-load efficiency, and understanding the effects of fuel on cyclic variations and emissions over the entire operating range [3]. Unfortunately, as of today practical control strategies do not exist to confidently introduce this combustion mode to industry. Therefore, it is crucial to further our understanding of cycle-to-cycle dynamics and how these variations impact performance parameters in order to develop robust strategies to control the onset of combustion in HCCI engines.

Commercialization of HCCI has been inhibited by the fact that this combustion mode is not sensible at all engine speeds and loads. This reality indicates the need to be able to shift from HCCI and conventional spark-ignition (SI) combustion in order to achieve a wide range of speed and loads that an engine would encounter under normal operating conditions. Potentially HCCI could be integrated into an engine operating strategy, where at low or part-load the engine could operate on HCCI and transition into

SI where there would be flame propagation at high-loads [1]. However, achieving the necessary level of control during this transient engine condition is complex and difficult when there are no means of an external trigger to initiate combustion, unlike in traditional SI combustion. The timing of autoignition relies heavily on the pressure-temperature-composition history of the newly inducted air-fuel mixture during the compression process. This goes to say that if the thermal conditions and composition of the charge at intake valve closed (IVC) are insufficient then there is no readily available means to avoid a misfire. Consequently, these mixture qualities at IVC need to be precisely controlled in order to obtain the optimum combustion timing. This transition period has been studied by several investigators [11-15] and the term dual-mode SI combustion or spark-assisted HCCI has been coined. This combustion mode utilizes a spark to initiate a flame that elevates the temperature and pressure in the cylinder, driving the rest of the charge into autoignition.

One such strategy that could be used for controlling this auto ignition event is the cyclic addition of synthesis gas (syn-gas). By replacing part of the base fuel with syn-gas, or reformed gas, one can alter HCCI combustion characteristics in varying ways depending on the replacement fraction and the base fuel's resistance to auto-ignition, or octane number. This addition of syn-gas, or reformed gas, has been studied [27-31], but only on a cycle averaged sense. A barrier to using this production of reformed gas on-board an engine platform for combustion control is the variation of the H_2/CO ratio within the syn-gas composition and proves to be challenging for applied use with small scale reformers.

In summary, it looks as if a practical combustion strategy of an automotive engine running on HCCI would have to be designed to operate in a dual or multiple-mode before further research can be conducted on extending the full range of operation to HCCI. The engine system has to be able to easily switch from one mode to the other, especially during sudden load transients. Even though dual-mode operation proves to circumvent problems like high pressure rise rates and excessive engine noise that HCCI encounters at high-load instances, additional research and improvement efforts are necessary to understand this advanced combustion mode in the partial burn regime, where the transition into SI combustion would take place, in order to take full advantage of its technology.

This thesis outlines the impact that internally trapped exhaust gas residuals have on the combustion parameters in the partial burn regime. This is beneficial as understanding the feed forward mechanism that is the cause of these high instabilities in this region will lead to the development of control schemes that are capable of pushing the engine toward more stable operating regimes. This work also introduces a simple burned/unburned residual model into a much larger 5-state physics based thermodynamic control model in order to capture and correctively predict the cycle-to-cycle dynamics regarding the operational regime of an HCCI engine in an attempt to capture this feed forward mechanism so that an adaptive neural network control can utilize the model and be capable of real-time onboard control. Lastly, this work explores preliminary results that show the effect of cyclically injecting syn-gas as a possible control scheme in HCCI combustion. This syn-gas has a profound effect based on

injection pressure, amount of mass (and thus energy) injected, and species injected. By using this syn-gas as a control knob and the information acquired from the residual study, one can develop a better understanding of HCCI in the partial burn regime, and work toward operating strategies to be able to transition between modes, such as HCCI-SI and SI-HCCI so that the full advantage of these low temperature modes can be discovered.

2. REVIEW OF THE LITERATURE

2.1. CYCLIC VARIABILITY

Few experimental studies have been presented on the cause of cyclic dynamics in an HCCI engine, mainly due to the fact that cyclic dynamics are small outside of the partial burn regime. Some have attributed the cyclic variation to the charge temperature at IVC while others have investigated the residuals left over in the cylinder and/or the back flow of the exhaust gases, in other words the residual gas fraction. In some cases using hot residual gas is advantageous in order to increase the temperature of the freshly inducted charge either through an exhaust gas recirculation (EGR) valve or utilizing a second opening of the exhaust valve during the intake stroke to induct hot exhaust gases.

A fundamental study on understanding the mechanism underlying the cycle-to-cycle variations was conducted by Koopmans et al. [4]. In this experiment, HCCI was achieved by the early closing of the exhaust valve and trapping a portion of the hot exhaust gas. This gas is compressed during the exhaust stroke and due to the pressure/temperature relationship its temperature is elevated and then mixed with the newly inducted charge. This higher overall temperature at IVC causes early ignition timing and a higher peak pressure. The exhaust gas temperature was lower due to the amount of time for heat transfer to occur in the exhaust stroke. This lower residual temperature is carried through into the next charge at IVC. The lower temperature causes a late timing and lower peak pressures. This cycle's exhaust gas temperature was at a much higher temperature than the previous cycle. This cyclic patterned continued

causing unstable combustion in the partial burn regime and would eventually lead to a misfire. A misfire does not produce any residuals at an elevated temperature, the mixture of the next cycle does not reach the ignition temperature, and thus combustion does not occur. These oscillations must therefore be avoided. This study found that combustion phasing is not affected by the residual gas temperature at the end of the expansion stroke, but rather it is influenced by the gas temperature at the beginning of the compression stroke. This work focused on the temperature effect of the residual gas fraction and no chemical effects were considered.

In a following investigation [5] there was a strong emphasis on cycle-to-cycle and cylinder-to-cylinder deviations and how they limit the operating range of HCCI, mainly how these effects can change in different zones of the operating region and how they can be controlled. HCCI was achieved by the use of negative valve overlap and utilizing trapped residuals to elevate charge temperatures. It was noted that on the borderline between where ordinary HCCI occurs and the partial burn region, (or where spark-assisted HCCI would take place) the temperature after the compression stroke is at the energy limit for reaching auto ignition. High load HCCI was limited by the extremely high heat release rate and pressure rise rates due to the lowered amount of residuals if the engine was run without boost pressure. On the other hand, low load HCCI was found to be restricted by cycle-to-cycle behavior causing combustion timing to oscillate to the point of misfire. The most important thing to note from this study was that an increased negative correlation for some engine speeds indicated that it is more than just temperature that governs this cyclic phenomenon.

In an effort to further understand the cause of these cycle-to-cycle variations and combustion stability, an experimental study was performed using HCCI and varying fuels from neat n-heptane to primary reference fuels (PRF) 20, 40, 50, and 60 [6]. The basis for this work is understanding that the chemical kinetics of fuel/air mixtures dominate HCCI ignition and combustion. Thus, by varying the research octane number (RON) test fuel, one would expect to gain a better understanding of the combustion behavior. From this study it was evident that the chemical properties of the test fuels play an important role in the combustion stabilities and cycle-to-cycle variations of HCCI combustion. The results revealed that cyclic variability increases significantly with an increase in the fuels RON however the residual gas fraction composition and exhaust temperature were not investigated for these fuels.

To further explore the cyclic variability of HCCI combustion, [7] focuses on the cyclic variation of SOC and its correlation with other parameters. The optimal combustion process depends on the gradient of charge properties from the initial localized ignition sites outwards. The development of this combustion can be uniform and look like a propagating flame front, or it can be random with several secondary autoignition sites. This study concluded that there are, in general, five key players in causing cyclic variations in HCCI engines; temperature inhomogeneity and thermal stratification, mixture compositional inhomogeneity, fluctuations in air/fuel ratio (AFR), fluctuations in diluents, and turbulence intensity. It was found that variations in SOC are the most sensitive to temperature at IVC while AFR, pressure at IVC, and rate of EGR are

in a decreasing order of importance. While the overall rate of EGR was studied, there was no discussion on the speciation of the residual or the chemical composition therein.

Another investigation [8] by the same authors in [7] is an extension on the cyclic variability of SOC. The motivation for this work is to expand on the discussion of the main sources of cyclic variation in an HCCI engine. The sensitivity of combustion timing to certain input variables and conditions is important to both understand the cyclic variation and to control combustion timing effectively. If the physics behind these variations could be better understood then effective control strategies could be developed. In this experiment the ignition timing was studied for a range of charge properties by varying the intake temperature, intake pressure, AFR, EGR rate, speed, and coolant temperature. This was done for two different fuels on two different single cylinder engines totaling up to over 430 operating points. From this massive data set three distinct patterns in cyclic variability were observed; normal cyclic variations, periodic cyclic variations, and weak/misfired cyclic variations. These distinct patterns go to show that HCCI cyclic dynamics are not always a random phenomenon. The normal cyclic patterns observed in the output parameters are a product of the four main sources of cyclic variation; temperature inhomogeneity and thermal stratification, mixture compositional inhomogeneity, fluctuations in air/fuel ratio (AFR), and fluctuations in diluents. This was concluded since the variations in these sources do not follow any specific pattern or structure. These variations tend to increase with an increase in EGR rate, but decrease with an increase in equivalence ratio, intake temperature and coolant temperature. The periodic cyclic variations that were observed

were determined to be a direct cause of a fluctuating air mass flow rate. This was due to experimental setup and not a natural oscillation of HCCI combustion. However, the weak/misfire cyclic variations indicate that the engine was approaching the misfire limit and was operating in the partial burn regime. This pattern resulted in heavy amounts of partially burned fuels (i.e. unburned hydrocarbons) that become part of the residual gas and are added to the next cycle's fresh charge. This accounts for the severe oscillations observed in this operation zone. As discussed before, in order to control this kind of combustion behavior, the periodic and weak/misfire patterns must be avoided and the engine should be run in the normal cyclic variation zone. It goes without saying that the variations in SOC in the normal zone need to be minimized as much as possible. The cyclic dynamics of the output parameters depends on many different variables, some correlated to each other and some independent. Further investigation of these variables is needed to comprehend the physics of the combustion phenomenon that occur.

In a more recent study, [9], researchers were motivated to gain an improved understanding of the HCCI combustion process by further investigating these cycle-to-cycle variations. As seen in the previous paragraphs many have examined this phenomenon and many of the sources that might cause this kind of behavior. In this experiment the objective was to exclusively observe the cyclic effects of intake air temperature and AFR in an ethanol fueled, two cylinder engine, at a constant engine speed. HCCI was achieved by preheating the intake air and was only operated with one piston. The other piston was run on conventional diesel. It was found that at higher intake temperatures it is possible to ignite very lean mixtures. The coefficient of

variation (COV) of maximum in-cylinder pressure increased with a decreasing AFR (richer mixtures) and also increased with intake air temperature. However, for all test points, the variation of maximum in-cylinder pressure is less than 3 percent. This indicates that the engine was not operated in the partial burn regime where a high COV of maximum pressure would be observed due to misfired cycles and partially burned cycles. Another parameter observed was indicated mean effective pressure (IMEP). IMEP is a valuable measure of an engine's capacity to do work that is independent of engine displacement. The COV of IMEP increases with an increase in AFR and decreases with increasing intake air temperature. This is expected as the energy available for combustion to occur is decreasing with higher AFR and increasing with hotter charge temperatures. This study was primarily focused on the effects of AFR and intake temperature, while those sources alter the chemical kinetics, the study did not investigate the effects of internally trapped residuals or chemical effects of EGR on the HCCI combustion process.

A more refined investigation of [9] was conducted in [10] where cyclic variability was categorized ranging from stochastic behavior to a more deterministic behavior. This was done by analyzing the temporal dynamics of these cyclic variations using statistical methods and chaos theory. The analysis was performed on the cyclic variation of combustion timing as the combustion timing directly affects the engine’s performance. A symbol-statistics method was utilized to find the occurrence of probabilities of data points at the same operating condition. It was found that as AFR increases, the determinism in the ignition timing increases. This determinism was also confirmed by

the engines return map of the cycle based time series of ignition timing values for an increase in intake air temperature. By using a 'symbol sequence statistic method' it was determined that the signature of the engine, that is the history of previous cycles, last for a minimum of 3 cycles. This goes to say that the current combustion process could be affected by the previous 3 cycles. Therefore, it would be advantageous for an HCCI combustion controller to retain more information than just the immediate previous cycle. These findings highlight the importance of symbol sequence statistics and how useful these tools are in understanding nonlinear cyclic dynamics.

Primarily, investigations of the cyclic dynamics in a homogeneous charge compression ignition engine are limited to operating regimes that steer clear of the partial burn regime and the misfire limit. Most push their engines to the misfire point in order to map out the working limits of the engine but they do not investigate these cycle-to-cycle variations in detail. It would be in this regime where a multi-mode engine may transition into another mode of operation, when the HCCI combustion process cannot maintain stable combustion timing and power output. In the next section, this multi-mode operating strategy is discussed in greater detail.

2.2. SPARK-ASSISTED HCCI

It has been shown that it may not be possible to maintain HCCI combustion under all speeds and loads that an engine would experience under transportation applications. An important technical development to help overcome this problem and achieve a wide spread use of HCCI is the ability to switch between HCCI and SI combustion rapidly as speed and load change. It is evident that there are many engine

conditions where HCCI is physically possible but has been noted to be very unstable. Appropriate stabilizing strategies must be implemented in order to maximize its range to fully use the potential that HCCI combustion represents. This development of multi-mode switching and HCCI stabilization techniques require that the fundamentals of this transition between HCCI and SI be well understood, specifically from the perspective of realistic engine operating conditions.

In a study conducted at Oak Ridge National Labs in Oak Ridge Tennessee [11-12] experimental observations of cyclic variability in combustion during the transition region between traditional propagating flame combustion or SI and HCCI is recorded. The measurements within this region disclose a complex sequence of high COV in combustion parameters. It was shown that an increase in the zone of stable HCCI like combustion was possible when using spark assist. This “spark assist” is when a spark is required to add just enough energy into the system in order to obtain auto ignition. It was discovered that the cyclic dynamics in the transition zone are dominated by nonlinear, nonrandom processes. This research suggests that nonlinear EGR feedback is most likely the major source of these variations. It should be noted that the type of EGR used in the study was internally trapped residuals achieved by an early closing of the exhaust valve using variable valve actuation (VVA). The observed patterns of combustion variability give the impression that they are produced by the strong nonlinear feedback of the re-circulated gas on succeeding combustion reactions. The transition starts with the destabilization of SI combustion and ends with steady HCCI combustion as EGR is increased. Several attempts at making a fast switch from either SI

to HCCI or HCCI to SI seem to indicate that the forward and reverse processes may require different paths of control. These variations within the transition period are predictable in nature and suggest the possibility of developing on-line diagnostics and control for expanding stable HCCI operation and helping to improve transition between the two operating modes. This work goes to show that further analysis of the unstable region in HCCI would be beneficial in order to exploit future control strategies for this advanced combustion mode.

In a following investigation [13], methods are described for using cyclic determinism to extract global kinetic rate parameters that can be used to pinpoint multiple distinct combustion states and develop a more quantitative understanding of the SI-HCCI transition region. This application was implemented on indolene-containing fuels and a never before seen HCCI switching mode was observed. It was concluded that variations in exhaust temperature tend to be slower and have less of an immediate impact on SOC on a cycle-to-cycle basis than when compared to the variations in residual fuel-air charge. However, exhaust temperature variations appear to be filtered due to the thermal stratification of the combustion chamber and require several cycles before a noticeable change takes place. This “signature” or combustion history of the engine due to the previous cycles caused a switching between two distinct types of HCCI combustion that occurred after top dead center (TDC). One exhibited a strong correlation as the burn rate constant decreased with increasing temperature and the other exhibited a weak correlation. These results indicate that the global kinetics that

are tied to an engine can be empirically observed during the transition process and these observations can be used when trying to implement realistic control strategies.

After initial investigations of spark assisted HCCI focused on the sequence of low-dimensional bifurcations driven by nonlinear feedback between combustion events for on board control, [14] performed an investigation on wavelet analysis of the time series combined with conventional statistics and multifractal analysis which revealed previously undocumented features in the combustion variability during the transition region. From these results it appears that real-time wavelet decomposition of engine cylinder pressure may be useful for on-board control and tracking of SI-HCCI combustion regime shifts. These tools can be beneficial for on board diagnostics but a statistical breakdown of the patterns in the data do not add any new information to the actual physical phenomena behind the cyclic dynamics that drive the cyclic variability in the partial burn region of HCCI combustion. A further understanding of the driving mechanism for cyclic variability will be of great value to control this onset of auto ignition.

In [15] a variable compression ratio (VCR) engine was used to investigate the mixed combustion region and operating conditions from lean SI limit to spark-assisted HCCI to pure HCCI without spark assistance. The VCR is achieved by tilting the monohead, which is comprised of the cylinder head and liners, around a pivot so that the clearance volume changes. It was found that the main drawback of spark-assisted HCCI is typical SI combustion initiation fluctuations that become present. These combustion fluctuations are present due to the cycle-to-cycle differences in combustion

phasing that were introduced with the initial SI flame kernel development. The investigators found that spark assistance can be used for controlling the combustion phasing during mode transitions however there are large fluctuations in the transition region where cycles experience both auto ignition and flame propagation, and other cycles only experience partial burn. It was concluded that these intermediate cycles need to be minimized during mode transfers and that closed loop control of several different parameters are needed in order to make a smooth and fast transfer. There was no closed loop control of the VCR in this study; instead several different set points were tested with different compression ratios. The emissions reported were for the spark assisted HCCI and only briefly mentioned during the transition region. If a better understanding of the HCCI limits could be achieved then the use of spark assistance could be fine-tuned to find optimal combustion phasing when in mode transfer.

2.3. SYNTHESIS GAS ADDITION

The generation of chemically active gas species can be performed through "on-board" partial reforming of primary hydrocarbon fuels. Such reforming techniques have been used on a large scale for years in the commercial production of hydrogen gas. Various fuel reforming techniques exist through which synthesis gas (syn-gas) can be produced with varying $CO/H_2/N_2$ compositions, along with additional trace species. When properly understood and utilized, the addition of these reformate gases to engine combustion can be used to impact engine performance. One such strategy that could be used for controlling the HCCI auto ignition event is the cyclic addition of this syn-gas. By replacing part of the base fuel with syn-gas, or reformed gas, one can alter HCCI

combustion characteristics in varying ways depending on the replacement fraction and the base fuels resistance to auto-ignition, or octane number.

The impact and potential benefits of reformate addition to HCCI combustion is an area that is attracting attention and has been investigated under several lights. One group of investigators observed that the impact of the reformed gas on combustion phasing depends on the primary fuel's octane number [29,30]. The results from these investigations show that the addition of a reformed gas composed of H_2 and CO tends to retard SOC, based on 10% total heat release, of low octane fuels, but that the impact on high octane is dependent on inlet charge temperature. HCCI combustion with diesel fuels and pure H_2 enrichment has been shown both through modeling and experimental investigations to retard the combustion phasing and reduce combustion duration [28].

Some work has been done investigating the effect of CO addition to the HCCI combustion event in quantities similar to what is present in EGR [27]. These studies investigate the impact that EGR has on the combustion of several fuels (n-heptane, 75% n-heptane/25% isooctane, 80% n-heptane/20% toluene). However, since they are investigating from an EGR standpoint, the quantities introduced are only a fraction of what might be expected from a reformed gas. The maximum amount introduced in these studies is 2000 ppm [27]. It is not surprising that these low concentrations of CO showed little to no effect on the combustion characteristics examined.

However, the composition extremes of syn-gas and their effect on n-Heptane HCCI combustion have been investigated by Hosseini et al. [31]. In this work, it was demonstrated both experimentally and through numerical simulation that the two

extreme cases of reformed gas compositions, with H_2/CO ratios of 3/1 and 1/1 by volume, effectively retard SOC over a wide range of conditions, implying that any currently known method of producing on-board syn-gas would result in a H_2/CO ratio that would have a similar impact on combustion. These results also showed that the syn-gas composition with a higher H_2 content had a greater impact on combustion. The same authors investigated the syn-gas addition's effect on other high and low octane fuels [29].

Replacing a portion of the total intake fuel energy with an equal amount of reformed gas energy has been shown to impact diesel type fuels. Enrichment with pure hydrogen has been shown to have a stronger retarding effect on combustion than carbon monoxide enrichment, and it is likewise accepted that hydrogen is typically the dominant species affecting combustion during mixed syn-gas addition. However, as calculated by Subramanian et al. [28], CO has potential to retard combustion at low initial temperatures (600K) and advance combustion during higher initial temperatures (1000K) [28]. Hydrogen, on the other hand, is only believed to possess the capability of retarding combustion to varying degrees.

The inhibiting effect of syn-gas addition on low octane fuels, at low temperatures, is believed to be the result of initial consumption of active OH radicals in the presence of syn-gas being replaced by less active HO_2 radicals [28]. At high temperatures, it is believed that the addition of CO increases the net production of OH radicals, accelerating the reactivity of the mixture [28].

Work to date seems to be on a cycle averaged basis and with reformate that is introduced upstream from the intake valve. While this leads to a broader understanding of the syn-gas impact on combustion in a general sense, it does not provide the cycle resolved detail of the stochastic-deterministic effects that is necessary to understand the time correlation of multiple engine cycles and successfully implement cycle-to-cycle control methodologies. Researchers have acknowledged the potential use of syn-gas addition as a cyclic control mechanism, but have not investigated the effect that the gas addition has on the higher order trends driving the dynamics as their experiments are based on cycle-averaged experimental results [29].

2.4. SCOPE OF THE INVESTIGATION

Mainly, investigations of cyclic variability in HCCI engines have been focused within stable combustion limits. However, the limits of stable HCCI combustion have been tested and are noted to be different from engine to engine and test stand to test stand. Interestingly, little investigation has been done with regard to the cycle dynamics in the partial burn regime at these limits of operation. It is well established that in order to fully utilize the operating benefits of HCCI, a multi-mode operating strategy must be implemented. Therefore, the most recent idea is to use spark-assisted HCCI to aid in the transition between these two combustion modes. It has been shown that transitioning causes severe cyclic variations in performance parameters of the engine and the risk of a misfire is prevalent, losing combustion completely.

For the current study, the effects of internally trapped residuals at the partial burn limit are considered to determine under what conditions these cyclic variations are

present and how indicative they are to the transition region in spark-assisted HCCI combustion. This investigation will provide a fundamental study of the internal EGR and the “residual signature” on an HCCI combustion engine operating at the partial burn limit. The goal is to study the relationship between cyclic variations and how these cycle-to-cycle instabilities affect combustion through the internally trapped residual that is carried over to the next cycle. Extremely fast thermal sensing equipment will provide experimental information that will shed insight on cyclic exhaust temperatures and poimnt to thermal management strategies for HCCI. Using a single cylinder small displacement engine will eliminate the cylinder-to-cylinder cross talk that occurs in multi-cylinder engines exhaust manifolds. Currently, most studies focus on engine performance on a cycle averaged basis to determine if combustion was in a stable operating zone and only one [4] measured cycle-to-cycle temperatures in order to capture the physics of the variations. None have operated in the partial burn regime while investigating the effects of internally trapped residuals on the engines performance. Cycle-to-cycle comparisons will be conducted to establish any relation between the exhaust temperature and the newly inducted charge temperature at IVC. In order to have the ability to control the auto ignition and overall combustion rate of HCCI, it is important to have a strong understanding of the interaction between the fuel/air/residual, the chemical kinetics, and the pressure-temperature history of the cylinder during the combustion process.

Experiments were conducted by using a residual gas injector that was developed to cyclically inject a reactive species gas, in this case carbon monoxide, to perturb the

fresh intake charge through its chemical composition. This perturbation allowed the chemical effects to be separated from the thermal effects in order to study the kinetics behind HCCI combustion development. These experiments allowed further insight to the effects that modulating syn-gas had on SOC and RHR. This was done by running the engine at a steady operating point and observing how the combustion parameters such as SOC and RHR were affected. A range of experiments were developed once the engines response to cyclic addition of syn-gas was understood in order to fully assess the chemical kinetics behind this non-linear deterministic processes in HCCI at the partial burn regime/misfire limit.

Found in the following chapters of this thesis is an outline of the experimental setup and data collection and analysis system at Missouri University of Science and Technology's Engine and Spray Dynamics Laboratory. It was on this system that all the data presented in this thesis were collected and analyzed. Chapter 4 outlines the equations and methodology behind the data collection and analysis. Here, important metrics to quantifying engine output and performance measures are discussed and in detail the signal processing involved in the computation of these metrics. Following this section is investigation and results on cyclic dynamics in the partial burn regime and the set points that Missouri S&T's engine was operated at. This section will compare the steady state operating regime to the partial burn regime and discuss the stochastic effects that are influenced by both boundary and inlet conditions, as well as the deterministic effects from the cycle-to-cycle coupling that inherently exists. Then Chapter 6 will explore the capability of a 5-state non-linear thermodynamics based

engine model [17] to predict the cyclic dynamics regarding the operational partial burn regime of an HCCI engine. Here a sub model was added that changed the composition of the residual due to limits set for the partial burn regime. This residual model was comprised of a burned and unburned residual through the inclusion of unburned hydrocarbons. The last chapter of results, Chapter 7, outlines preliminary results of the underlying cycle-by-cycle dynamic impacts of carefully controlled in-cylinder injections of synthesis gas. By injecting this perturbation gas, in this work carbon monoxide was used, one can isolate the chemical composition effects of the residuals from the thermal effects in order to explore the extent of the non-linear effects seen in regions of instability. This thesis is wrapped up with conclusions and an overview of the data collected as a result of the aforementioned experiments.

3. EXPERIMENTAL SETUP

3.1. MISSOURI S&T EXPERIMENTAL FACILITY

The experimental data is collected at Missouri University of Science and Technology in the Internal Combustion Engine Laboratory. Here engine performance, emissions data, and combustion analysis can be collected and analyzed to further understand cyclic variability of an engine, whether it is an SI, CI, or HCCI engine. This chapter describes the experimental test bed utilized for this investigation.

3.1.1. Engine Setup and Control. Cyclic dynamics were studied using a small, single-cylinder, air-cooled compression ignition (CI) engine. A Hatz 1D50Z diesel engine was modified to operate in a HCCI combustion mode using a high compression ratio of 14.5. It is advantageous to use a single cylinder engine so that collected data would be uninfluenced by other variables and outside excitations that would arise in a multi-cylinder engine. The engine properties and timing parameters are listed in Table 3.1.

Table 3.1. Hatz HCCI engine specifications

Engine	Hatz 1D50Z (modified)
Number of Cylinders	1
Number of Strokes	4
Bore (mm)	97
Stroke (mm)	70
Compression Ratio	14.5
Displacement Volume (L)	0.517
Cooling	Air
Intake Valve Opening* (ATDC)	345
Intake Valve Close* (BTDC)	133
Exhaust Valve Open* (ATDC)	116
Exhaust Valve Close* (BTDC)	342
Intake/Exhaust Valve Overlap (CAD)	33

*Valve events referenced at TDC of the power stroke and defined at the point of 0.15 mm lift

The output shaft of the engine was connected to a 30 HP absorbing/motoring eddy current dynamometer. This shaft assembly housed data acquisition instrumentation including a BEI Optical Shaft Encoder and a Lebow 1604 series torque transducer, as seen in Figure 3.1. The shaft encoder allows the data collected from the engine to be cyclically (0-720 CAD) viewed in 1/5th crank angle degree measurements.

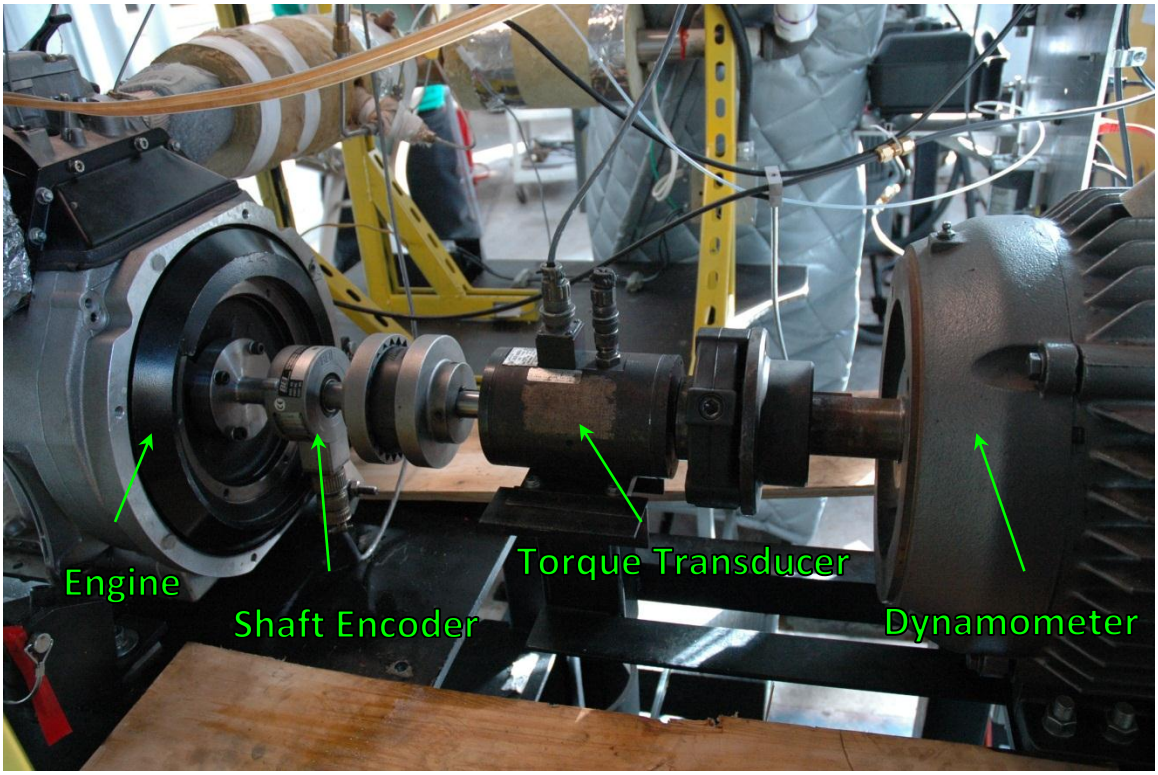

Figure 3.1. Engine/dynamometer coupling system with instrumentation

To experimentally achieve HCCI combustion in the Hatz, pre-heated intake air is mixed with vaporized fuel in order to obtain a truly homogeneous mixture in the intake manifold just before being inducted into the engine cylinder. The intake air

temperature is controlled using a 6 kW process air heater controlled by a process controller, as seen in Figure 3.2.

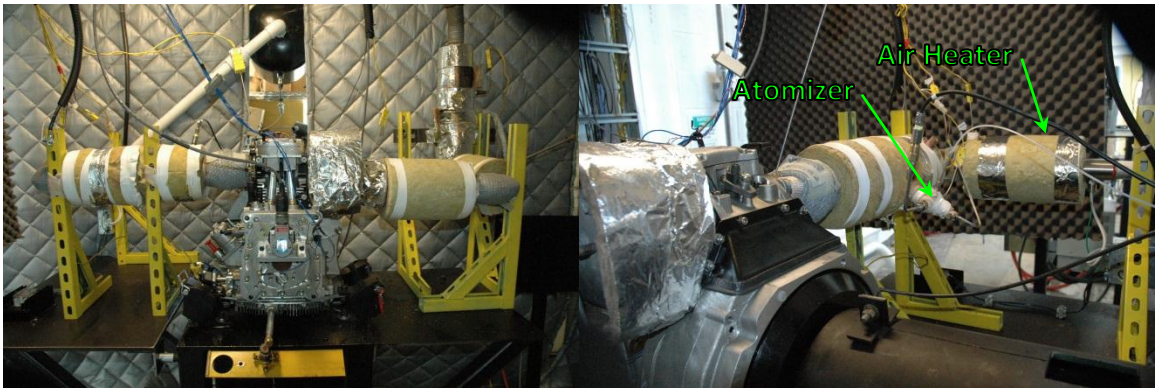

Figure 3.2. Hatz 1D50Z engine setup with the HCCI intake system

The intake air flow is measured using a laminar flow element. The fuel is vaporized by using a custom fabricated atomizing device. A schematic of the atomizer construction is shown in Figure 3.3. This atomizer is comprised of a cartridge heating element encased in an array of pipe fittings and is operated above the boiling temperature but below the auto-ignition temperature of the fuel. The heating element is powered by a variable transformer that allows a constant low level voltage to be applied to the cartridge heater as to eliminate small fluctuations in the temperature. A small amount of air flow (5.5 liter per minute) is introduced into the atomizer to push the fuel vapor into the intake manifold. A low flow FMI metering pump is used to precisely meter a constant flow of fuel into the atomizer. In order to ensure accurate fuel flow, a fuel drip nipple is placed close enough to the heating element as to alleviate

the formation of droplets. The fuel flow is verified by using a rotameter calibrated to the specific fuel used during testing.

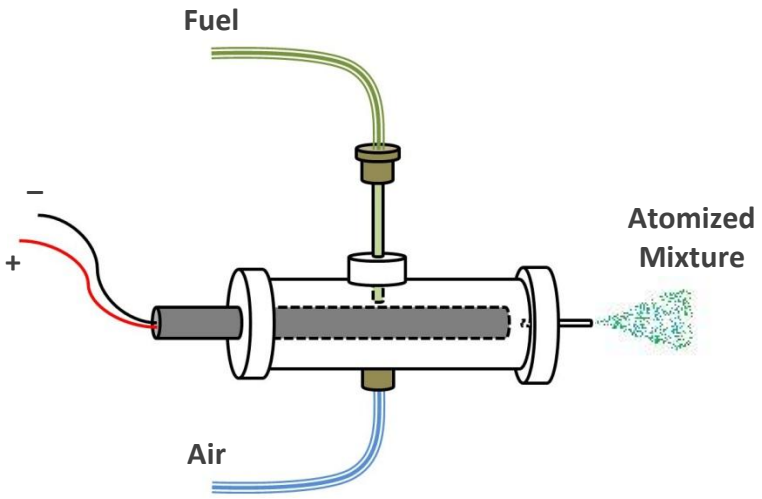

Figure 3.3. Schematic of custom fabricated atomizing device

The engine does not have an OEM exhaust gas residual recirculation valve. In order to increase the engines internally trapped residual amount, a gate valve was installed in line with the exhaust piping system as seen in Figure 3.4. This valve is then used to create more back pressure in the exhaust manifold, forcing more residuals to back flow into the engine during the valve overlap period, increasing the internal exhaust gas residual amount.

Figure 3.4. Exhaust piping – exhaust manifold back pressure valve

3.1.2 Engine Performance Instrumentation. In-cylinder pressure measurements are measured using a Kistler 6045A pressure transducer. The pressure transducer is flush mounted to the inside of the cylinder in the engine's aluminum head. This is done to prevent affecting the cylinder volume. A flush mount sensor as close to the center of the cylinder as possible is ideal when investigating engine knock, and since HCCI

combustion is an autoignition event, the pressure transducer was chosen to be flush mounted. The Kistler 6045A pressure transducer is a charge type transducer and requires a charge amplifier for use. A Kistler Dual Mode Amp Type 5010 charge amplifier set to 10 MU(bar)/Volt is used to convert the transducer charge into a readable voltage in the data acquisition system via BNC connections.

In order to complete a full combustion analysis, a number of different exhaust gas species must be monitored and measured. Three separate California Analytical Instruments (CAI) emissions analyzers are utilized to determine the concentrations of each of these species that are contained in the exhaust. Two wet gas analyzers are used to measure total unburned hydrocarbons (uHC) and nitric oxides (NO_x). A wet gas analyzer requires that the exhaust sample be maintained at an elevated temperature so that the water vapor does not condense out and harm the machine. This is achieved by using heated sample lines. A model 300M-HFID flame ionization detector determines uHC in parts per million while a model 4000-HCLD determines the NO_x concentration. Carbon monoxide (CO), carbon dioxide (CO_2), and oxygen (O_2) percentages are measured by a model 300 NDIR dry gas analyzer that condenses the H_2O out of the exhaust stream prior to analysis. In addition to the combustion pressure and emissions measurements, there are other various temperatures and pressures that are monitored around the engine test cell.

3.1.3. Cyclic Exhaust Measurements. For a study on exhaust gas residuals and its effect on the combustion performance parameters, the exhaust temperature and pressure must be collected on a cyclic basis. A fast response thermocouple developed

by ECM, Engine and Control Monitoring, called the FastTEMP Kit was used to measure the exhaust gas temperature on a 0.2 CAD resolution. The thermocouple is a 1/16" Type-K TC that is six inches long, with a response time of 0.004 seconds. The temperature gradient across the thermocouple sensor cable is minimized for the best accuracy since the data collection system is very sensitive. The thermocouple was hard mounted in the exhaust manifold as to reduce mechanical stress and vibration that might cause strain to the thermocouple wires in the senor resulting in noise in the data and reduced sensor life.

With this Type-K thermocouple it is necessary to correct for the non-linearity introduced to the voltage reading by the Seebeck coefficient. The Seebeck coefficient, also called thermoelectric power, for specific materials is a measure of the magnitude of an induced voltage due to a temperature difference across that material, in this case the thermocouple itself. In order to compensate for this effect, the following formulas were used to correct the temperature.

$$T_{corrected} = T_{exhaust} + \Delta T_{Seebeck} \tag{1}$$

A plot showing the correction curve ($\Delta T_{Seebeck}$) for the specific material used for this fast response thermocouple is displayed in Figure 3.5.

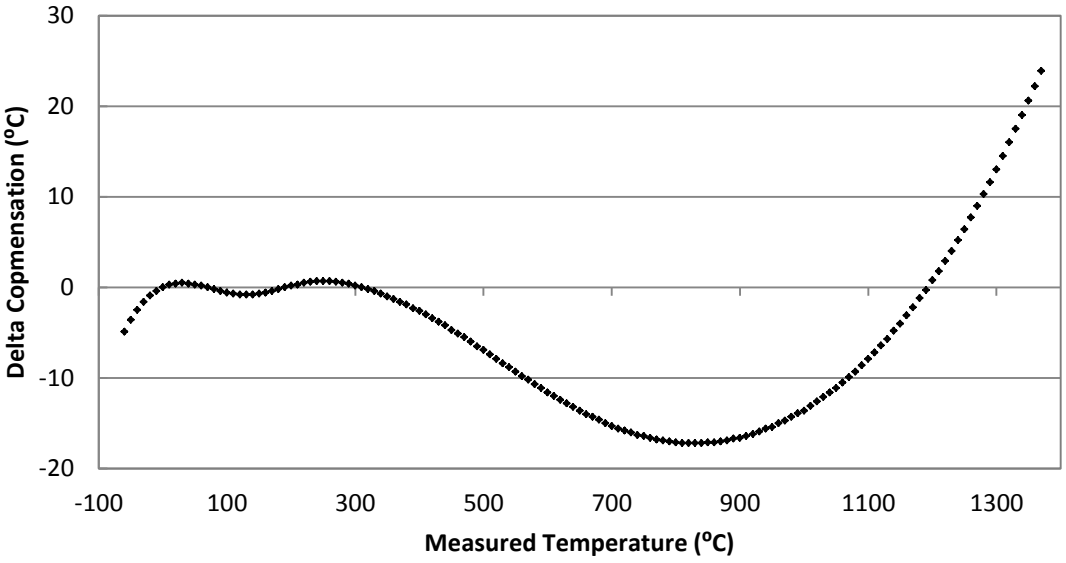

Figure 3.5. Seebeck coefficent compensator chart for FastTEMP thermocouple

$For\ \ T_{exhaust} < 125\ °C$

$$\Delta T_{Seebeck} = \frac{1.6617794 * T_{exhaust}}{33.855045 + \ e^{(0.0091689527 * T_{exhaust})}} - \ 0.017613953 * T_{exhaust} - 4.5852666 \quad (2)$$

$For\ 125\ °C \leq T_{exhaust} \leq 375\ °C$

$$\Delta T_{Seebeck} = \frac{1.6617794 * T_{exhaust}}{33.855045 + \ e^{(0.0091689527 * T_{exhaust})}} - \ 0.017613953 * T_{exhaust} - 4.5852666 \quad (3)$$

$For\ T_{exhaust} > 375\ °C$

$$\Delta T_{Seebeck} = 1.3147694E^{-13}{T_{exhaust}}^{5} - 6.1788807E^{-10}{T_{exhaust}}^{4} + 1.1867514E^{-6}{T_{exhaust}}^{3} - 0.0010330437{T_{exhaust}}^{2} + 0.36326078 * T_{exhaust} - 44.138569 \quad (4)$$

The curves are represented mathematically in Equations 2-4. Depending on the measured value, the correct function is selected and the compensation value is calculated. This value is then added to the measured value to accurately and correctly record the exhaust gas temperature, which is used to estimate the residual gas temperature.

In order to estimate the exhaust gas residuals properties, one must measure these exhaust parameters with accuracy. Therefore the instrumentation was installed close to the exhaust valve. A unique exhaust manifold was fabricated so that both transducers were mounted in such a way that the thermocouple junction was 1 cm from the exhaust valve stem in the exhaust port. The thermocouple junction was placed extremely close to the valve seat. It was made sure that the TC junction was outside of the flow separation layer in order to capture bulk gas temperature. Shrouding due to the back side of the valve was taken into consideration such as to not inhibit the flow of hot exhaust gas on to the thermocouple. This is illustrated in Figure 3.6. At this location, since there is little time for mixing to occur, the levels measured should be relatively close to those present in the cylinder at the end of the exhaust stroke. The exhaust temperature is quantified by a 100 CAD average over the cycle of the exhaust stroke.

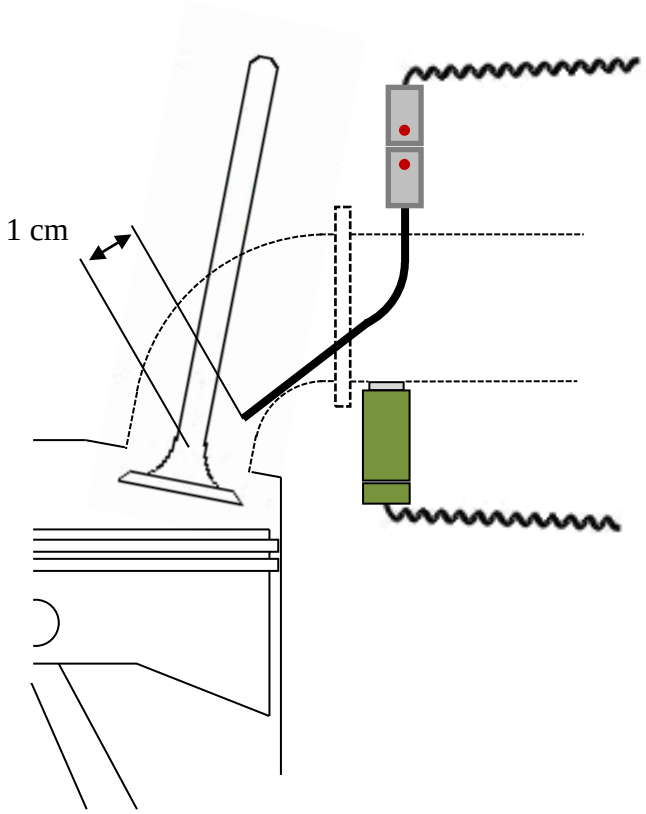

Figure 3.6. Probe position for cycle resolved temperature and pressure measurements

The thermocouple junction can be seen in Figure 3.7. This figure shows the bottom side of the head, or the top surface of the combustion chamber, with the exhaust valve removed in order to locate the tip of the TC in relation to the valve stem. The exhaust manifold pressure was collected using a water cooled Kistler 4049A high temperature gas pressure transducer in line with a PR-Amplifier Type 4622A, with a response time of 0.1 milliseconds. The sensor is mounted in the same relative location in the custom exhaust manifold as the temperature transducer.

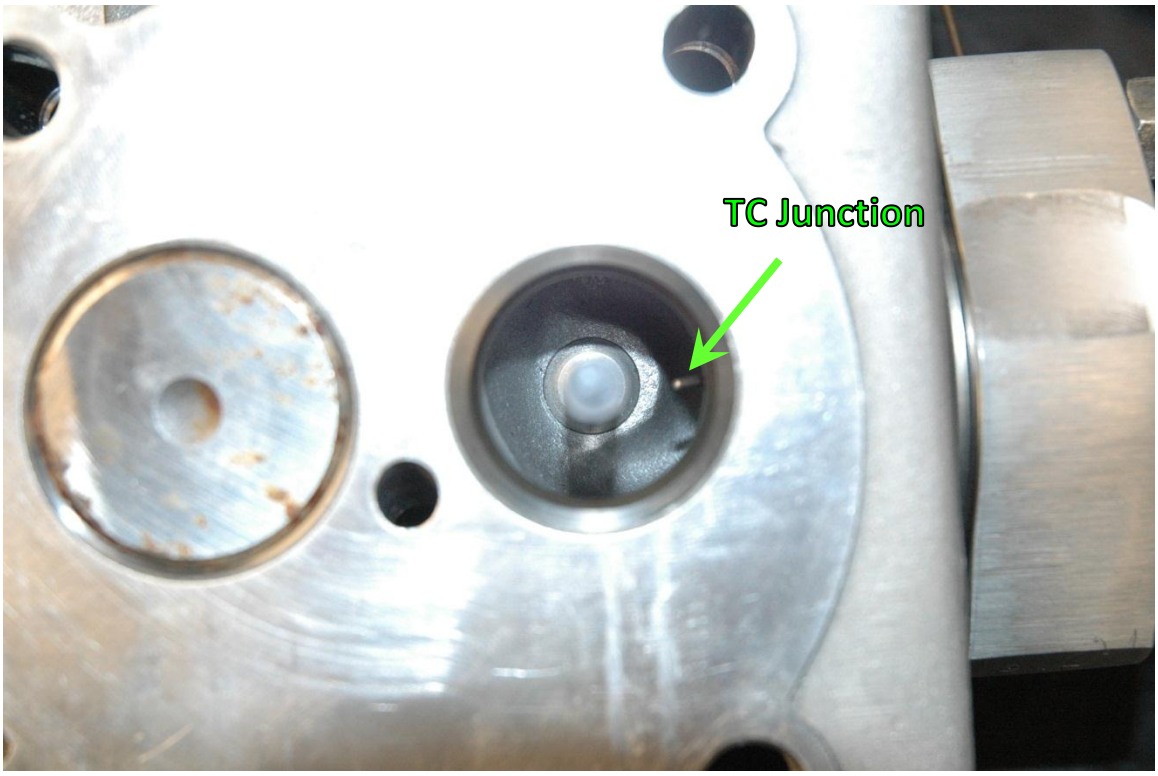

Figure 3.7. Thermocouple junction location, engine head with exhaust valve removed

3.1.4. Residual Gas Injector. Since the occurrence of HCCI combustion relies on chemical kinetics, we know that the thermodynamic state and the dilution levels of the charge mixture will directly affect the start of combustion process. In order to further investigate these effects on this process, it would be beneficial to be able to carefully perturb the intake charge on a cyclic basis with certain exhaust products. With this in mind, it was desired to isolate the chemical composition effect of the residuals from the thermal effect by directly injecting a reactive species gas, like CO or H_2. These gasses would be directly injected during the induction process and end just before IVC to achieve adequate mixing in-cylinder and observation of the combustion process would be performed.

An injector, called the Residual Gas Injector (RGI), was developed to do just this. In order to directly inject into the cylinder cycle-by-cycle, the preexisting port for the original diesel fuel injector was used. The diesel fuel injector is a design of the OEM engine and is not used for HCCI combustion; however it is installed to keep the geometry of the cylinder intact during operation. To minimize modifications to the original head, a residual mass injector was designed and constructed from the original diesel injector, shown in Figure 3.8.

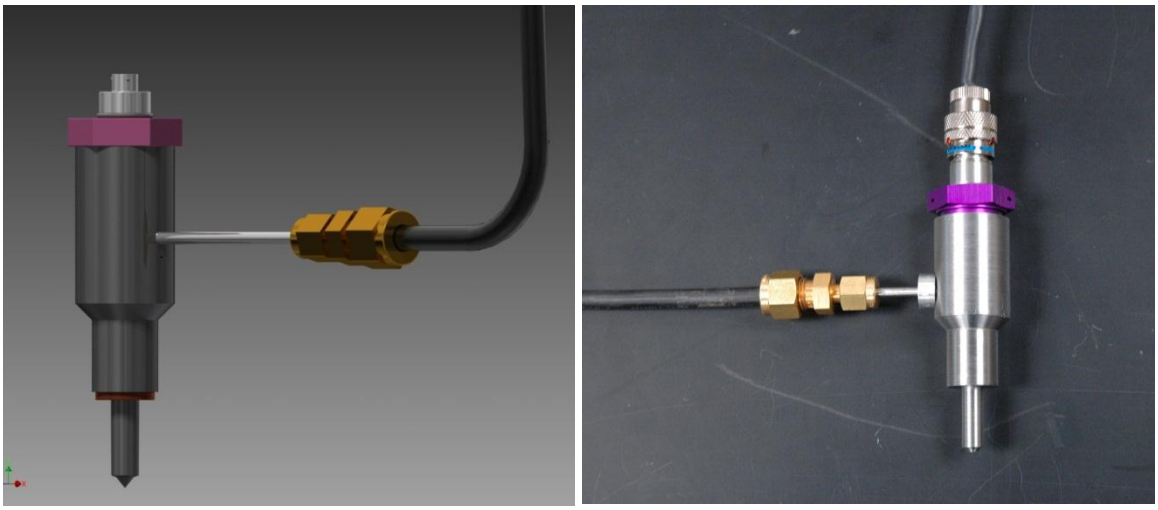

Figure 3.8. In-cylinder Residual Gas Injector a. solid model and b. prototype

The main body of the injector was turned from high grade steel to accept the gas port tube and the valve body. A single-coil solenoid valve, manufactured by the Lee Company, with a response time of 0.015 second will allow gas injections of up to 7% by mass of the inlet charge to be mixed with the fresh charge in-cylinder. The valve is designed to withstand pressures of 4000 psi. The use of a multi-seal allows these kinds

of pressures, developed by the Lee Company. Further figures of the RGI and its construction can be seen in Appendix A.

The RGI is operated by a product from Drivven, a National Instruments Company. The use of LabVIEW with Drivven support cards allows the RGI to operate very similarly to a fuel injector. The Port Fuel Injector Driver Module Kit seen in Figure 3.9 provides a CompactRIO (cRIO) module for driving low and high impedance Port Fuel Injectors (PFI) and general purpose automotive solenoid valves. A LabVIEW FPGA VI was developed to control each driver channel on the PFI support card. Each channel is individually controlled for timing and duration and can be operated in real time.

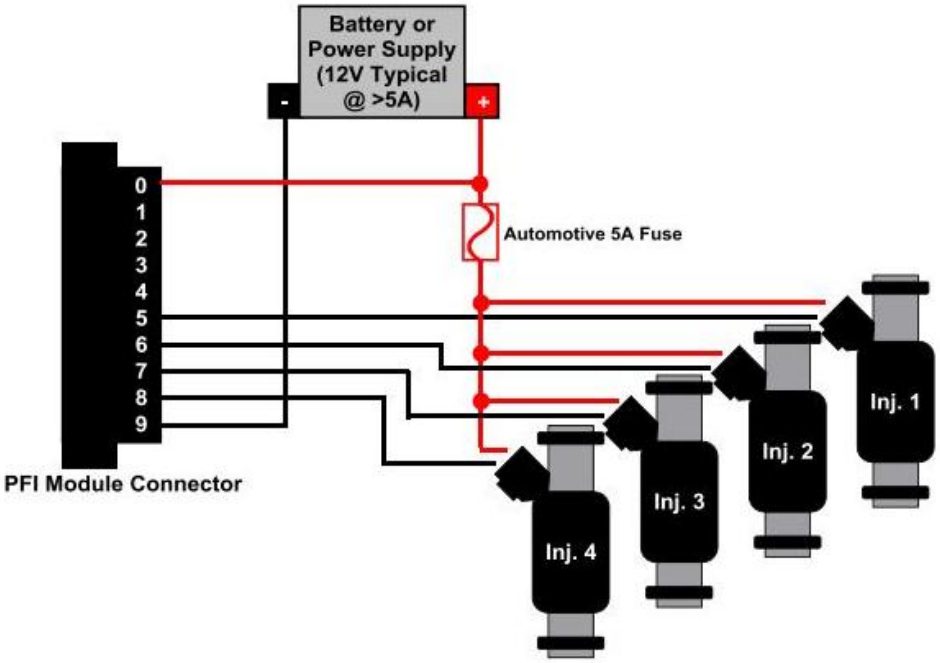

Figure 3.9. Drivven PFI support card with individual injectors

Since the Hatz is a single cylinder air cooled engine, only one of the fuel injector driver ports were utilized. The system was set up with a NI-cRIO 9022 Real Time

Controller as the base chassis that communicates with the top level programs in LabVIEW nested in the computer mainframe. This system in shown in Figure 3.10.

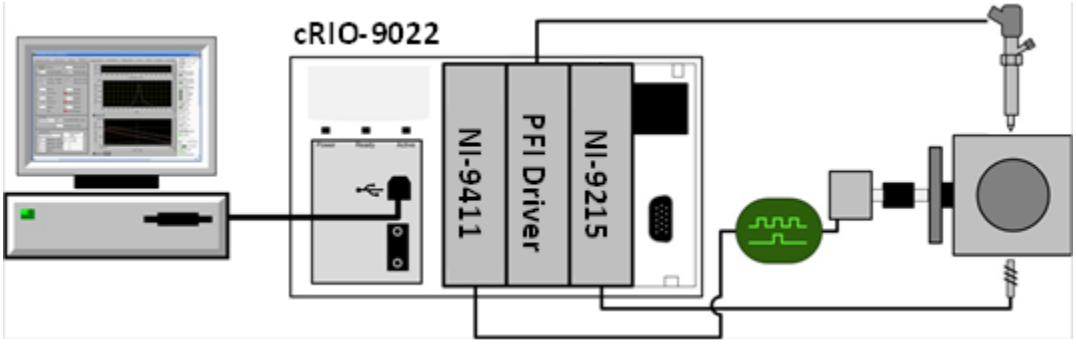

Figure 3.10. c-RIO FPGA residual gas injector driver system

The use of a NI-9411 and ESTTL card allowed for engine position tracking, while the RGI was driven by the PFI Driver card. The engine pressure was monitored as an analog input using a NI-9215 card. All of this, used in parallel with the data collection system already installed on the Hatz, allowed for the fast perturbations of reactive species gas to be added in-cylinder to the intake charge prior to compression and combustion.

3.2. EXPERIMENTAL PROCEDURE

For this study, there were several engine set points selected for the firing test of the HCCI engine that includes a range of different loads at one single engine speed. The details of the set points are shown in Table 3.2. The speed selected for this study is 1800 revolutions per min (rpm). At this speed, there were four different variations in fueling

rate allowing for a change in engine load. The engine load is quantified as the net indicated mean effective pressure (IMEPn). More details about IMEP calculations can be found in §4.2.1. The fuel used in this research is indolene, which is a research grade gasoline with a research octane rating number (RON) of 96.

Table 3.2. Observed engine set points

Operating Regime	Intake Temp (K)	Eq. Ratio (φ)	Fueling Rate (grams/min)	Avg. CA50 (CAD)	IMEPg (bar)	COV (%)	Fuel Efficiency ($\eta_{f,i}$)
Steady State	*503*	*0.29*	*6.0*	*361.5*	*3.34*	*1.57*	*58.5*
Partial Burn	*466*	*0.28*	*6.0*	*374.9*	*2.47*	*13.00*	*43.2*
Steady State	*495*	*0.36*	*7.5*	*361.3*	*3.79*	*1.58*	*53.1*
Partial Burn	*460*	*0.34*	*7.5*	*377.9*	*3.12*	*10.60*	*43.7*
Steady State	*468*	*0.41*	*9.0*	*364.3*	*4.57*	*1.20*	*52.7*
Partial Burn	*452*	*0.40*	*9.0*	*380.6*	*3.88*	*8.99*	*44.8*
Steady State	*437*	*0.50*	*11.2*	*368.7*	*5.38*	*1.72*	*50.4*
Partial Burn	*442*	*0.50*	*11.2*	*383.7*	*4.96*	*5.96*	*46.5*

**All set points at constant engine speed – 1800 rpm*

At each engine set point, the intake air temperature was varied in order to change combustion phasing within the combustion cycle. Engine phasing is most commonly referred to as when the combustion duration starts and stops within the current cycle. At each load the intake temperature was increased until the combustion phasing was advanced early in the cycle. The set point that is of interest here is when CA50 is close to TDC. This is important as this is when the engine has the highest fuel conversion efficiency and will be referred to as the *steady state* operating location from here on. This limit is reached based solely on operator's judgment. In some instances it is not possible to reach CA50 at TDC; therefore a constraint on pressure rise rates (PRR)

of 10 bar/CAD is set. In fact it is rarely the case where you will have both CA50 at TDC and a pressure rise rate of 10 bar/CAD. This constraint limit is set because it is where the engine is audibly loud and noise, vibration and harshness (NHV) are of concern. This NHV will eventually lead to the degradation of engine components. Once the set point of CA50 at TDC, or the pressure rise rate limit is reached, the data is collected. The intake temperature is reduced in order to phase combustion late in the cycle. Here, engine variations become very high and the engine approaches a misfire limit. The coefficient of variation (COV) becomes very high and partial consumption of the fuel/air charge leads to calling this set point as the *partial burn regime*. This COV is defined as the cyclic variability in indicated work per cycle. When the COV is high, greater than 10%, then the engine is considered to be in a region of instability, or partial burn regime. It is in the partial burn regime where the main focus of this study is localized where the cyclic dynamics are not fully understood.

The equivalence ratio, φ, is the ratio of actual fuel/air ratio to the stoichiometric fuel/air ratio. This defines the mixture composition at each set point and is found from Equation 5.

$$\varphi = \frac{(F/A)_{actual}}{(F/A)_{stoich}} \tag{5}$$

The fuel properties of indolene are given by the manufacturer and the $(F/A)_s$ was found, through thermochemistry, to be 0.0674. This is a constant for this fuel as the

carbon-hydrogen ratio is fuel specific. When the equivalence ratio is equal to 1 then the fuel/air mixture is considered to be at stoichiometric conditions, φ=1. If φ<1 then the fuel/air mixture is considered to be lean, and if φ>1 then it is considered rich. HCCI combustion is a very fuel efficient process and part of this is contributed to HCCI operating in the lean condition, φ<1. This is done due to the rapid release of chemical energy when autoignition occurs within the cylinder, attributing to the high PRR's. The higher the equivalence ratio, the higher the engine load, and the more violent the combustion becomes, relating to NVH. The highest equivalence ratio used in this study was φ=0.5.

At the steady state operating points, 400 consecutive cycles of engine data were collected. These measurements were taken after the engine had stabilized at each intake temperature for that load. A stable operating point is when there are no longer any transients in exhaust temperature, pressure rise rates, and amount of heat released. In the partial burn regime, 1000 consecutive cycles where collected. It is important to collect this many cycles when studying cyclic dynamics as this information helps to reveal the cycle-to-cycle dependence. Further details about all engine set points and averaged observed parameters can be found in Appendix B.

4. DATA COLLECTION AND ANALYSIS

4.1. CYLINDER PRESSURE DATA

One of the challenges to operating in HCCI is the difficulty in accurately detecting the start of combustion in cylinder due to the autoignition process. In order to analyze the combustion event and determine metrics such as SOC, 50% of heat released (CA50), and burn duration, the combustion energy release process was quantified by a zero-dimensional single-zone heat release analysis. This heat release curve is computed from the measured in-cylinder pressure (P_θ), in-cylinder volume (V_θ), and their respective derivatives, $dP_\theta/d\theta$ and $dV_\theta/d\theta$. This particular section sheds light on the signal processing involved in the computation of these metrics. The equations that are used to compute the variables within the heat release calculation will be presented first and the heat release calculation will follow.

4.1.1. Cylinder Volume and Volume Derivative. In-cylinder volume as a function crank angle degrees, θ, that is the instantaneous cylinder volume, V_θ, is one of the necessary variables for the heat release calculation. By using the current crank angle degree and the geometrical position equations given by Heywood [16], the cylinder volume at any crank position θ is

$$V_\theta = V_c + \frac{\pi B^2}{4}(l + a - s) \tag{6}$$

where V_c is the clearance volume in the cylinder at full compression, *B* is the cylinder bore (cylinder diameter), *l* is the connecting rod length to the crank radius, *a* is the crankshaft radius, and *s* is the distance between the crank axis and the piston pin axis. This dimension *s* is given by the following equation.

$$s = a\ cos\,\theta + (l^2 - a^2 \sin^2\theta)^{\frac{1}{2}} \tag{7}$$

In order to better understand the geometrical variables within the engine that are comprised of the connecting rod, crankshaft axis, and this distance *s* as defined by Equation 7, a graphical representation of the geometry is available in Figure 4.1.

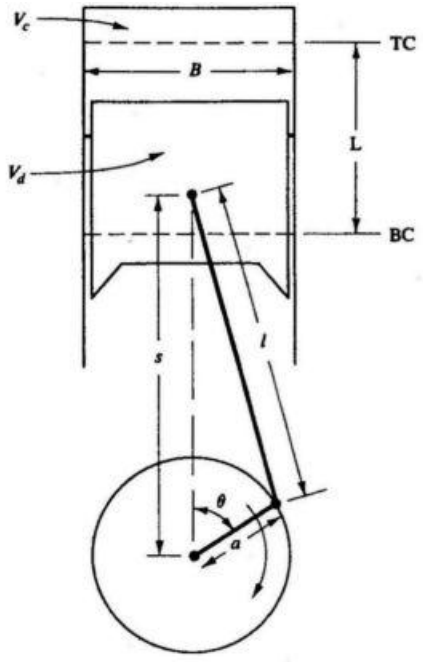

Figure 4.1. Geometry of cylinder, piston, connecting rod and crankshaft

To calculate the volume derivative with respect to crank angle degrees, $dV_\theta/d\theta$, one would take the derivative of Equation 6 with respect to θ.

$$\frac{dV_\theta}{d\theta} = \frac{d}{d\theta}\left[V_c + \frac{\pi B^2}{4}(l + a - s)\right] \tag{8}$$

Given that the clearance volume, the bore, the connecting rod length, and the crankshaft axis are all fixed constants, Equation 8 condenses to

$$\frac{dV_\theta}{d\theta} = -\frac{\pi B^2}{4}\frac{ds}{d\theta} \tag{9}$$

Next calculate the derivative of *s* with respect to crank angle degrees ($ds/d\theta$)

$$\frac{ds}{d\theta} = -a\sin\theta\left[1 + \frac{a\cos\theta}{(l^2 + a^2\sin^2\theta)^{\frac{1}{2}}}\right] \tag{10}$$

Finally, by substituting Equation 10 into Equation 9, the equation for in-cylinder volume as a function crank angle degrees, that is the instantaneous cylinder volume, is

$$\frac{dV_\theta}{d\theta} = \frac{\pi B^2}{4} a \sin\theta \left[1 + \frac{a\cos\theta}{(l^2 + a^2\sin^2\theta)^{\frac{1}{2}}}\right] \frac{T_{IVC} P_\theta T_\theta}{P_{IVC} V_{IVC}} \qquad (11)$$

4.1.2. Cylinder Pressure Smoothing. As the pressure evolves within the cylinder during compression and expansion after combustion, there tends to be high frequency pressure waves from cavity resonances. With consideration to the heat release computation, it assumes spatial homogeneity of the combustion process so these resonances can affect the pressure curve causing miscalculations within the heat release data. They can occur at very high loads and have been witnessed on the S&T engine platform. Therefore, a low-pass filter is applied to the raw pressure data as to smooth the pressure data and eliminate these cavity resonances. It can be seen in Figure 4.2 how the smoothing technique affects the raw data curve.

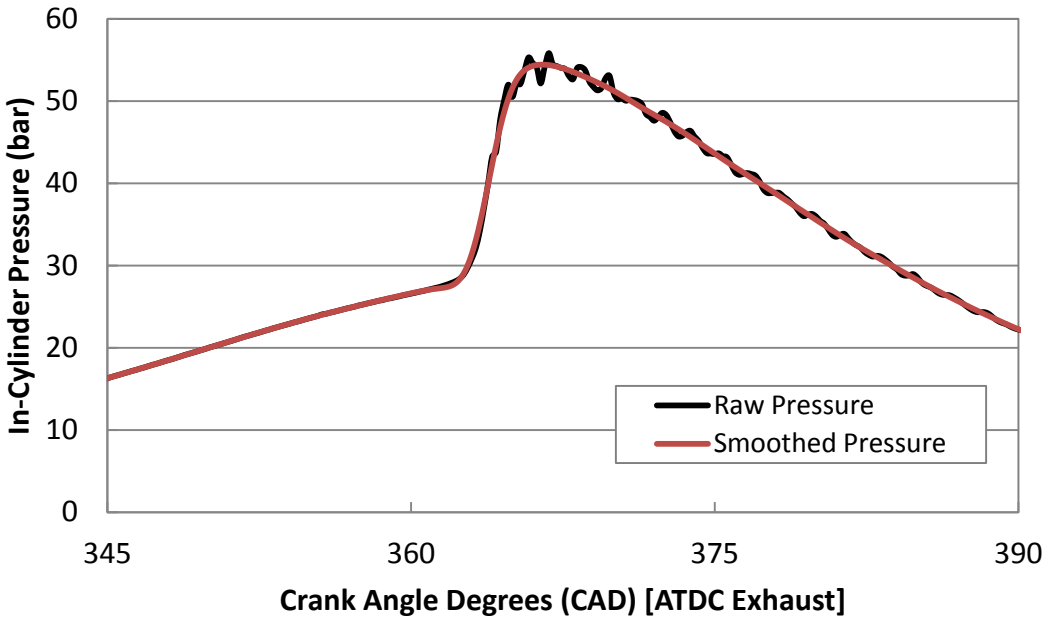

Figure 4.2. High frequency resonances at TDC and smoothed pressure data

The cosine low-pass filter works by performing the Fourier transform on the raw data, then multiplying the cylinder pressure spectrum by the cosine filter and then by using an inverse Fourier transform, the filtered data is converted back into the time domain. This filtered data is plotted in Figure 4.3.

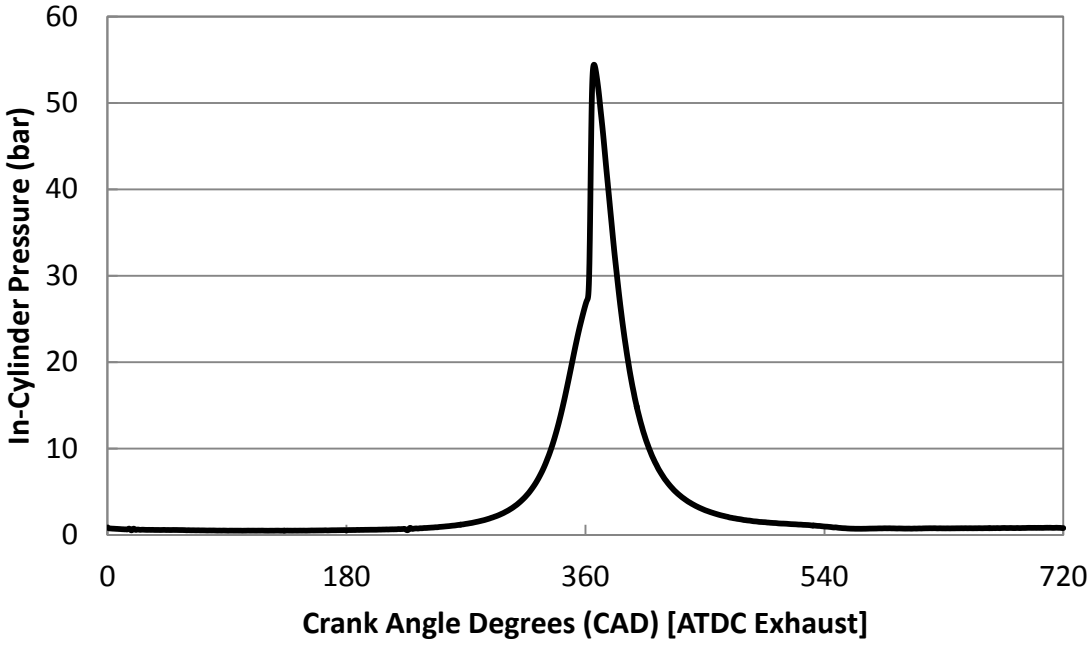

Figure 4.3. Smoothed pressure evolution within the cylinder

4.1.3. Cylinder Pressure Derivative. The pressure rise rate (PRR), or in-cylinder pressure derivative as a function of crank angle degrees, θ, that is the instantaneous in-cylinder pressure derivative, is calculated using Equation 12. The pressure rise rate is not calculated for the entire engine cycle. The range of crank angle degrees is from intake valve closed to exhaust valve open.

$$\frac{dP_\theta}{d\theta} = PRR = \frac{P_{\theta+h} - P_{\theta-h}}{2h} \tag{12}$$

In Equation 12, the variable *h* is defined as the resolution of the shaft encoder. For this study the BEI Optical Shaft Encoder had a resolution of 1/5th CAD (0.2 crank angle degrees).

4.1.4. Cylinder Temperature. In-cylinder temperature as a function crank angle degrees, θ, that is the instantaneous in-cylinder temperature, T_θ, is another one of the necessary variables for the heat release calculation. For this calculation, the fuel/air charge is assumed to behave like an ideal gas. In order to treat the system as a closed thermodynamic system with no mass crossing the boundaries, one can only apply this technique to the time when the engine is actually a closed system. That is from intake valve closed (IVC) to exhaust valve open (EVO). During this time the engine is a closed thermodynamic "chamber". With these assumptions in mind, the instantaneous in-cylinder temperature, T_θ, can be calculated by relating the ideal gas equation to the conservation of mass, yielding Equation 13.

$$T_\theta = \frac{T_{IVC} P_\theta T_\theta}{P_{IVC} V_{IVC}} \tag{13}$$

Here the variables T_{IVC}, P_{IVC}, and V_{IVC} are the in-cylinder temperature, in-cylinder pressure, and in-cylinder volume at IVC, respectively. Due to the measured intake fuel/air charge temperature, it is assumed that T_{IVC} is fairly well approximated.

4.1.5. Heat-Release Calculation. The heat-release analysis is taken from Heywood [16]. When calculating heat-release (HR) from the cylinder pressure data analysis, one can quantify the effects of heat transfer, crevices, and leakage based on the first law of thermodynamics. An advantage to this approach is that the pressure fluctuations in cylinder can be directly related to the amount of fuel chemical energy that is released throughout the combustion process. The first law for this system is shown in Equation 14.

$$\delta Q_{ch} = dU_s + \delta Q_{ht} + \delta W + \sum h_i dm_i \tag{14}$$

Where dU_s is the change in sensible energy, the term δQ_{ch} represents the chemical energy released by combustion, the piston work (δW), δQ_{ht} is the heat transfer to the chamber walls, and the mass flux term represents the flow across the boundary. For these parameters, we monitor and calculate onboard the heat release and heat release rate. Therefore a gross heat release analysis is used instead of a net HR in order to be quick enough to be calculated in real time. The difference between this net and gross HR is the heat transfer to the cylinder walls, head, and piston top and the small crevice effects. By eliminating these from the first law, replacing piston work with $p\,dV$, and assuming that the change in sensible energy is given by $mc_v(T)$ where T is the mean charge temperature and m is the mass within the system boundary then the equation is reduced to:

$$\delta Q_{ch} = mc_v\, dT + p\, dV \tag{15}$$

By use of the ideal gas law, and neglecting the change in gas constant R, the system's equation becomes:

$$\delta Q_{ch} = \left(\frac{c_v}{R}\right) V\, dp + \left(\frac{c_v}{R} + 1\right) p\, dV \tag{16}$$

Recall that for this calculation the heat transfer effects and the crevice effects have been removed, yielding a gross heat release for the fuel chemical energy released. Figure 4.4 shows the results of heat-release analysis showing the effects of heat transfer, crevices, and combustion inefficiency [16].

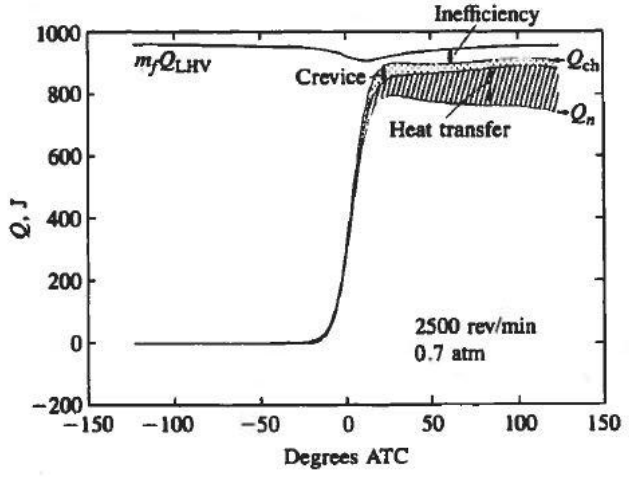

Figure 4.4. Heat-release analysis showing the effects of losses in chemical energy released [16] [Heywood, J.B. "Internal Combustion Engine Fundamentals."]

In order to accurately calculate the term c_v/R, the ratio of specific heats (γ) for burned and unburned gases is used, shown in Equation 17. For an approximate approach γ is held constant during combustion and has been shown to give adequate results [16].

$$\frac{c_v}{R} = \frac{1}{\gamma - 1} \tag{17}$$

Finally, the heat release rate (RHR) is calculated using Equation 18. This HRR is used to compute the cumulative heat release (HR) by numerically integrating the RHR equation using the composite trapezoidal rule. This method has been used significantly in engine combustion analysis and has proven to be a robust method [16].

$$\frac{dQ_{ch}}{d\theta} = HRR = \frac{\gamma}{\gamma - 1} P_\theta \frac{dV_\theta}{d\theta} + \frac{1}{\gamma - 1} V_\theta \frac{dP_\theta}{d\theta} \tag{18}$$

The HR, RHR, and PRR are all useful in this study of HCCI cyclic dynamics. The pressure rise rate allows us to maintain a limit of 10 bar/CAD as the pressure evolves within the cylinder, informing us that we do not want to advance the engine any more as noise, vibration, and harshness (NVH) becomes a problem and could degrade the internals of our engine. The HR and RHR inform us of SOC (which for this study we are

calling CA10), CA50 and burn duration. All these metrics are used to determine cycle-to-cycle dependence and can be seen in further detail in Chapter 5. CA10 is defined as the location or crank angle degree, where 10 percent of the total heat released occurs. That is determined from a maximum heat released value, as seen in Figure 4.4, and then 10 percent of that value is used to determine the relative location of CA10 in crank angle degrees for that cycle. CA50 is computed in the same fashion; except that its location is where 50 percent of the total heat released occurs.

4.2. ENGINE PERFORMANCE MEASURES

With regard to homogenous charge compression ignition combustion, the maximum heat-release rate and the duration of the heat release (burn duration) can vary between cycles significantly when operating in the partial burn regime close to the misfire limit. Then the peak cylinder pressure varies accordingly. The faster burning cycles have substantially higher values of maximum pressure (steady state operating case) than do the slower burning cycles (partial burn regime), where the steady state case has maximum RHR near TDC. Operation in the partial burn regime is obviously undesirable as there is risk of a misfire and from the point of fuel efficiency, hydrocarbon emissions, torque variations, and roughness. Various measures of cycle-by-cycle combustion variability are used. It can be defined in terms of variations in the cylinder pressure between different cycles, or in terms of variations in the details of the burn process which cause these differences in pressure.

4.2.1. Indicated Mean Effective Pressure. While torque is a valuable measure of a particular engine's ability to do work, it is dependent on engine size. A more appropriate performance measure is net indicated mean effective pressure (IMEPn). This is defined as the net work per engine cycle divided by the engines displacement volume. For a single cylinder engine, it is divided by the cylinder displacement volume, which is the engine's displacement volume. IMEPn is represented mathematically as

$$\text{IMEPn} = \frac{1}{V_d}\int_{V_0}^{V_{720}} P_\theta \, dV \tag{19}$$

In Equation 19, the limits of integration are V_0 and V_{720} which represent the initial and final volumes of the cylinder in terms of crank angle degrees. 720 degrees of rotation, or 2 cycles, indicates integration over all four strokes of a four stroke engine, or the entire engine cycle. After applying the composite trapezoidal rule, IMEPn can be acquired from the measured cylinder pressure as seen in Equation 120. Note that this cylinder pressure is the smooth pressure curve and not the raw data that includes the cavity resonances.

$$\text{IMEPn} = \frac{1}{2V_d}\sum_{i=1}^{720/h}\left[P_{\theta_i+h} + P_{\theta_i}\right]\left[V_{\theta_i+h} - V_{\theta_i}\right] \tag{20}$$

As mentioned above, *h* is once again the resolution of the shaft encoder and θ_i is the crank angle at index *i*.

4.2.2. Fuel Conversion Efficiency. The ratio of the work produced per cycle to the amount of fuel energy supplied per cycle that can be released in the combustion process is used as the engine's efficiency. Since it is with respect to fuel energy in, this efficiency is more commonly referred to as the fuel conversion efficiency, η_f. The fuel energy supplied which can be released by combustion is given by the mass of the fuel supplied to the engine per cycle time the heating value of that fuel (Q_{HV}). The fuel conversion efficiency is given by Equation 21.

$$\eta_f = \frac{P}{\dot{m}_f Q_{HV}} \tag{21}$$

Where $\dot{m}_f$ is the mass flow rate of the fuel into the cylinder per unit time and *P* is unit power out for that cycle.

4.2.3. Coefficient of Variation. One important measure of cyclic variability, which is yet another parameter derived from pressure data, is the coefficient of variation (COV) of IMEP. The COV is defined as the standard deviation in IMEP divided by the mean IMEP as shown in the following mathematical representation.

$$\mathrm{COV}_{IMEP} = \frac{\sigma_{IMEP}}{\overline{IMEP}} * 100 \tag{22}$$

COV is usually expressed as a percent, hence the multiplication by 100. It defines the cyclic variability in indicated work per cycle, and has been found that when operating in steady state it is near 1-2% and when the engine is found to be in the partial burn regime, when CA50 is retarded very late in the combustion process, the COV_{IMEP} exceeds 10%.

4.2.4. Return Maps. A method for examining inherent interactions between cyclic events is to plot return maps. Return maps show the correlation between each individual pair of consecutive events in the data set without averaging. By plotting each successive value of the measured parameter against the succeeding cycle's measured parameter we can see when they are related. This return map reflects whether or not one can represent this oscillation process in terms of some type of simple function such as:

$$\Psi(i+1) = f\,[\,\Psi(i)\,] \tag{23}$$

Where $\Psi(i)$ is the current cycles observed parameter, or measured metric. Return maps can be advantageous in this study on cyclic dynamics, because return maps may reveal strong but rarely occurring correlations which sometimes are overwhelmed in spectral densities by the signals from weaker but more frequently occurring correlations, and even other "patterns" referred to as noise. Some example return maps of IMEP of an engine set point are shown in Figure 4.5.

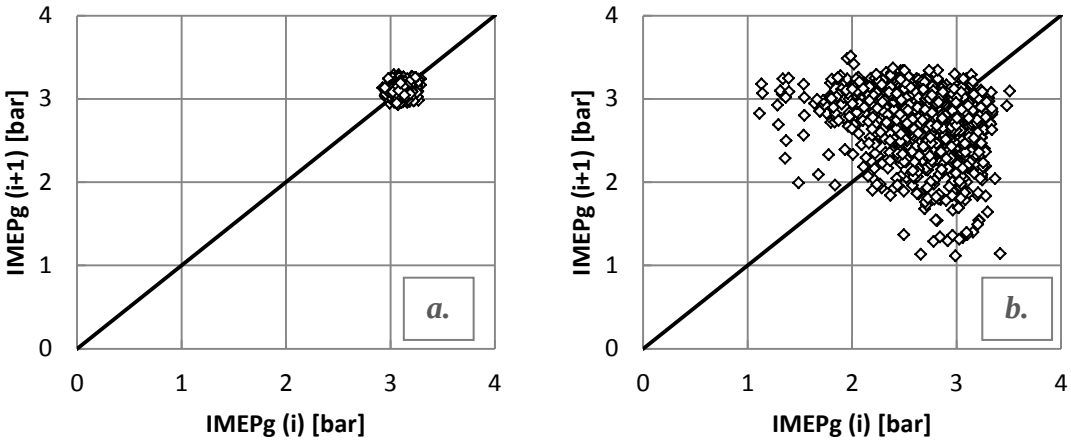

Figure 4.5. Experimentally determined return maps of IMEPg for an engine set point

A return map is a good tool to check the probable interaction between parameters of each cycle with its next consecutive cycle. If the observed parameter or measured metric is anti-correlated (i.e. if ***Ψ(i)*** is low then ***Ψ(i+1)*** is high and vice versa), then it is reflected in the extended armatures that appear on either side of the diagonal in Figure 4.5.b. This kind of behavior will be referred to as determinism or as showing a deterministic behavior. Correlated events, as opposed to anti-correlated events would tend to lie on the diagonal as seen in Figure 4.5.a. This type of grouping shows a circular unstructured pattern representing a Gaussian random distribution, more commonly referred to as stochastic or showing stochastic behavior.

4.3. RESIDUAL GAS FRACTION

The residual gas fraction affects the combustion process in HCCI engines through both the reactant concentrations and the charge temperature, which makes it an

important parameter to study when trying to understand the cyclic dynamics that are present in the partial burn regime of HCCI combustion. Therefore, a practical and accurate model for predicting the residual amount, α_r, is needed in order to confidently draw conclusions about the physical relationships that exist in this advanced combustion mode. The predictive model used for this study taken from [18] predicts the overall residual gas fraction as a combination of two mechanisms: the trapped gas in the cylinder at exhaust valve closing (EVC), and the contribution of back-flow from the exhaust to cylinder during valve overlap. The amount of residual trapped in the cylinder at EVC can be estimated fairly accurately with knowledge of the compression ratio. The flow processes during the valve overlap period, however, are very complex and are therefore difficult to model correctly. For most engine speeds, the cylinder contents equilibrate with the exhaust system during the exhaust stroke and are roughly at atmospheric pressure. The intake port, on the other hand, is generally below atmospheric pressure, which results in a net flow of burned gas into the cylinder from the exhaust manifold. This back-flow contributes significantly for each individual engine cycle. A parameter often used to describe this back-flow is the valve overlap factor (OF). An empirical expression for OF is given in [34] when the valve overlap duration is known, and can be seen in Equation 24 below.

$$OF = \frac{1.45}{B}\left(107 + 7.8\Delta\theta_{ov} + {\Delta\theta_{ov}}^2\right)\frac{L_{v,max}D_v}{B^2} \tag{24}$$

In Equation 24, OF is the valve overlap factor in degrees/meter, $\Delta\theta_{ov}$ is the valve overlap in crank angle degrees, B is the engine bore in mm, $L_{v,max}$ is the maximum valve lift in mm, and D_v is the valve inner seat diameter in mm. This expression gives a good estimate of OF for most typical engine geometries. This OF was calculated for the Missouri S&T engine, and was found to be 0.6585. Once the overlap factor, OF, is known, an expression for the overall residual gas fraction can be determined. An empirical expression from [18] is given below in Equation 25 that was used to determine the overall residual gas fraction.

$$\alpha_r = 0.401\frac{OF}{N}\left[1 - e^{\left(-4.78\left(1-\frac{P_i}{P_e}\right)^{0.7} - 153.8\left(1-\frac{P_i}{P_e}\right)^{4.5}\right)}\right]\frac{P_e}{P_i}\frac{T_i}{T_e} + \frac{1}{r_c}\frac{P_e}{P_i}\frac{T_i}{T_e} \qquad (25)$$

This resulting model relates the residual gas fraction to six independent parameters: engine speed (N), inlet and exhaust pressures (P_i and P_e), the overlap factor (OF), the inlet temperature (T_i), and the compression ratio (r_c). The first part of the expression relates the residual from the valve overlap period, while the second part contributes to the amount of gas trapped in the cylinder at EVC. The sum of these two gives the total predicted residual. It should be noted that the residual gas fraction will be fairly small for most operating conditions, less than 7%. Since the S&T Hatz does not include external EGR at this time, any effect on the next cycle's combustion event from residual gases will be an effect solely from the internally trapped residuals.

5. CYCLIC DYNAMICS INVESTIGATION

The experiments performed in this work are focused on the *partial burn regime* of HCCI combustion, where the cyclic variations are high. This cyclic dispersion tends to present itself in these low temperature combustion (LTC) modes as a result of combined stochastic and deterministic effects. Stochastic effects are influenced by both boundary and inlet conditions to the cylinder, while the deterministic effects are generated from the cycle-to-cycle coupling that inherently exists. As charge dilution is increased, these factors result in regions of instability and large cyclic variations in SOC and RHR. Upon entering these partial burn regimes, the deterministic mechanism of combustion tend to amplify the stochastic variations in a non-linear manner. In order to compare the partial burn regime to a baseline, the engine was also operated in a region of stable combustion and high efficiency, known as the *steady state* operating zone. This steady state operation is defined as a region where the engine is pushed to a pressure rise rate (PRR) limit of 10 bar/CAD. The engine phasing, or CA50, is near TDC and this is achieved by increasing the intake temperature on the engine test bed at S&T. Others achieve HCCI differently. The partial burn regime is when the engine is phased much later in the cycle, sometimes as late as 20 degrees after TDC given certain loads. Here partially consumed charges and misfires lead to increased emissions in NO_x and uHCs. It is at these two operating regimes where most of the data is collected and analyzed.

5.1. BASELINE EXPERIMENTS

The baseline experiments are experiments solely running the engine in HCCI and monitoring the combustion evolution and studying the cycle-to-cycle dynamics that the internally trapped exhaust gas residual will have on the next cycle's SOC at the partial burn regime. The experimental test matrix used in this section is shown in Table 5.1.

Table 5.1. Baseline Experimental Data Summary

Operating Regime	Intake Temp (K)	Equiv. Ratio (φ)	Fueling Rate (grams/min)	Engine Speed (rpm)	Avg. CA50 (CAD)	IMEPg (bar)	COV (%)
Steady State	*503*	*0.29*	*6.0*	*1800*	*361.5*	*3.34*	*1.57*
Partial Burn	*466*	*0.28*	*6.0*	*1800*	*374.9*	*2.47*	*13.00*
Steady State	*495*	*0.36*	*7.5*	*1800*	*361.3*	*3.79*	*1.58*
Partial Burn	*460*	*0.34*	*7.5*	*1800*	*377.9*	*3.12*	*10.60*
Steady State	*468*	*0.41*	*9.0*	*1800*	*364.3*	*4.57*	*1.20*
Partial Burn	*452*	*0.40*	*9.0*	*1800*	*380.6*	*3.88*	*8.99*
Steady State	*437*	*0.50*	*11.2*	*1800*	*368.7*	*5.38*	*1.72*
Partial Burn	*442*	*0.50*	*11.2*	*1800*	*383.7*	*4.96*	*5.96*

The experimental matrix shows 4 different equivalence ratios (engine loads) all run at the same engine speed of 1800 rpm. As the intake temperature is increased for the steady state operating regime, the engine is phased earlier in the cycle as shown by the matrix. The engine's work output, quantified by IMEPg, is also increased due to the completely consumed fuel/air charge. The COV at steady state is in between 1-2%, indicating stable operating conditions, however in the partial burn regime the COV is significantly higher indicating instabilities in the engine's work output. These set points

are an average 400 consecutive engine cycles at the steady state and 1000 cycles at the partial burn regime.

5.1.1. Pressure Traces and Pressure Rise Rates. A pressure trace is a plot of the engine's in-cylinder pressure as it evolves throughout the combustion cycle. In HCCI, the combustion process is considered to be a constant volume process due to combustion occurring within 3-5 CAD. The pressure trace will climb the consistent motored pressure as the volume inside the cylinder decreases, and then when the conditions are right, the chemical kinetics control the auto-ignition of the fuel and a very sharp pressure spike is seen. This is consistent at the steady state operating point. In the partial burn regime, the engine will motor through the compression stroke at TDC and then the fuel will combust giving a very late phasing of the engine and resulting in partial consumed charges.

Figure 5.1 shows pressure traces for the steady state operating regime where combustion phasing is near TDC. It can be seen that as load is increased, the overall peak pressure also increases. This is due to the increase in chemical energy released within the same cylinder volume. When operating at different loads and hence different amounts of chemical energy introduced into the system through fuel, the autoignition event changes with respect to available energy in the system. The intake temperature is how this autoignition event is phased in the engine. As inlet temperatures increase then the amount of available energy is increased and the autoignition event occurs sooner. This is considered phasing the engine. The intake temperature is adjusted to phase the

combustion event earlier or later within the cycle, all while keeping pressure rise rates in check.

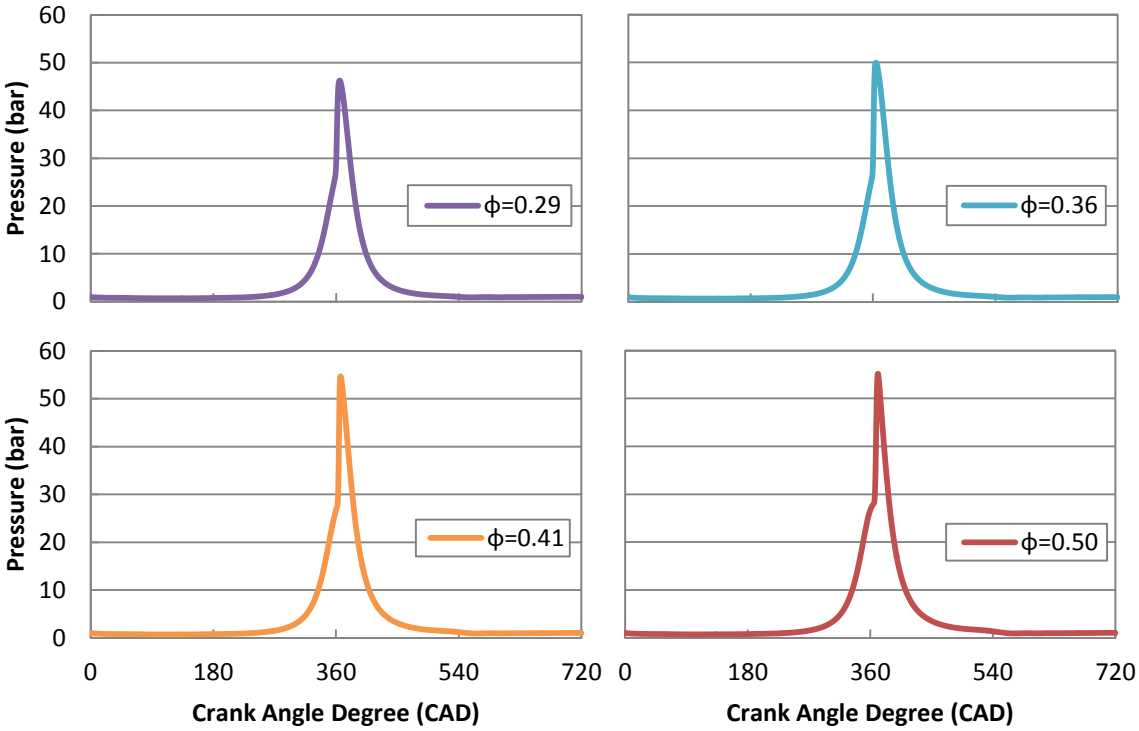

Figure 5.1. Steady state pressure traces for all engine loads

Figure 5.2 is a zoomed in version of the peak pressure, showing the 4 different loads. Here it can be seen that the higher loads are phased slightly later in the cycle. This is due to reaching a pressure rise rate (PRR) limit of 10 bar/CAD before ideal phasing could be reached, at TDC.

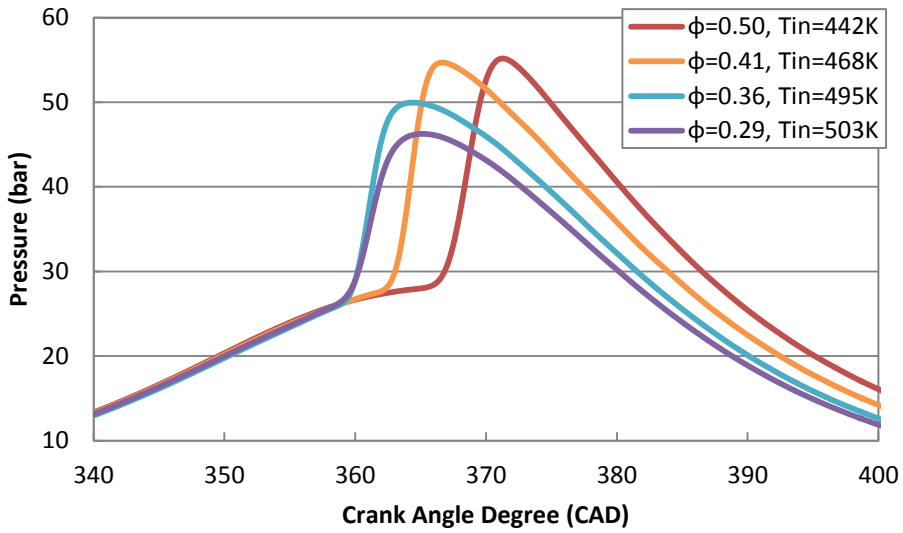

Figure 5.2. Pressure trace for steady state operating conditions

The PRR is defined as the rate at which the pressure increases on a crank angle resolved basis. HCCI combustion sees very high PRR's and even more so when the load is increased. The PRR's for each load are shown in Figure 5.3. It should be noted that the average PRR was kept under the 10 bar/ CAD limit, as to not harm the engines internal structure.

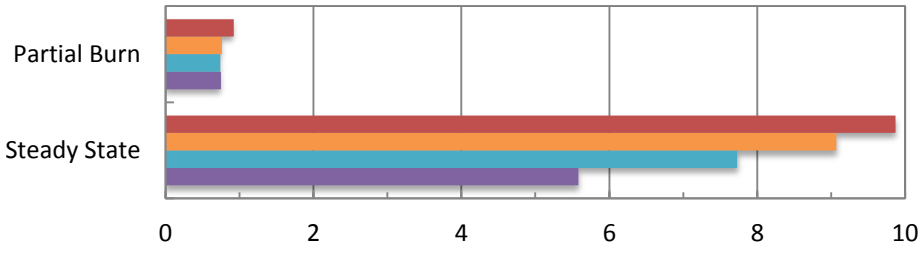

	Steady State	Partial Burn
0.50	9.87	0.92
0.41	9.07	0.76
0.36	7.73	0.74
0.29	5.58	0.75

Figure 5.3. Experimentally determined pressure rise rates

The partial burn regime pressure evolution appears as different due to the combustion phasing and location of this regime. Since combustion occurs very late in the cycle, the pressure trace will normally show the motored pressure crest when the engine reaches TDC at 360 CAD, then a small peak will appear after the pressure starts to decrease indicating combustion. The average CA50 in the partial burn regime is relative to the load and can be seen in Table 5.1 above. Again, with increased load the pressure curve is slightly higher due to the amount of energy released from that fuel/air charge.

The partial burn regime was reached by decreasing the intake temperature slowly until the engine started to show instabilities. These instabilities are noticeable audibly, and also through the real-time pressure trace, IMEP values, and in the monitored exhaust pressure at EVO. The engine was allowed to sit at a set point for approximately 10 minutes before reducing intake temperature again. Eventually the partial burn regime is reached and the collected data confirms the trends mentioned above. If the engine is pushed too far toward the misfire limit, there will be several consecutive cycles where combustion does not occur and the engine will then start to motor due to the lack of energy in the intake temperature to start the autoignition process. Figure 5.4 shows the partial burn pressure traces as they progress with equivalence ratio. Figure 5.5 is zoomed in on the pressure trace for all 4 loads.

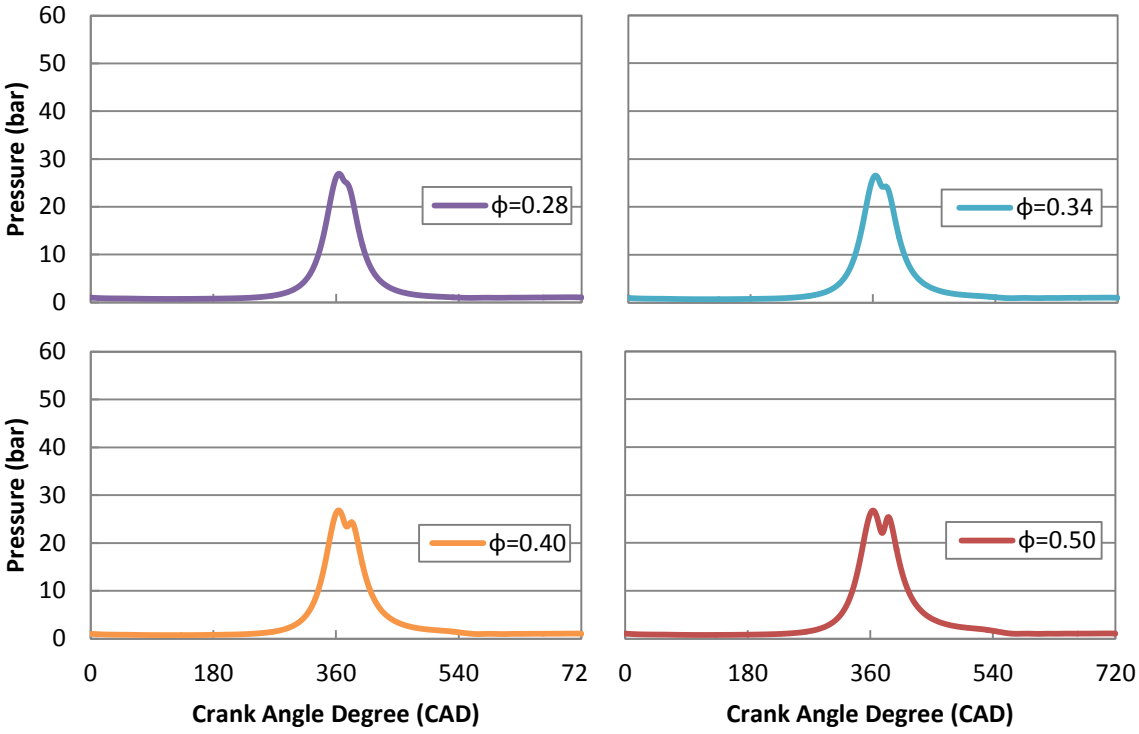

Figure 5.4. Partial burn pressure traces for all engine loads

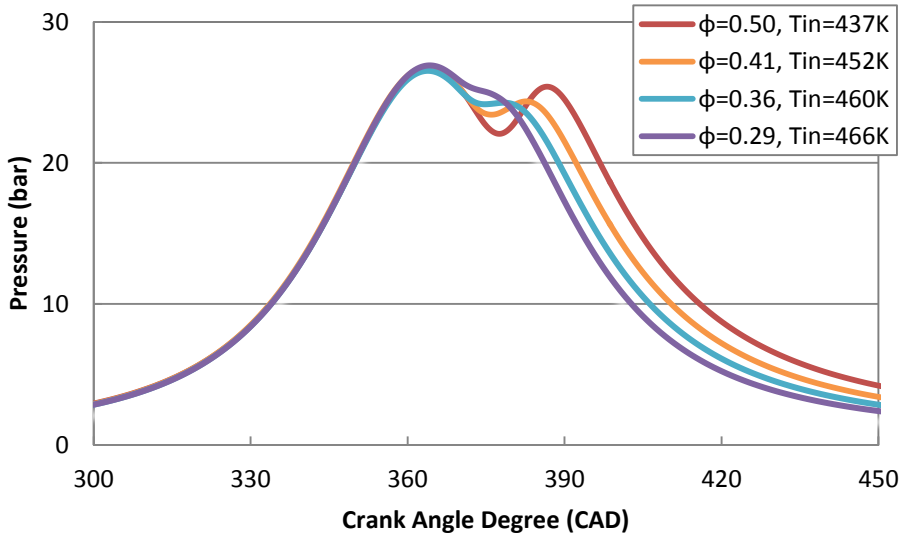

Figure 5.5. Pressure trace for partial burn regime

5.1.2. Heat Release and Heat Release Rates. The heat release of a combustion event is derived from the pressure evolution within the cylinder and the computations as outlined in §4.1.5. The heat release curve is representative of the sensible energy change and work that is transferred to the piston. The curve is normalized to give unity at is maximum value and is interpreted as the burned mass fraction versus the crank angle profile. This profile allows parameters such as SOC, defined as CA10 in this work, and CA50 to be determined. Figures 5.6 and 5.7 show the steady state and partial burn heat release curves for all 4 equivalence ratios, respectively. Heat release-rate or rate of heat release (RHR) is defined as the rate at which the chemical energy of the fuel is released by the combustion process.

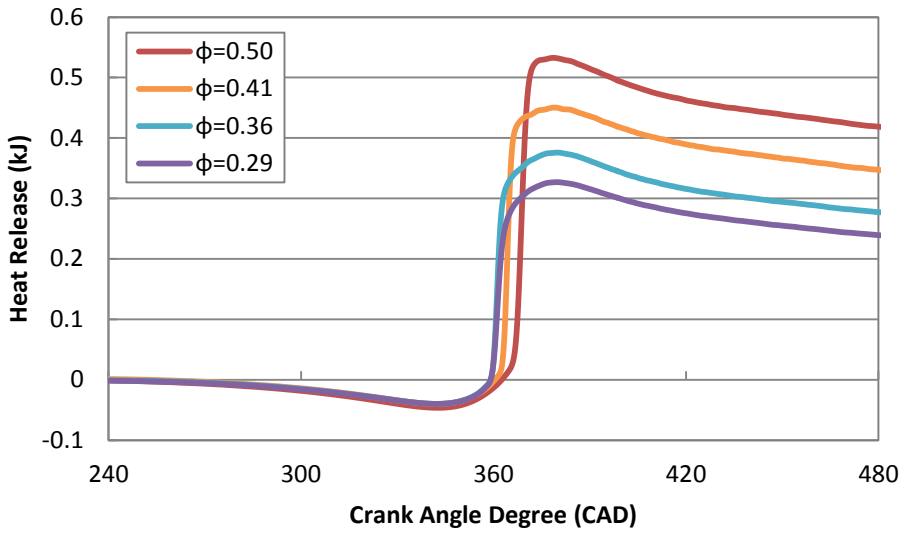

Figure 5.6. Cumulative heat release curve for steady state operating conditions

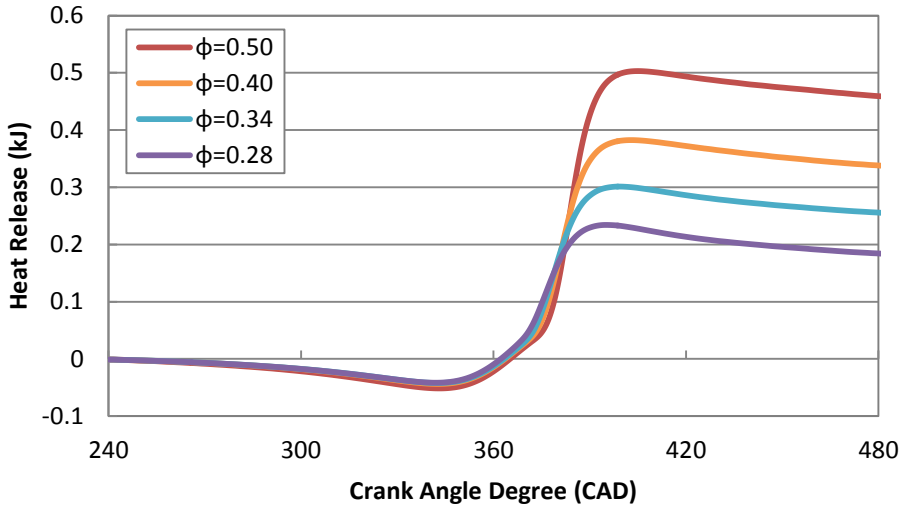

Figure 5.7. Cumulative heat release curve for partial burn regime

These figures show that the higher the equivalence ratio, the greater the fuel mass, the greater the chemical energy, and thus higher amounts of energy released per cycle. It can be seen that when the engine is operated in the partial burn regime, the heat release curves are not nearly as steep indicating a longer combustion event and hence larger burn durations. Figures 5.8 and 5.9 show the RHR for the steady state operating zone and the partial burn regimes, respectively.

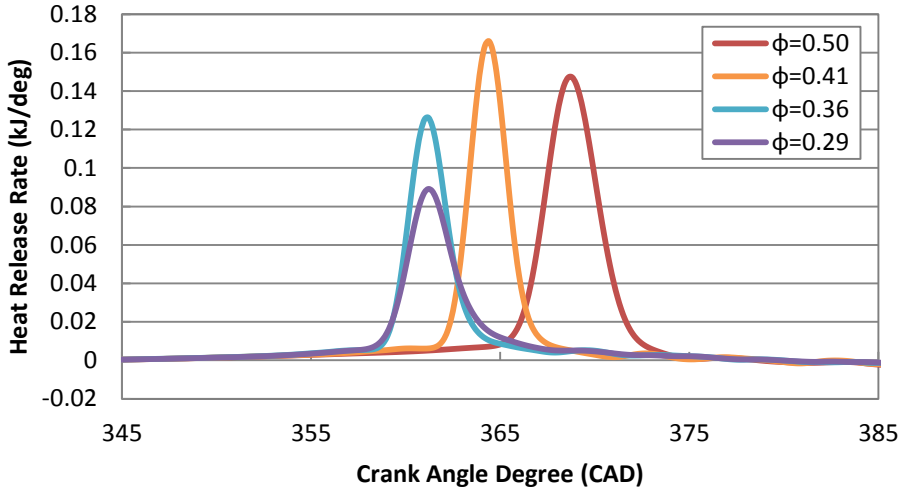

Figure 5.8. Rate of heat release for steady state operating conditions

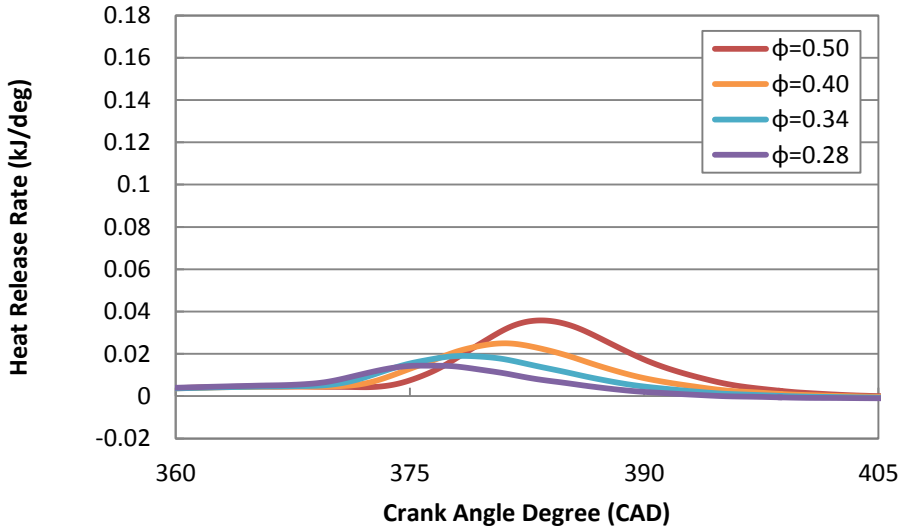

Figure 5.9. Rate of heat release for partial burn regime

It can be seen that in the partial burn regime the rate of heat released is significantly lower than when compared to the steady state set points. This is due to the late combustion timing of the autoignition event and the fact that the volume is increasing at a faster rate as the piston accelerates downward toward bottom dead center of the expansion stroke. This is indicative of partially consumed charges resulting in a lower IMEPg and significantly higher uHC emissions.

5.1.3. Capturing Cyclic Exhaust Temperatures. The FastTEMP fast response thermocouple is installed in the exhaust manifold and is utilized to capture cyclic exhaust temperatures for this study on the partial burn regime in HCCI combustion. The exhaust temperature was collected on a cyclic basis, in temporal form, and can be seen in Figure 5.10.

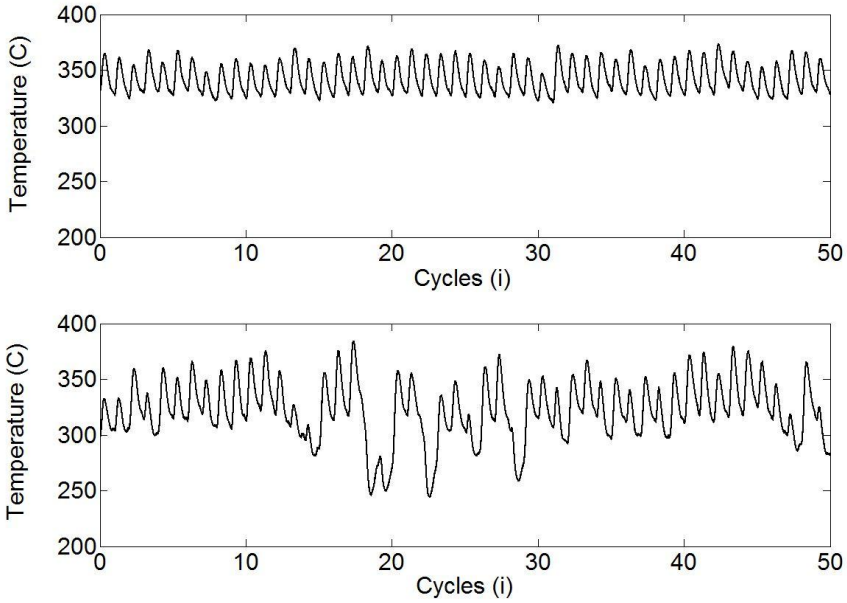

Figure 5.10. Experimentally measured cyclic exhaust temperatures
a. steady state b. partial burn regime (*φ=0.36, 0.34*)

Shown are exhaust temperatures for both the steady state and the partial burn cases. When combustion is phased early in the cycle, HCCI is a very stable form of combustion which is shown in the repeatable and stable exhaust temperatures measured at that set point. At the partial burn regime, however, combustion is very unstable and can result in misfired cycles as well as partially burned/consumed charges. These phenomena are seen through the captured cyclic exhaust temperatures. Figure 5.10b shows that when a partial burn combustion event happens, the time series temperature will decrease far below the time series temperature average of the complete fired cycles. This exhaust temperature is representative of the internally trapped residual temperature which is then carried over to the next cycle to mix with the newly inducted charge, affecting the new charge's thermodynamic state. These

plots show experimentally measured cyclic exhaust temperatures for 50 consecutive cycles at a fueling rate of 7.5 grams/min and an engine speed of 1800 rpm.

5.1.4. Exhaust Manifold Pressures. Recall that the internally trapped residual model used for this study, taken from [18], predicts the overall residual gas fraction as a combination of two mechanisms: the trapped gas in the cylinder at exhaust valve closing (EVC), and the contribution of back-flow from the exhaust to cylinder during valve overlap. The amount of residual trapped in the cylinder at EVC can be estimated fairly accurately with knowledge of the compression ratio. The flow processes during the valve overlap period, however, are very complex and are therefore difficult to model correctly. For most engine speeds, the cylinder contents equilibrate with the exhaust system during the exhaust stroke and are roughly at atmospheric pressure. The intake port, on the other hand, is generally below atmospheric pressure, which results in a net flow of burned gas into the cylinder from the exhaust manifold. Exhaust manifold pressure was measured for the baseline testing set points at both the steady state case and the partial burn regime for all engine loads and can be seen in Figures 5.11 and 5.12, respectively.

In Figure 5.11, near TDC compression, there are small pressure fluctuations seen in the exhaust manifold pressure. These fluctuations are a result of the combustion event occurring causing modal vibrations within the engine structure itself. Even more so, the intake valve actuation is also seen in the structure vibrations near 227 CAD. These vibrations are also observed in Figure 5.12 but they are not as significant. The

pressure rise, or blow down, is higher in the partial burn than in the steady state due to combustion occurring 20 CAD closer to EVO.

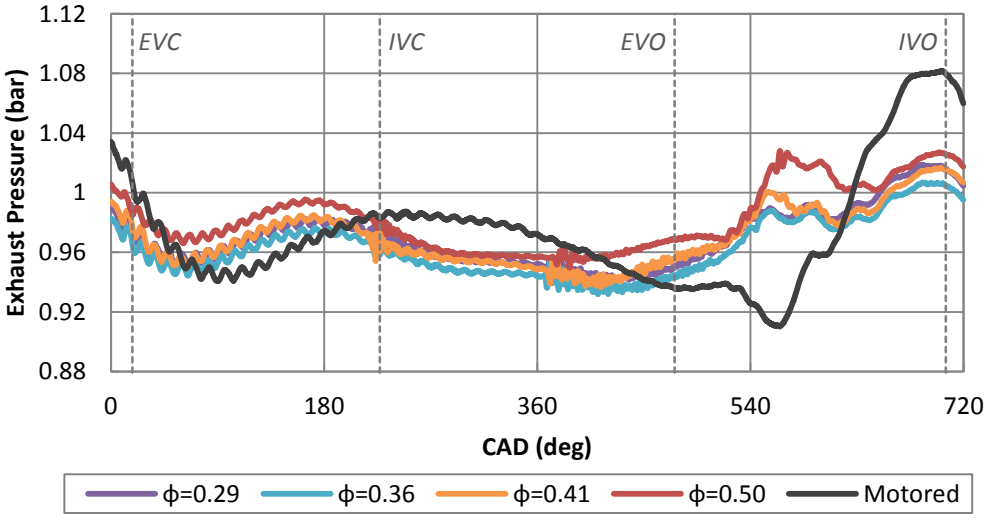

Figure 5.11. Exhaust manifold pressures for the steady state case

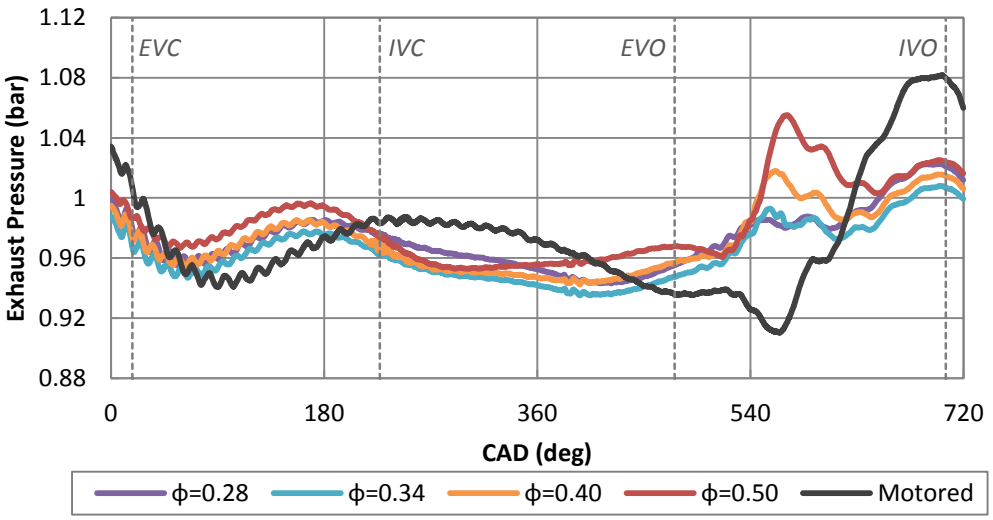

Figure 5.12. Exhaust manifold pressures for the partial burn regime

5.1.5. Baseline Return Maps. In order to understand the cyclic behavior of the engine at the different operating regimes, experimentally determined IMEPg return maps for 400 consecutive engine cycles at the steady state and 1000 cycles at the partial burn set points are plotted in Figure 5.13.

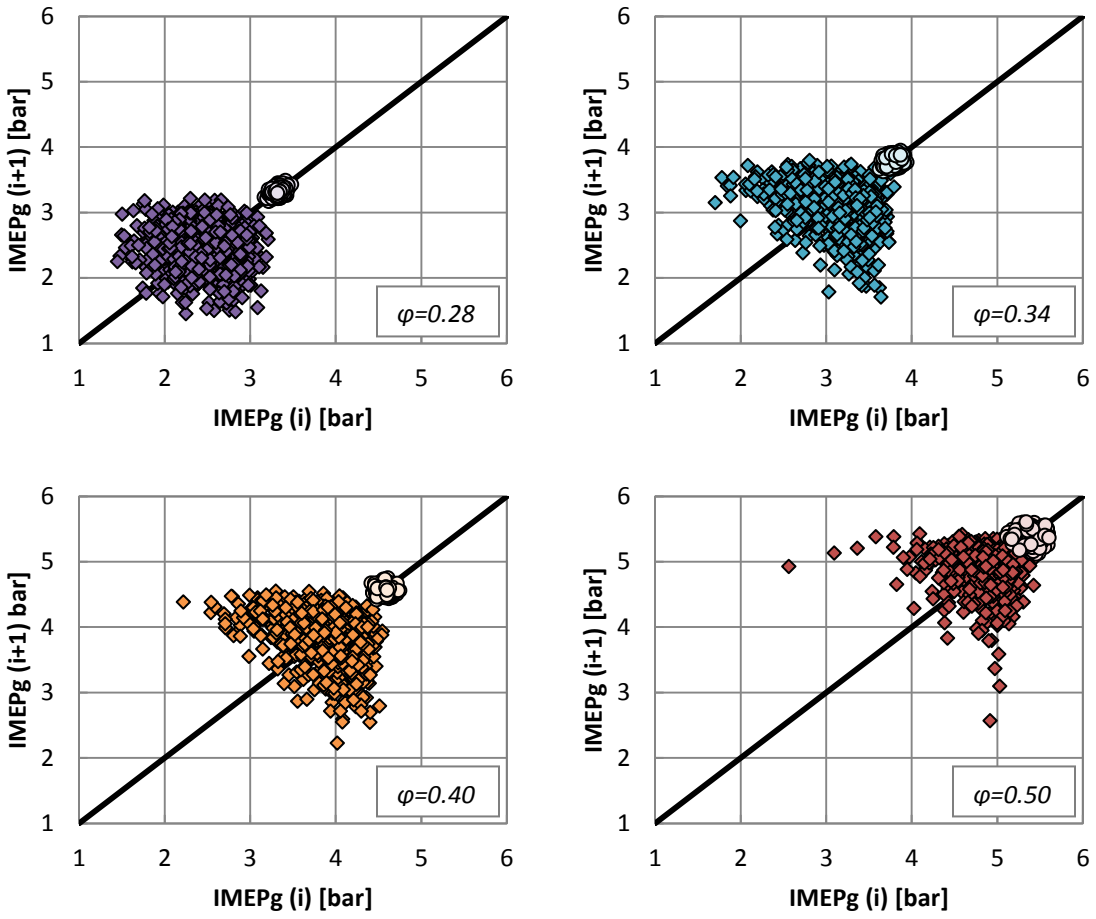

Figure 5.13. Indicated Mean Effective Pressure (gross) return maps for all engine loads

Here, one can see that the cyclic dynamics are stochastic in nature, which is a circular unstructured pattern, representing a Gaussian random distribution when combustion is phased close to TDC, or steady state having minimal cyclic variation.

However, as combustion is phased later in the cycle, the engine approaches the misfire limit and displays a different structure in the return maps. This is indicative of the engine operating in a partial burn regime, and some deterministic behavior is present. When investigating these four set points, it is observed that as load is increased, and hence exhaust temperatures increase, there is more structure in the IMEP return maps of the data. For this work CA10 (crank angle where 10% heat is released) will be used to determine SOC. The engine was run in the partial burn regime in order to observe the cycle-to-cycle dependence and a return map of CA10, for all engine load set points, is plotted and displayed in Figure 5.14.

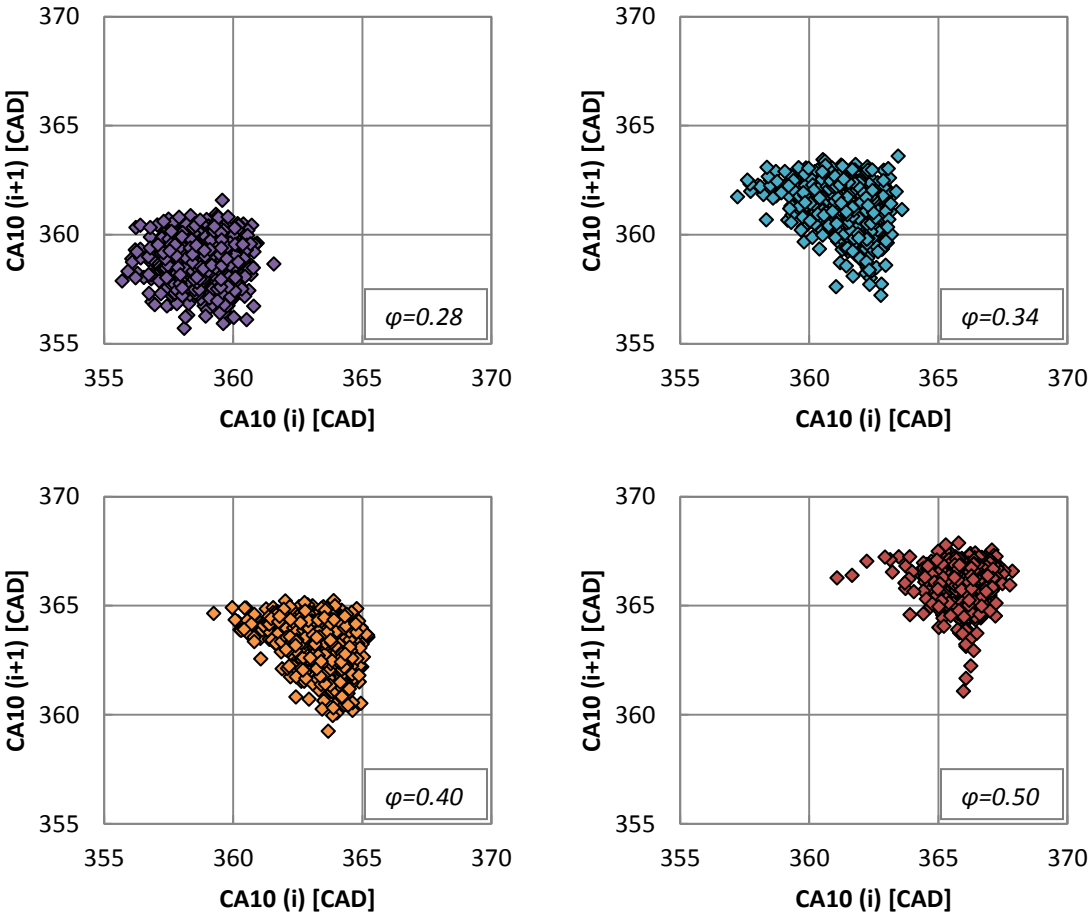

Figure 5.14. Start of combustion (CA10) return maps for all engine loads

These plots show some slight determinism between the current cycle and the next cycle through CA10. The correlation is not as strong in the lower load case, but more prominent in the higher load cases. Hence the current cycle is impacting the next cycle, through some phenomenon.

It is understood that the current cycle's start of combustion and energy release rate in the cylinder will affect that cycle's exhaust temperature. This is exactly what Figure 5.15 displays. There is a strong correlation between CA10 and the exhaust temperature for that cycle. It can be seen that as combustion is phased later in the cycle (later CA10), then the measured exhaust temperature increases. These higher temperatures of the exhaust gas residual will be carried over to the next cycle to mix with the freshly inducted charge anticipating an earlier SOC for the next cycle.

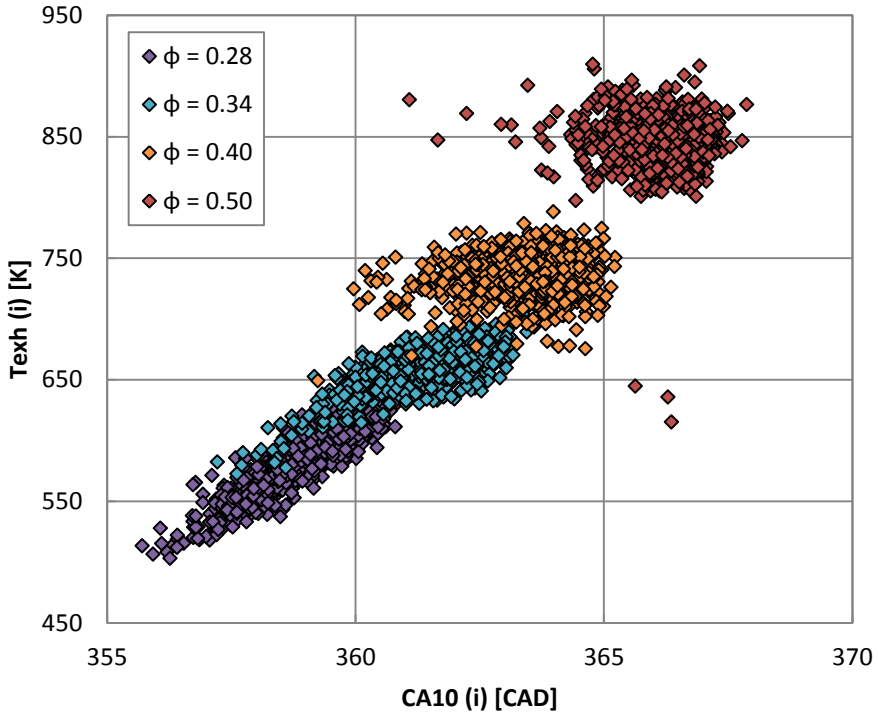

Figure 5.15. Effect of combustion phasing on cyclic exhaust temperature

There is a gap in the figure above due to a change in load. If the engine would have been run at an equivalence ratio of 0.45 then the linear trend would be more complete.

It was anticipated that hot residual gas from cycle i will mix with the fresh charge and elevate the temperature of the new charge, causing an earlier start of combustion for cycle i+1. A plot of the effect of exhaust temperature on CA10 (i+1) is displayed in Figure 5.16 in order to assess the cycle-to-cycle dependencies.

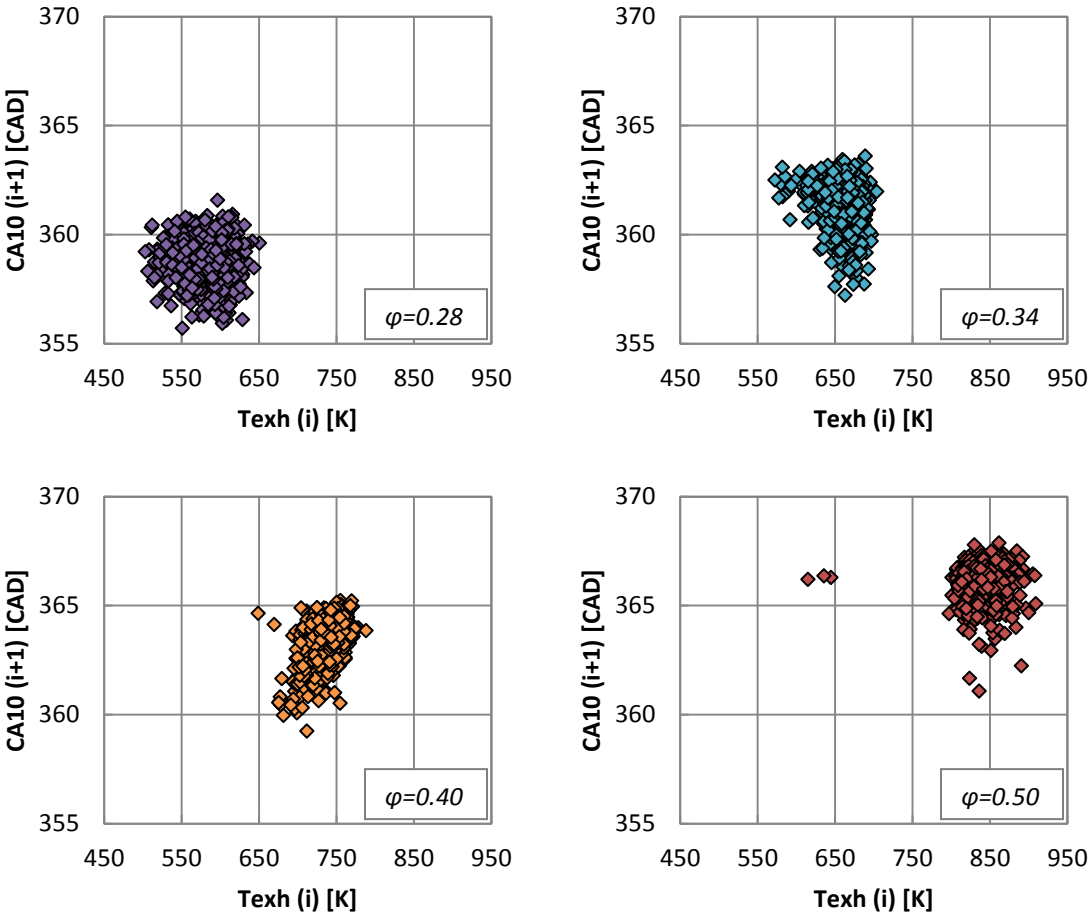

Figure 5.16. Exhaust temperatures correlation on next cycle's CA10

These results suggest limited correlation in the parameters plotted. Hence the residual temperature effect on the next cycle's start of combustion is not as strong as originally anticipated. This is an interesting result as exhaust gas residual not only changes the charge temperature, but also contributes to the reactant mixture composition. Hence, perhaps the compositional effect needs also to be considered in establishing cycle-to-cycle dependence.

5.2. INCREASED RESIDUAL AMOUNT

The internally trapped residual affects the next charge through reactant concentrations and charge temperature. The current work has shown that the temperature effect of the internal residuals does not have a strong effect on the start of combustion for the next cycle. To further investigate this phenomenon, the internally trapped residual amount was increased by increasing the exhaust manifold back pressure. By doing this, the residual gas fraction was increased by 30 percent. Table 5.2 and 5.3 compare the baseline exhaust test cases to the increased exhaust manifold pressure cases, respectively, for the different loads.

Table 5.2. Baseline exhaust pressure set points and residual amounts

Operating Regime	Fueling Rate (grams/min)	Equiv. Ratio (φ)	Exh. Temp (K)	Exh. Pressure (bar)	Residual Amount (%)
Steady State	*6.0*	*0.29*	*644*	*0.988*	*6.18*
Partial Burn	*6.0*	*0.28*	*584*	*0.987*	*6.32*
Steady State	*7.5*	*0.36*	*673*	*0.987*	*5.82*
Partial Burn	*7.5*	*0.34*	*662*	*0.987*	*5.50*
Steady State	*9.0*	*0.41*	*702*	*1.006*	*5.29*
Partial Burn	*9.0*	*0.40*	*736*	*1.003*	*4.87*
Steady State	*11.2*	*0.50*	*753*	*1.004*	*4.61*
Partial Burn	*11.2*	*0.50*	*844*	*1.008*	*4.18*

Table 5.3. Increased manifold pressure exhaust set points and residual amounts

Operating Regime	Fueling Rate (grams/min)	Equiv. Ratio (φ)	Exh. Temp (K)	Exh. Pressure (bar)	Residual Amount (%)
Steady State	*7.5*	*0.36*	*691*	*1.243*	*7.56*
Partial Burn	*7.5*	*0.34*	*647*	*1.247*	*7.21*
Steady State	*9.0*	*0.42*	*706*	*1.251*	*6.86*
Partial Burn	*9.0*	*0.40*	*732*	*1.265*	*6.25*
Steady State	*11.2*	*0.50*	*752*	*1.265*	*6.06*
Partial Burn	*11.2*	*0.50*	*806*	*1.285*	*5.67*

By studying the charts above, one can see that the exhaust pressure was indeed increased causing the residual amounts to increase by approximately 30 percent. The three highest loads were run in order to further study the effect on the cyclic dynamics since these were the test cases that were observed as having the most structure in the cyclic dynamics.

5.2.1. Increased Exhaust Manifold Pressure. The engine does not have an OEM exhaust gas residual recirculation valve. In order to increase the engines internally trapped residual amount, a gate valve was installed in line with the exhaust piping system as seen in Figure 3.3. This valve is then used to create more back pressure in the exhaust manifold, reducing the amount of residuals leaving the cylinder, and increasing the internal exhaust gas residual amount. Figure 5.17 is a plot of motored pressure traces comparing the standard operating back pressure used in the baseline tests to the increased exhaust manifold pressure case. The exhaust manifold pressure was also collected during the operating tests at steady state and at the partial burn regime. These plots are shown in Figures 5.18 and 5.19 respectively. The pressure dynamics are slightly different than the baseline tests shown in §5.1.4.

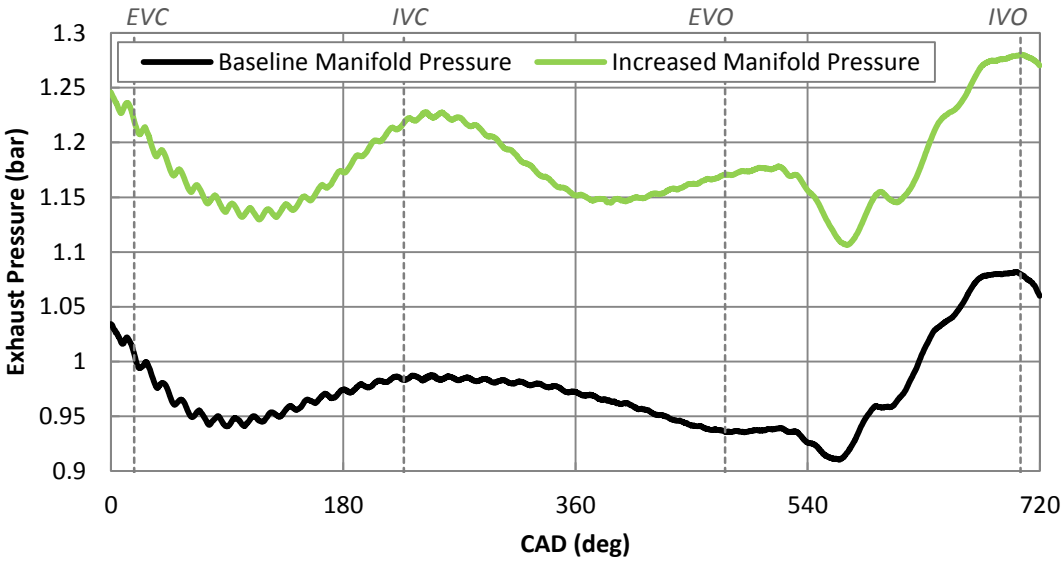

Figure 5.17. Motored exhaust manifold pressures - baseline and modified cases

Recall that the residual gas fraction is a combination of two mechanisms: the trapped gas in the cylinder at EVC, and the contribution of back-flow from the exhaust to cylinder during valve overlap. These exhaust gases, referred to as the internally trapped residuals, will mix with the fresh charge and cause fluctuations in engine performance.

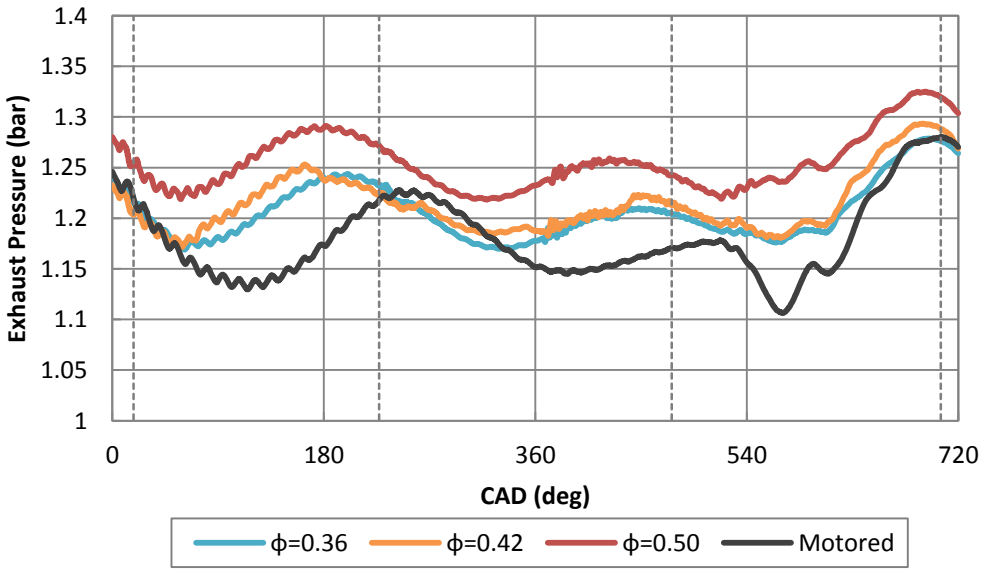

Figure 5.18. Increased exhaust manifold pressures for the steady state case

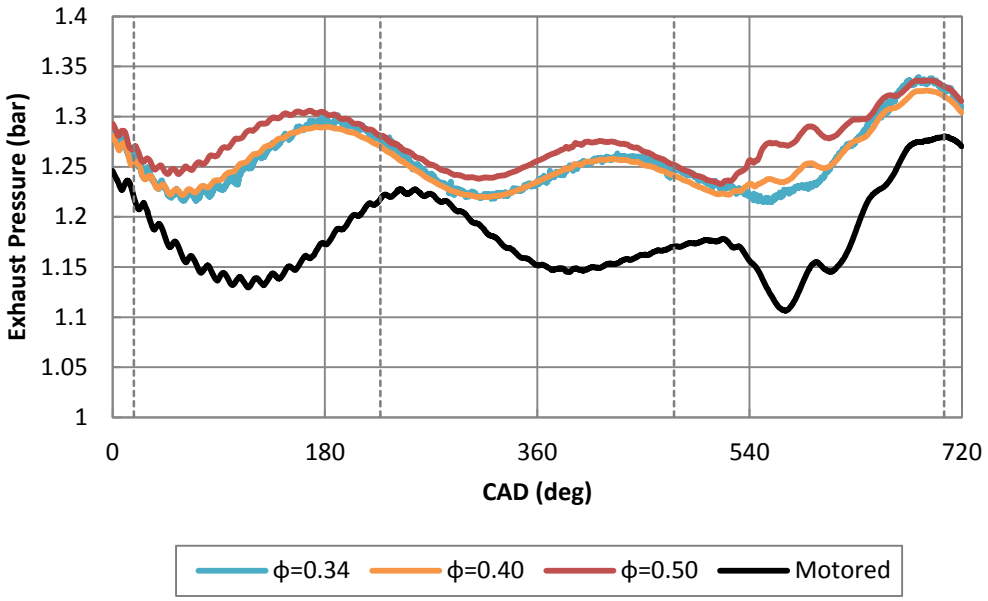

Figure 5.19. Increased exhaust manifold pressures for the partial burn regime

The pressure waves seen in the previous figures indicate slightly different exhaust pressure dynamics than when compared to the baseline tests. These pressure fluctuations are amplified due to the back pressure and occur after EVC, making them not of concern with respect to the internally trapped residual amount. The two smaller engine loads appear to operate similarly, however the highest engine load of ϕ=0.50 has a slightly higher pressure in the steady state case than compared to the partial burn. This could be partially due to the increase in exhaust temperatures that is seen at this set point.

5.2.2. General Engine Performance Results. The increased residual amount experiments are executed correspondingly to the baseline experiments. The engine operated just as the baseline tests, except it was able to sustain combustion longer in

the partial burn regime using the increased trapped residuals. The experimental test matrix used in this section is shown in Table 5.4.

Table 5.4. Increased Residuals Experimental Data Summary

Operating Regime	Intake Temp (K)	Equiv. Ratio (φ)	Fueling Rate (grams/min)	Engine Speed (rpm)	Avg. CA50 (CAD)	IMEPg (bar)	COV (%)
Steady State	*495*	*0.36*	*7.5*	*1800*	*361.0*	*3.74*	*1.31*
Partial Burn	*459*	*0.34*	*7.5*	*1800*	*378.1*	*2.70*	*19.07*
Steady State	*475*	*0.42*	*9.0*	*1800*	*363.2*	*4.27*	*1.44*
Partial Burn	*453*	*0.40*	*9.0*	*1800*	*381.3*	*3.30*	*17.45*
Steady State	*453*	*0.50*	*11.2*	*1800*	*366.4*	*4.87*	*1.69*
Partial Burn	*447*	*0.50*	*11.2*	*1800*	*382.0*	*4.16*	*9.97*

The set points were all run at the same engine speed of 1800 rpm as before. The intake temperature for these tests had to be increased approximately 10 degrees K in order to hit the same steady state operating point of 10 bar/CAD and phase combustion close to TDC. The partial burn regime intake temperatures are very similar to the baseline experiments. The engines work output, quantified by IMEPg, suffered when compared to the baseline tests as well. This is due to a greater dilution prior to induction of the fresh charge, so the fuel/air mass ratio is reduced, resulting in a lower IMEPg. The COV at steady state is in between 1-2% just as in the base line tests, indicating stable operating conditions; however in the partial burn regime the COV is significantly higher in comparison to the baseline partial burn tests indicating further instabilities in the engines work output. It was mentioned above that the engine was able to operate longer in the partial burn regime with the increased residual gas

fraction. This is shown by the increased COV values of these tests. The engine "stumbled" for longer in these tests due to the thermal and chemical energy leftover in the increased residual amounts. Recall that Table 5.3 presented the average exhaust temperature for these increased exhaust manifold experiments. The exhaust temperatures were significantly higher at these set points when compared to the baseline tests. This caused the cylinder walls to increase in temperature, allowing the engine to operate longer at this partial burn set point. The baseline tests however, lost combustion sooner due to the lack of energy (lower exhaust temperatures) for combustion to occur and thus lost combustion resulting in less of an operable time in the partial burn regime and lower COV values. In other words, a partial burned cycle in the increased residual gas fraction tests that sustained combustion longer might have been a complete misfire in the baseline tests due to lack of chemical and thermal energy. These set points are an averaged 400 consecutive engine cycles at the steady state and 1000 cycles at the partial burn regime.

5.2.3. Return Maps. Cyclic behavior of the engine at the different operating regimes is observed through experimentally determined return maps for 400 consecutive engine cycles at the steady state and 1000 cycles at the partial burn set points. The increase in back pressure allowed the engine to operate longer in the partial burn regime, causing large dispersion in the data as shown by the IMEPg return maps in Figure 5.20. When comparing these return maps to the baseline tests, it can be seen that the structure is not as strong for the increased residual gas fraction experiments. At

higher loads, the structure starts to become a little more defined however is still pretty dispersed in comparison.

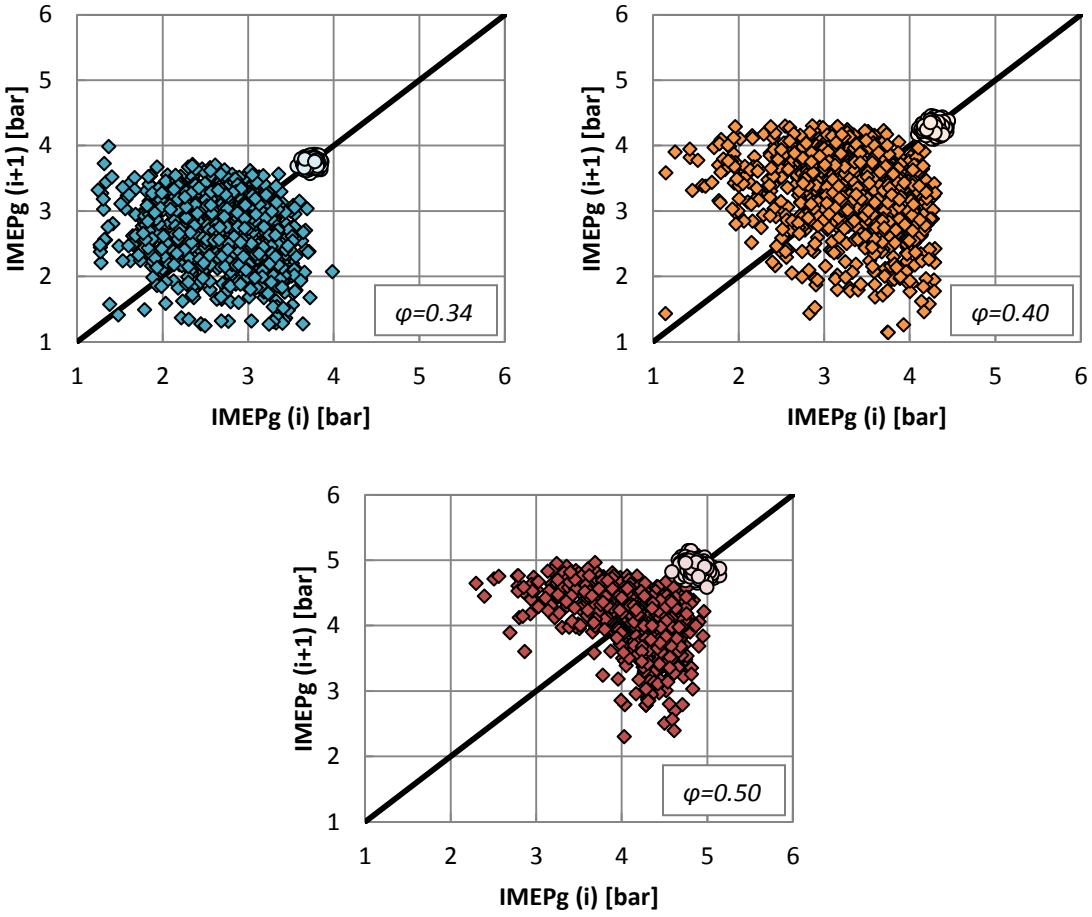

Figure 5.20. Increased residual gas fraction IMEPg return maps

Figure 5.21 displays the return maps for CA10 for cycle i versus cycle i+1. These plots show some slight determinism between the current cycle and the next cycle through CA10, however the dispersion of the data seen in IMEPg is reflected here in CA10. The correlation is not as strong in the lower load case, but more prominent in the higher load cases as seen in the baseline tests. This goes to say that cycle i is still affecting cycle i+1 by some phenomenon, and even more so at higher engine loads.

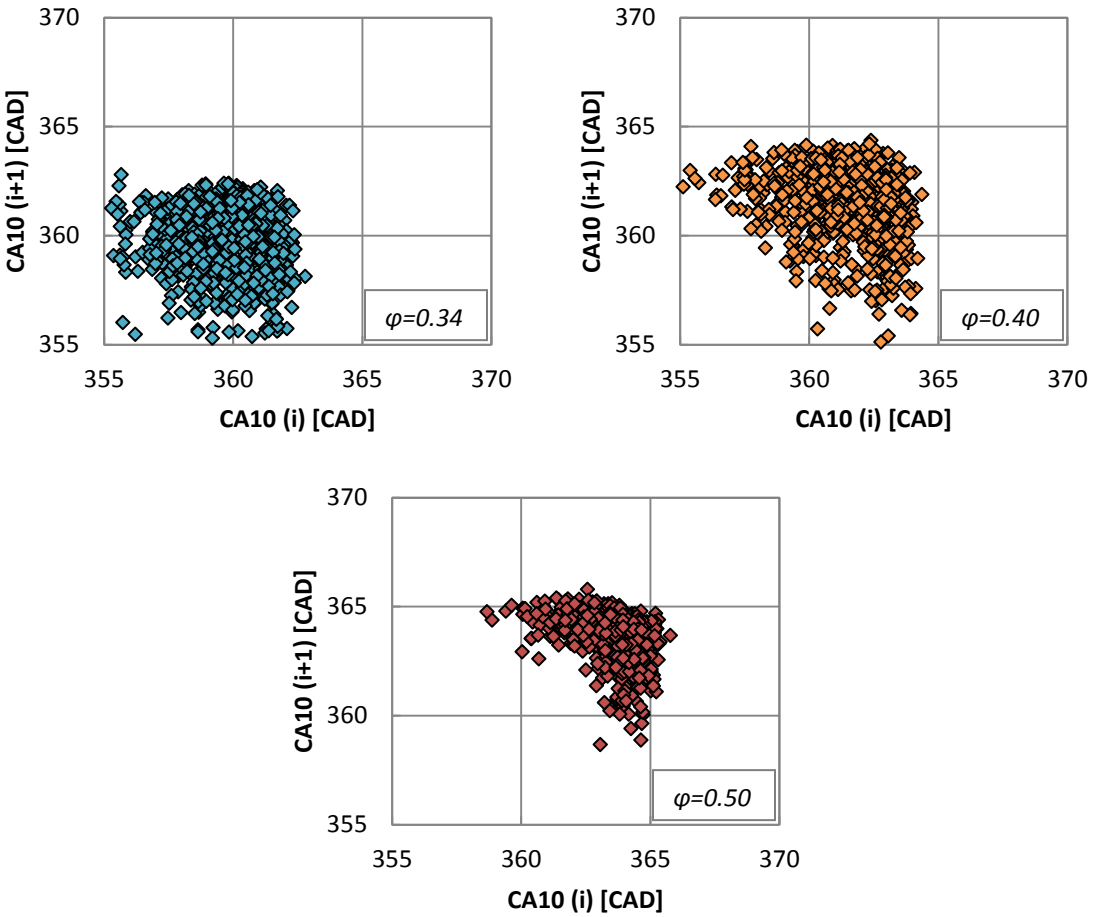

Figure 5.21. Increased residual gas fraction start of combustion (CA10) return maps

By increasing the residual gas fraction, and hence the thermal effects the residuals have on the fresh charge, one would expect a stronger correlation between the current cycle's start of combustion event and the previous cycle's exhaust temperature. However, this does not seem to be the case as Figure 5.22 plots the correlation between the previous cycle's exhaust temperature and the next cycle's CA10. These plots show that the HCCI start of combustion event once again is not near as dependent on temperature as originally conceived, and the higher load case that contains higher exhaust temperatures does not display any determinism, despite having

hot residual temperatures. This goes to say that the next cycle's combustion event is more dependent on the chemistry and composition of the residuals than the thermal effect of the residual gas fraction. This could be the reason that the middle load case, φ=0.40, has more structure than when compared to the baseline tests due to the residual gas fraction being increased by approximately 30% and operating in the partial burn regime could relate some unburned fuel through chemistry back to the fresh charge. Nonetheless, the case of φ=0.5 has the highest residual gas temperature and the weakest correlation.

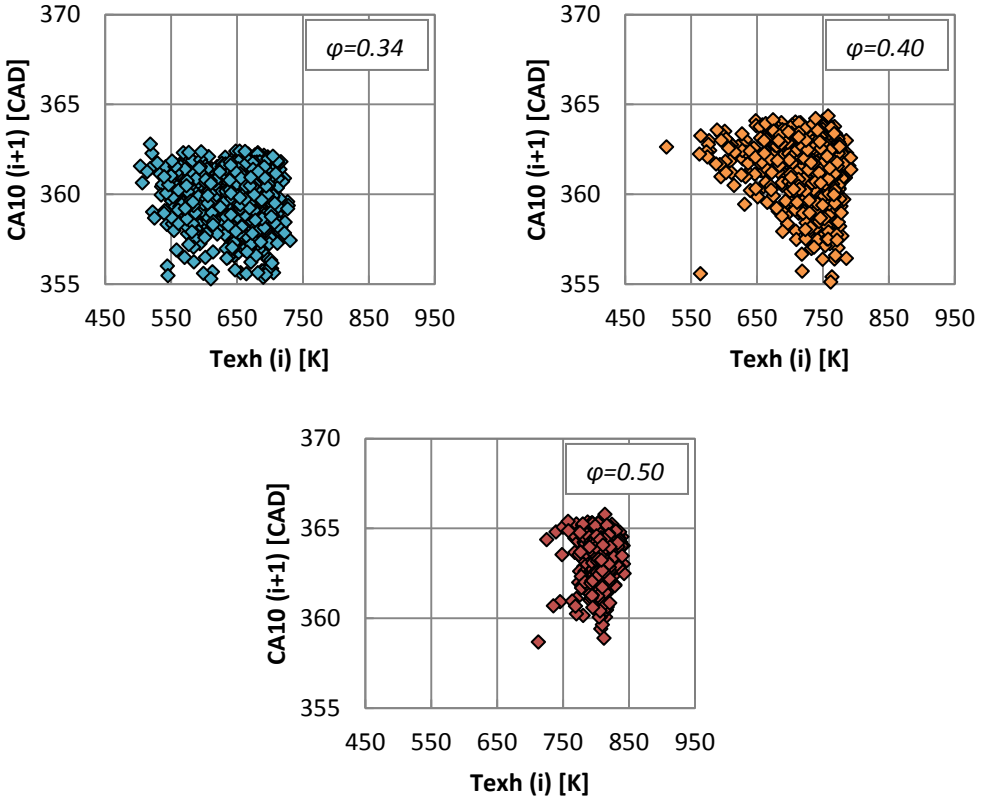

Figure 5.22. Increased residual gas fraction exhaust temperatures correlation on CA10

An interesting result of the increased exhaust manifold pressure, and hence the internally trapped residual gas fraction, is revealed in Figures 5.23 through 5.25. These

plots show that as the return map for the baseline test shows very stochastic behavior in the CA50 CAD location, the tests for the increased residual gas fraction display a very strong deterministic pattern. Also, when looking at SOC, both set points are combusting as the same relative time or location in CAD. Therefore, the increased exhaust residual amount is not affecting SOC; however it is affecting how the burn duration develops within the cylinder.

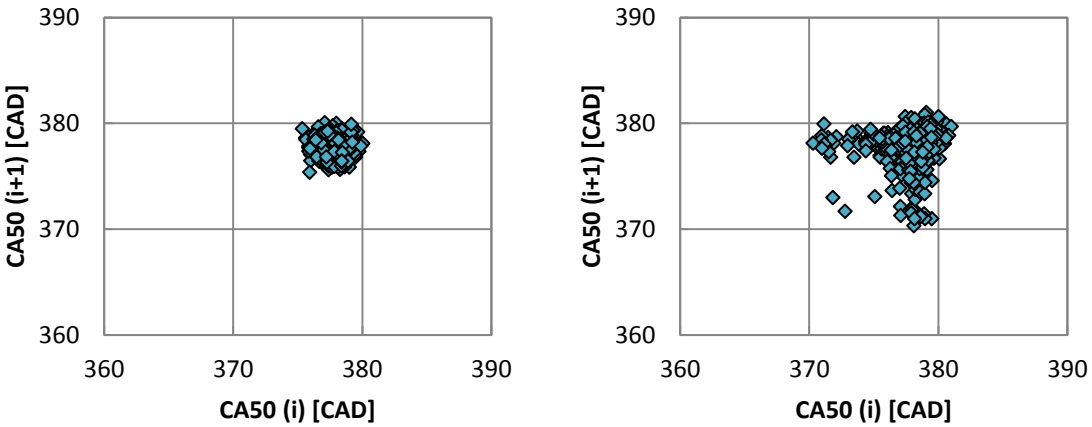

Figure 5.23. 50% heat release location (CA50) return maps for φ=0.34
a. baseline and b. increased residual gas fraction

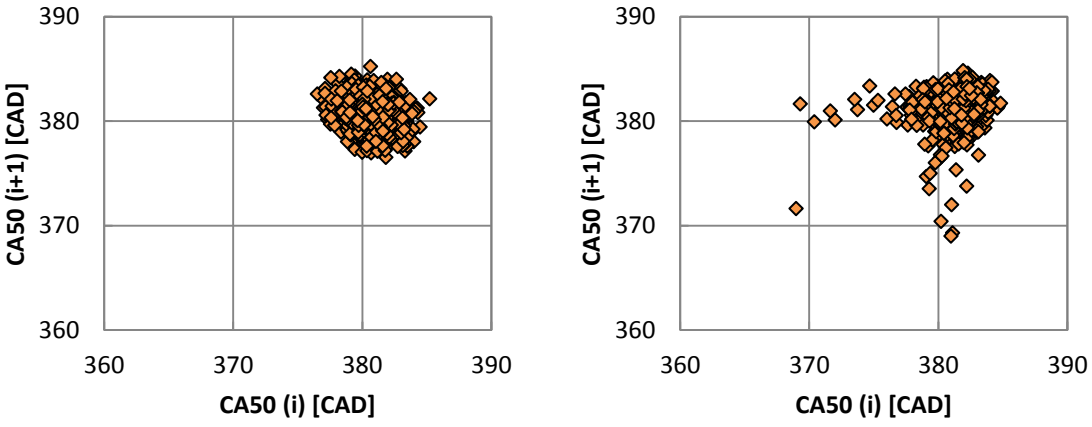

Figure 5.24. 50% heat release location (CA50) return maps for φ=0.40
a. baseline and b. increased residual gas fraction

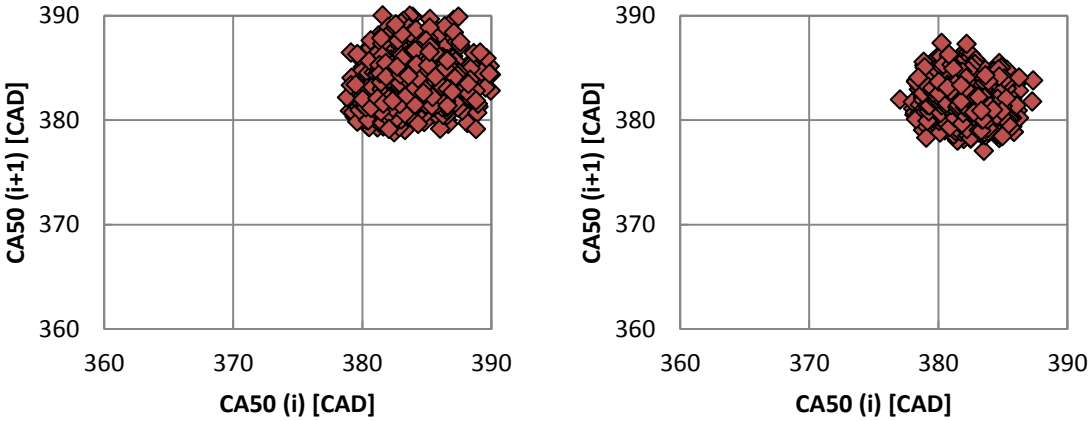

Figure 5.25. 50% heat release location (CA50) return maps for φ=0.50
a. baseline and b. increased residual gas fraction

6. MODEL DEVELOPMENT AND ADAPTATIONS

Initial work in Section 5 has shown that operation of HCCI combustion in a low pressure rise rate region (advantageous for engine NVH) pushes the engine close to a combustion misfire limit. Operating close to the misfire limit requires robust cycle-to-cycle control of ignition timing so as to not fall into unstable engine operation. In order to achieve such control, simple yet robust models of engine output are necessary as they can provide predictive capabilities to an engine electronic control unit. There are various techniques that could be considered (e.g. open loop control, closed loop linear control models, etc…) however for this work the focus is on controlling an HCCI engine using a non-linear thermodynamics based engine model in conjunction with a neural network (NN) closed loop controller. The advantage to the NN controller is the ability of such a controller to efficiently adapt to process perturbations. The advantage of a non-linear engine model is manifested in retention of certain non-linear system dynamics that are lost during linearization, e.g. linearization of a model for a given engine set point using a given fuel may require model recalibration when the fuel is changed. To this end, a non-linear thermodynamics based engine model for HCCI combustion has been developed [17]. The model has been shown to capture the general nominal time-averaged trends of the combustion behavior (quantified by peak cylinder pressure and 50% energy release location (CA50)) in an HCCI engine when parameters such as intake temperature or fueling rate are changed. The ability of the model to capture cycle-to-cycle combustion dynamics is yet to be considered. The following sections explore the

capability of such a model to predict these cycle-to-cycle dynamics regarding the operational partial burn regime of an HCCI engine.

For an HCCI engine, cyclic dynamics in measures such as temperature and species will result in next-cycle variations in energy release as well as combustion timing. Therefore, when considering the ability of a control model to capture the cycle-to-cycle dynamics of an HCCI engine it must be capable of qualitatively predicting both variations in ignition timing and engine work output to provide robust combustion control. Additionally, as will be discussed, the model should be capable of capturing some details of the residual temperature and composition effects.

6.1. ENGINE CONTROL MODEL

The model considered in this study is the non-linear thermodynamics based control model described in [17]. This model is a five state thermodynamic model which has been developed to be utilized in a NN type control scheme for cycle-by-cycle control of an HCCI engine. A pressure trace of this model is shown in Figure 6.1. The onset of combustion is modeled using an Arrhenius reaction rate expression which relates the combustion timing to both charge dilution and temperature. To account for the finite amount of time required for combustion to occur, a $\Delta\theta$ term is added within the model which shifts the point of instantaneous combustion from SOC to a point of very high energy release based on experimental heat release data. Additionally, the effect of internally trapped exhaust gas residuals on the next cycle's temperature and composition are also included. The model has been validated against experimental data from a single cylinder CI engine operating under HCCI conditions at two different fueling

rates. Parameters relevant to control such as combustion timing, peak in-cylinder pressure, pressure rise rates and work output from simulation agree very well with the experiment at both operating conditions. Since this nonlinear model is developed from a controls perspective, both the output and state update equations are formulated such that they are functions of only the control inputs and state variables, therefore making them directly applicable to state space methods for control. The result is a discrete-time nonlinear control model which provides a platform for developing and validating various nonlinear control strategies. For more detailed information on the model and validation see reference [17].

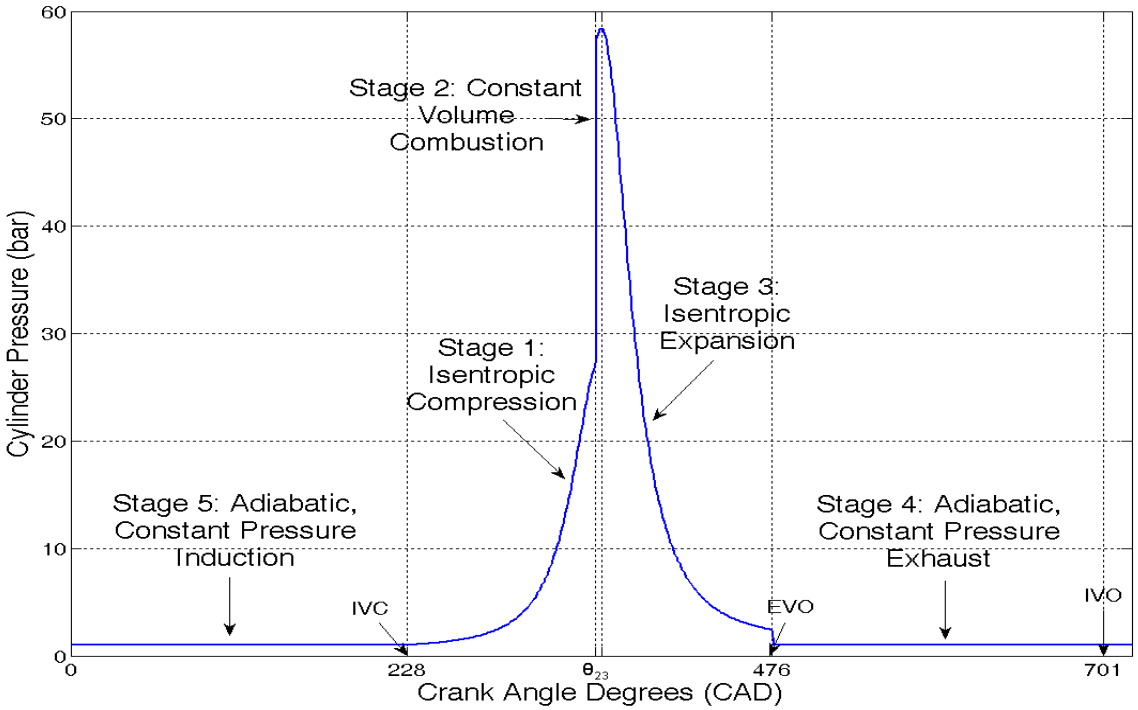

Figure 6.1. HCCI pressure evolution modeled as 5 discrete thermodynamic states

Note, the experimental engine does not incorporate EGR at this time thus the only effect the combustion products from a previous cycle will have in the current cycle's combustion event are through internally trapped exhaust residuals. All model results in this thesis do not include external EGR effects. The focus is on determining the ability that the simple five-state thermodynamics non-linear control model has in capturing the cyclic variations and elucidating the competing effects of trapped residual temperature and composition.

6.2. GENERAL MODEL COMPARISIONS

In order to understand the cyclic behavior of the engine at different operating regimes, the equivalence ratio (φ) was varied by adjusting fueling rate specified in grams per minute (gpm), in order to initially assess the ability of the model to capture changes in cyclic variation with engine load. Additionally, the intake air temperature (T_{IVC}) is varied to ascertain the ability of the model to capture cyclic variation due to combustion phasing at each φ. Three different engine speeds at these loads were chosen to represent the operating regime of the experimental engine (1800 rpm, 2200 rpm, and 2600 rpm). The higher fueling rates were used at the higher engine speeds in order to maintain a constant equivalence ratio due to the higher amount of air inducted into the cylinder. The experimental testing matrix used in this study is shown in Table 6.1. The fuel used is an unleaded test gasoline with a research octane number of 96 (UTG96). This fuel is chosen since the model was originally calibrated with this fuel's properties.

Table 6.1. Experimental set points for model development

Engine Speed (rpm)	CA50 (CAD ATDC Compression)	Intake Temperature (K)	Fueling Rate (gpm)	Equivalence Ratio (φ)	IMEPg (bar)	COV (%)
1800	-3.1	493	7.7	0.37	2.54	1.98
1800	16.6	465	7.7	0.35	2.31	11.89
2200	-3.4	518	7.7	0.33	2.15	2.98
2200	14.8	480	7.7	0.31	1.74	14.33
2600	0.1	516	7.7	0.29	1.79	3.86
2600	15.8	493	7.7	0.28	0.97	27.55
1800	0.4	473	9	0.43	3.11	1.88
1800	20.8	455	9	0.42	2.68	14.78
2200	-3.0	503	9	0.39	2.42	2.10
2200	13.7	473	9	0.36	2.47	5.44
2600	-2.6	517	9	0.35	2.10	2.80
2600	14.4	485	9	0.33	1.77	10.80
2600	-1.6	498	11.2	0.43	2.45	2.29
2600	12.3	475	11.2	0.41	2.55	3.51

**Same Equivalence Ratio*

To observe the cycle-to-cycle dynamics at these different engine set points, experimentally determined IMEPg return maps for 1000 consecutive cycles are plotted and shown in Figure 6.2. The cyclic dynamics show a circular unstructured pattern representing a Gaussian random distribution for the combustion phasing's close to TDC. However, when the engine is operated near the partial burn limit, that is a late combustion timing (CA50 = 20.8 ATDC), then a different structure is observed. This indicates that near the partial burn limit some deterministic behavior is present. Figure 6.3 compares how the model performs at these set points.

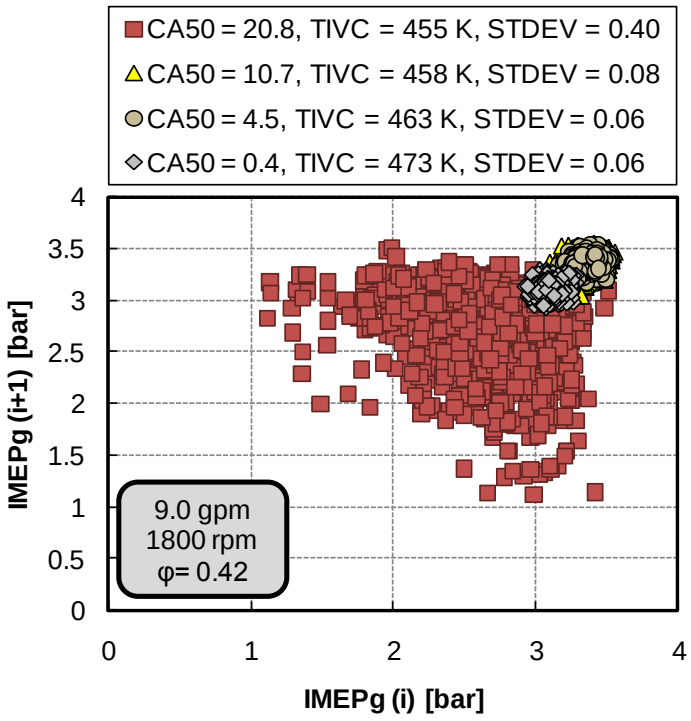

Figure 6.2. Experimentally determined IMEPg return map, 1800 rpm

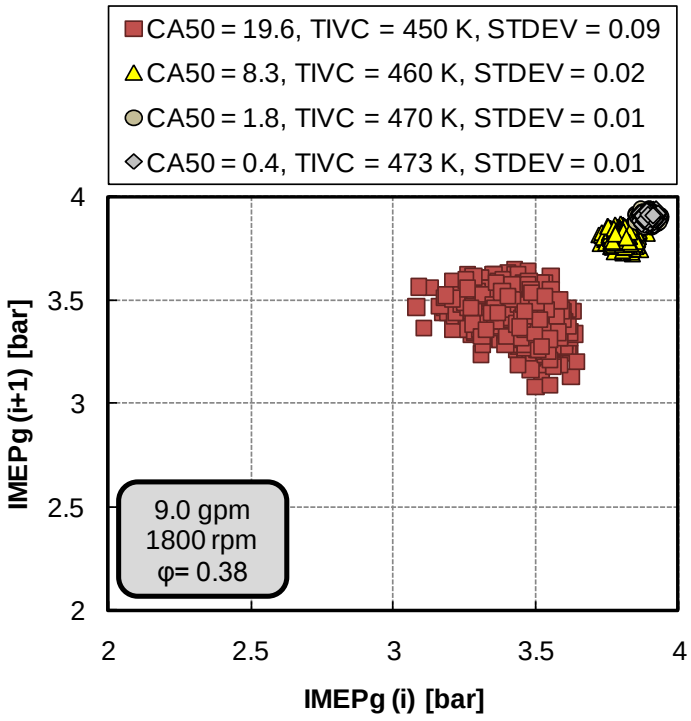

Figure 6.3. Model derived IMEPg return map, 1800 rpm

A simulation using the non-linear control model was run with the same T_{IVC}, fueling rate, and ϕ as the experiment. These results are shown in Figure 6.3. Indeed clear deterministic behavior in the partial burn regime is captured by the model. Note the IMEPg values from the model will be higher due to the idealistic assumptions made in the model, see reference [17].

In an effort to simulate more realistic variations, Gaussian random perturbations are added to the intake temperature and fueling rate based on the estimated experimental system's uncertainty in these variables. By comparing the experimental CA50 location to the model's CA50, it can be seen the model predicts an advanced combustion timing when compared to the experimental results for an equivalent T_{IVC}. This can be accounted for by adjusting the Arrhenius Reaction Rate threshold in the model, however, leaving this threshold equivalent to its original value is advantageous for assessing the capability of the model to apply across different engine platforms.

It should be noted here that the transition from a stable combustion operating point to the partial burn regime is quick. The model was also compared to a higher engine speed test case. These set points were also run at a high T_{IVC}, giving an earlier combustion timing as well as a lower T_{IVC} to phase the engine into the partial burn regime. These set points can be seen, experimentally and run in the model, in Figures 6.4 and 6.5, respectively.

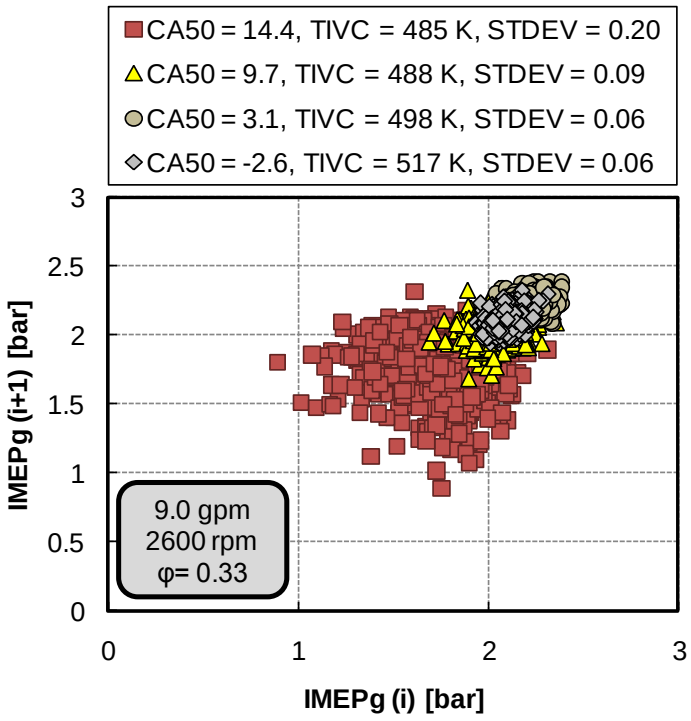

Figure 6.4. Experimentally determined IMEPg return map, 2600 rpm

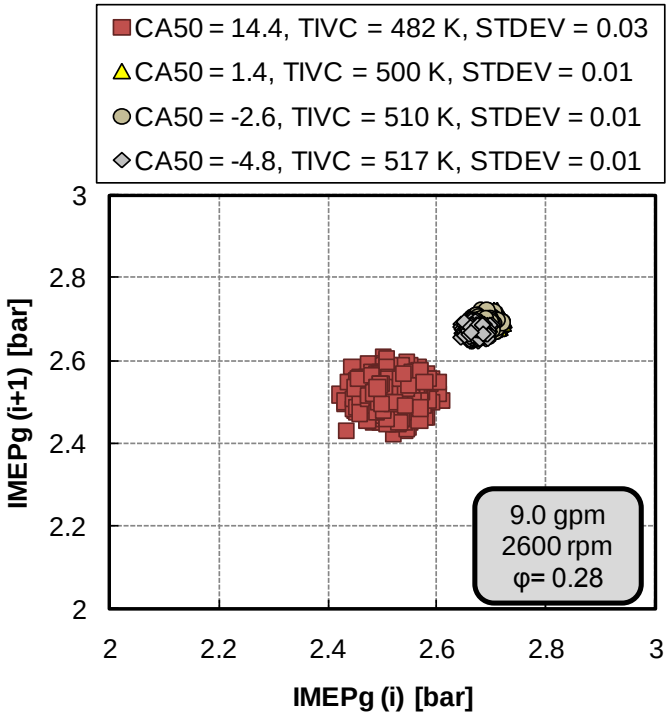

Figure 6.5. Model derived IMEPg return map, 2600 rpm

The experimental results indicate a more stochastic behavior at the partial burn limit for the higher engine speed of 2600 rpm. The model also predicts this stochastic behavior at the same combustion timing (CA50 = 14.4 ATDC). Although the amount of variation is different, the model is qualitatively predicting the behavior of the cyclic dynamics.

Since IMEPg varies from steady operating points to partial burn cases, it would be beneficial to use the entire experimentally determined data set and view the standard deviations of the IMEPg, as seen in Figure 6.6.

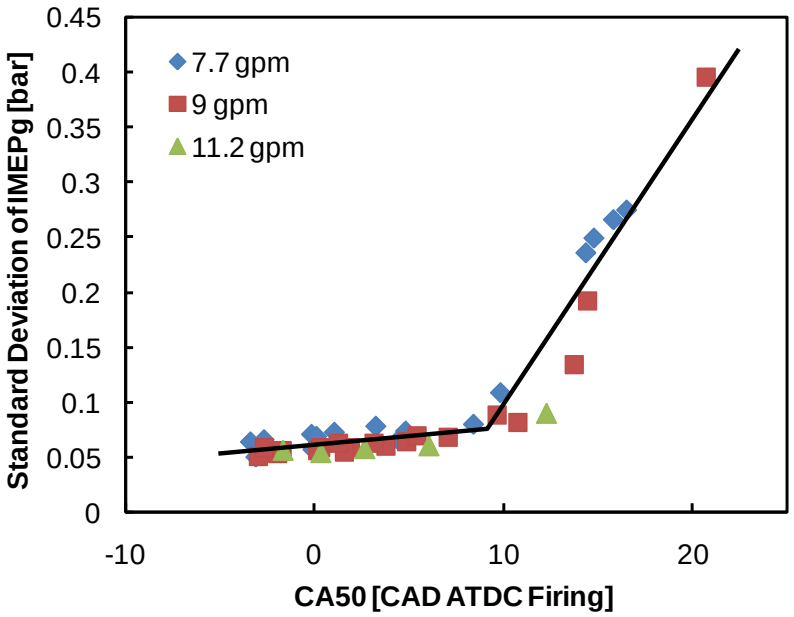

Figure 6.6. Standard deviation of experimentally determined IMEPg

This data set includes three different fueling rates, as seen in Figure 6.6 legend, and three different engine speeds (1800 rpm, 2200 rpm, and 2600 rpm). The standard deviation in IMEPg appears consistent as long as the engine operates near TDC. It can be seen that variation in work output (IMEPg) is a strong function of combustion phasing.

The variation in work output appears to be linear but changes slope after CA50 = 10 CAD ATDC which is a transition into a partial burn/misfire regime. In the partial burn regime, the fuel/air mixture is only "partially consumed", hence the name partial burn regime. If the inducted fuel is not fully oxidized then one would expect to see an increase in unburned hydrocarbons (uHC's). Indeed, as shown by Figure 6.7, the engine does in fact transition into this partial burn regime as indicated by the uHC's.

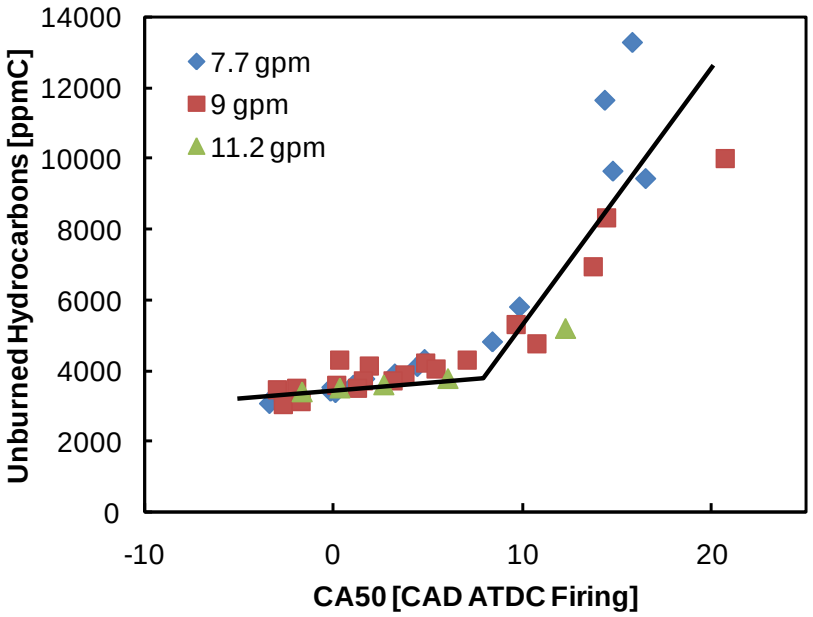

Figure 6.7. Measured uHC's of experimental set points

Figure 6.7 also includes 3 fueling rates, as indicated by the legend, and 3 different engine speeds. Consequently, the transition into a partial burn regime is governed more by combustion phasing rather than engine speed or equivalence ratio. The model must then be able to capture these trends that are seen once combustion enters into this partial burn regime, as defined by 10 degrees ATDC, or 370 CADs. The

misfire limit is when combustion does not occur and none of the fuel is consumed, causing the residuals for that cycle to be comprised completely of unburned fuel. This limit is set at 20 degrees ATDC, or 380 CADs. This is chosen as the engine experimentally has been found to lose combustion at or slightly before this location.

6.3. MODELING THE UNBURNED RESIDUAL

Recall that HCCI combustion is governed by two main parameters: the concentrations of fuel and oxygen, and the temperature. This means that changing the concentration and/or the temperature of the intake charge will cause the combustion phasing to change. The fact that the residual gas fraction directly affects both the reactant concentrations and the temperature, makes it an important parameter when trying to model combustion timing in an HCCI engine. Therefore, a practical and accurate model for predicting the residual gas fraction α_r is needed in order to accurately predict the combustion timing.

The predictive model used was taken from [18]. This model predicts the overall residual gas fraction as a combination of two components: the contribution of back-flow from the exhaust to the cylinder during valve overlap, and the trapped gas in the cylinder at exhaust valve closing. This back-flow contributes significantly to the residual gas fraction for each engine cycle. Recall that the parameter often used to describe this back-flow is the valve overlap factor (OF) [34] and is shown in Equation 24 in §4.3. Once the overlap factor, OF, is known, an expression for the overall residual gas fraction can be determined. The empirical expression from [18] is also given in in §4.3 as Equation 25. This resulting model relates the residual gas fraction to six independent parameters:

engine speed (N), inlet and exhaust pressures (P_i and P_e), the valve overlap factor (OF), inlet temperature (T_i), and the compression ratio (r_c). This expression explicitly accounts for the contributions from both the back-flow of exhaust gas into the cylinder during the valve overlap period and the gas trapped in the cylinder at exhaust valve closing. The sum of these two components gives the total predicted residual. The model correlated well with experiment over a wide range of intake pressures and engine speeds [18], which means that it should provide a fairly accurate prediction of the residual gas fraction.

The overall exhaust residual fraction, α_r, is computed using the model discussed above [18]. The changes made to the 5-state thermodynamic engine model include how the total residual, α_{tot}, is modeled. The new changes, and thus the new residual model, utilizes a linear scaling of the previous cycle's reactants mole fractions between two crank angle limits to determine the burned, α_i, and unburned, α_{ub}, exhaust residual amounts of α_{tot} as seen in Figure 6.8.

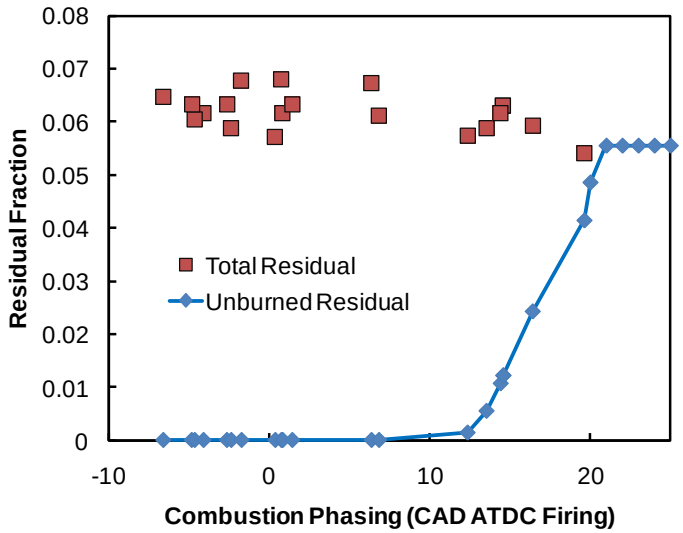

Figure 6.8. Residual components including burned/unburned residuals from the model

The limits are defined as the crank angle degree at which an initial partial burn limit is seen, CA_{PB}, and a complete misfire limit that is observed, CA_{MF}. The choice of CA_{PB} and CA_{MF} will effectively set the lean combustion limits of the model. The crank angle limits represent the onset of partial burn and misfire as discussed at the end of the previous section and are set to 370 and 380, respectively. The unburned residual fraction, α_{ub}, is scaled linearly proportional to the exhaust residual fraction, α_i, based on the following relationships:

$$\alpha_{ub}=\begin{cases} 0, & \text{Peak P}\leq CA_{PB} \\ \alpha_i\times\left[1-\dfrac{CA_{PB}\text{-Peak P}}{CA_{MF}\text{-}CA_{PB}}\right], & CA_{PB}<\text{Peak P}<CA_{MF} \\ \alpha_i, & \text{Peak P}\geq CA_{MF} \end{cases} \tag{26}$$

The residual temperature is computed by scaling the exhaust temperature by a residual heat transfer factor, X. Composition effects of the residual are captured through the thermodynamic properties of the mixture, specifically through the specific heat capacity of the residual. Note the inclusion of α_{ub} impacts the fuel and air in the reactants considered during computation for ignition while α_i influences only the amount of oxidizer present for combustion. The composition effect of including α_{ub} is through the specific heat capacity of high temperature unburned reactants and not from properties of individual chemical species. Other than the inclusion of unburned reactants, the model always assumes complete combustion products with excess oxygen.

6.4. UNBURNED RESIDUAL RESULTS

The ability of the model to capture the changes in uHC's concentration is manifested in the unburned residual model developed in §6.2. This unburned residual model varies linearly with combustion phasing and is scaled by the concentrations of the previous cycle's reactants. Recall that the model is constructed such that for an early combustion timing, CA50 near TDC, the total residual is made completely up of burned residual. This is the model assuming complete combustion. Once the phasing reaches the partial burn limit of 370 CAD, then the total residual is now comprised of partially burned and partially unburned residual as shown above in Figure 6.8. Figure 6.9 shows the models trend in variation of work output, while Figure 6.10 shows the trend in unburned hydrocarbons.

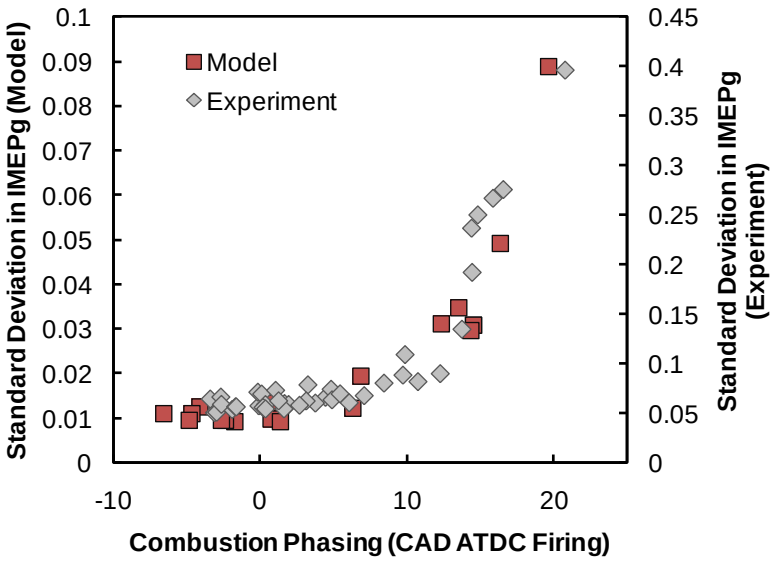

Figure 6.9. Standard deviation of models IMEPg compared to experiment

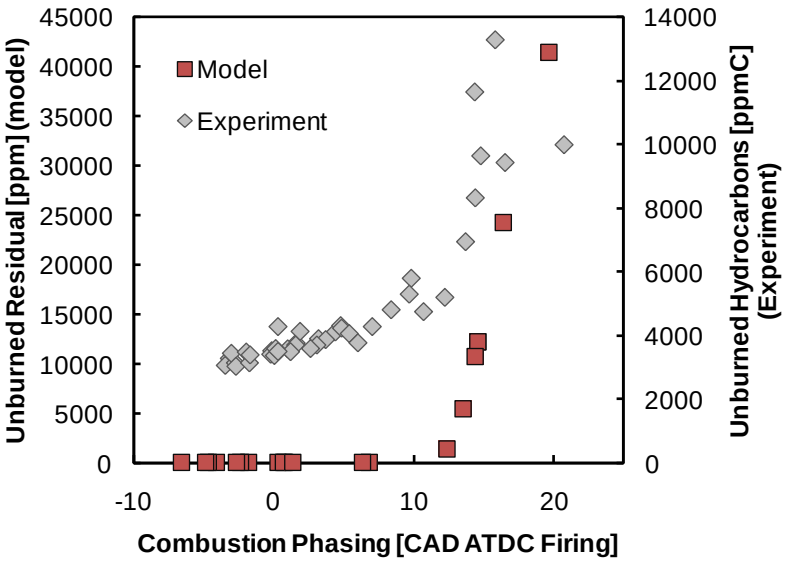

Figure 6.10. Modeled uHC's compared to experiment

Figure 6.9 shows that the model clearly captures the trend seen in variation of work output. These test cases also include varying engine speed and fueling rate. Even though the magnitudes of the values in the model are not quantitatively accurate, correctly predicting this trend is all that is required in order for the control model to be able to effectively control the combustion phasing, and hence efficiency. Since the uHC's increase in the experiment, the level of uHC's in the exhaust gas residual will also increase. This trend is captured by the model in Figure 6.10 however the levels of unburned residual are much higher in magnitude. These plots show that the model is *qualitatively* predicting the trend in variations of IMEPg and unburned residual concentration with changes in combustion phasing. It should be noted that these experimental results indicate that a linear scaling of the burned/unburned residuals with combustion phasing after a partial burn limit is valid up to the misfire limit where combustion does not occur.

A good question to ask is: Is this inclusion of an unburned residual, which effectively introduces a chemical composition effect in the simple model, responsible for the increase in output variation at late combustion timings? The model was modified to run the same experiments, but this time it was forced to assume all the residual amounts were burned residuals, including the linearly scaled unburned residuals. These data points are shown in Figure 6.11 below as the yellow circles.

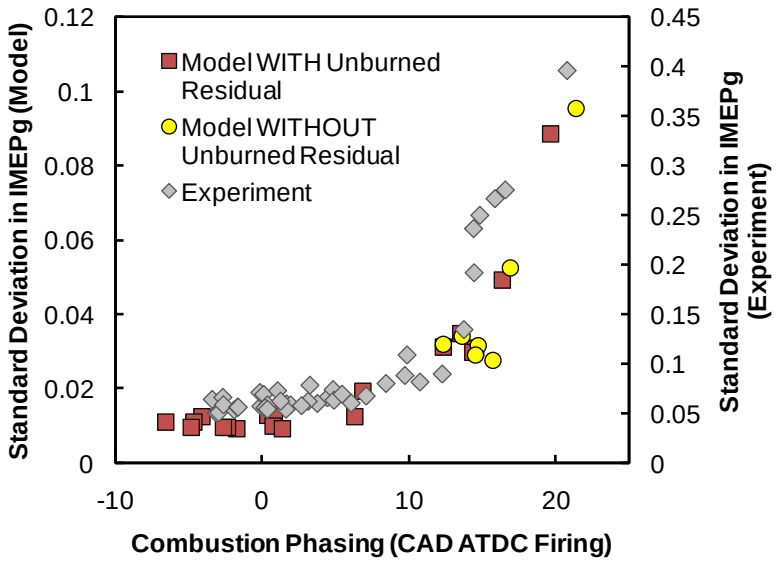

Figure 6.11. Variation in models output with all residuals forced to be burned residuals

The answer clearly shows that the level of variation in output in the model is not impacted by the compositional effect of the unburned residual. Even as the combustion phasing is pushed to the misfire limit, the standard deviation in engine work out still climbs the linear trend following the partial burn limit of 10 CAD ATDC. With these kinds of trends seen, then one must ask: Does the unburned residual impact the predicted deterministic behavior? (i.e. does the model even need to include an unburned

residual?). Figures 6.12 and 6.13 show the inclusion of the unburned residual versus the without the unburned residual in the model.

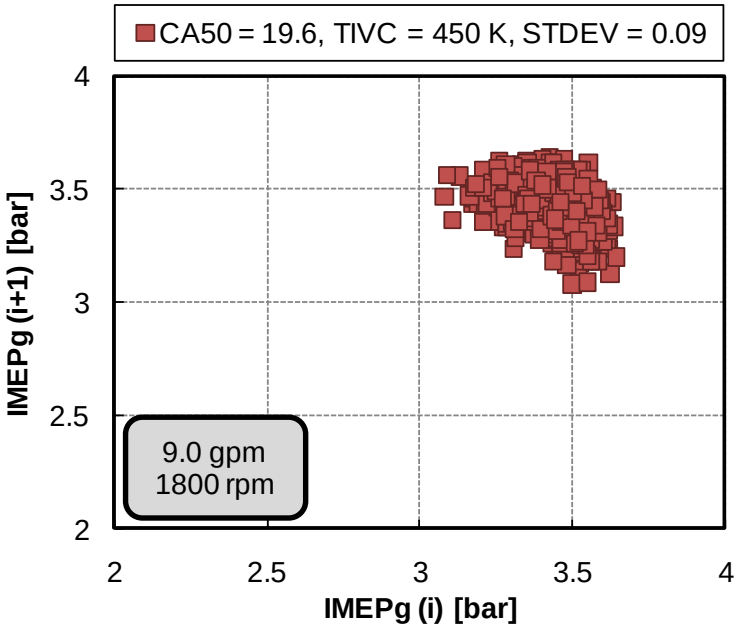

Figure 6.12. Model return map at a partial burn case *with* unburned residual

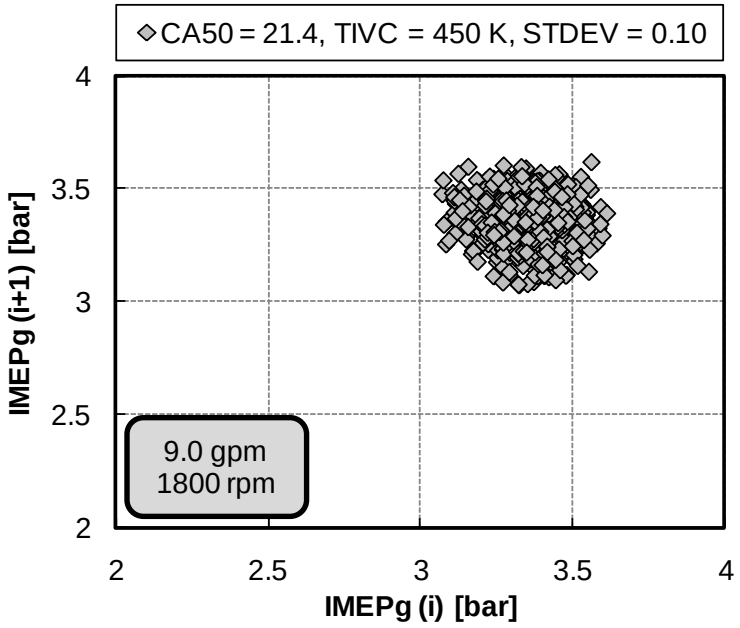

Figure 6.13. Model return map at a partial burn case *without* unburned residual

The model was run at one set point with a fueling rate of 9.0 grams/min, at an engine speed of 1800 rpm, and at an intake temperature of T_{IVC} = 450K. Figures 6.12 and 6.13 undoubtedly show that the inclusion of the unburned residual impacts the deterministic behavior in the cyclic variations predicted by the model. Therefore the residual impacts the deterministic behavior at partial burn through enriching the mixture, but there are other phenomena impacting the overall level of variation in output. Hence residual species (composition) are not necessary to capture the level of instability (i.e. COV) as long as the increase in the unburned residual is captured for late combustion phasing. However, this work does indicate that the composition of the residual does seem to impact determinism when observing IMEPg return maps. This is an intriguing result as the work presented in Chapter 5 seems to indicate that the temperature of the residual does not seem to impact determinism. All of this said, it would be beneficial to separate this chemical and temperature effect of the residual in order to study kinetically what is occurring in HCCI combustion that is causing this determinism to appear.

7. REACTIVE SPECIES GAS INJECTION

Since the occurrence of HCCI combustion relies on chemical kinetics, we know that the thermodynamic state and the dilution levels of the charge mixture will directly affect the start of combustion process. A more complete understanding is sought on the role of residual gas properties on the next cycle's start of combustion and heat release rate. Work presented in Chapters 5 and 6 demonstrates that the deterministic effect seen in the partial burn regime is more due to chemical composition of the residual than the temperature of the residual gas. A more complete understanding is sought of the role of this chemical composition effect on the kinetics of HCCI combustion development. This chapter outlines preliminary results of the underlying cycle-by-cycle dynamic impacts of carefully controlled in-cylinder injections of perturbation gases, in this case carbon monoxide, using a residual gas injector (RGI) on an individual cycle basis. By directly injecting a reactive species gas, like carbon monoxide or hydrogen, one can isolate the chemical composition effects of the residuals from the thermal effects in order to explore the extent of the non-linear effects seen in the regions of instability.

7.1. FLOW BENCH TESTING

Mass injections of certain percentages are to be added to the inlet fuel/air charge during the intake stroke. The hardware and details about the RGI can be found in §3.1.4. This section outlines how the RGI was benchmarked off the engine test stand in order to verify that the mass being injected into the cylinder was the correct amount thought to be injected. The RGI works on having back pressure from the reactive species

compressed gas bottle, and then the valve (activated by a solenoid) opens and closes with injection timing referenced from the engine's crank signal to pass high pressure syn-gas through the valve and out the tip of the injector into the combustion chamber. In order to verify the mass flow rates of carbon monoxide (CO), the syn-gas used, a flow bench test was constructed. Figure 7.1 depicts how the setup was fabricated.

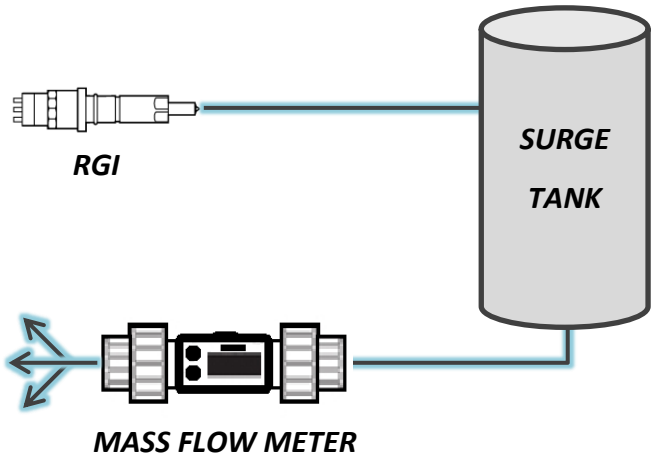

Figure 7.1. Residual gas injector flow bench setup

The mass injections have to be run through a surge tank in order to smooth the pulsations in the mass flow meter. This helps smooth the mass flow curve for that back pressure in the compressed gas bottle. The mass flow meter used was a CMOSens® EM1 Mass Flow Meter produced by SENSIRON. The gas was then vented to atmospheric pressure as this is what the injector will see when injecting into the engine during the intake stroke. It should be noted that nitrogen (N_2) was used instead of CO, because

venting CO into the room would be toxic and dangerous. Refer to the next section, §7.1.1, for details regarding bench testing with N_2 instead of CO.

7.1.1. Methodology. Carbon monoxide is the syn-gas to be injected into the engine in order to study the effects it has on the combustion process. Injections of up to 15%, by mass of the inlet charge, can be done with using the RGI. It would be beneficial to flow test using CO however as mentioned above, N_2 was used to flow test the injector instead of CO. Normally flowing a different gas would give different flow rates due to the previous comment about molecular weights. N_2 and CO just happen to have the same molecular weights and therefore have the same density. This is given in Table 7.1 which lists the two gases and their respective properties.

Table 7.1. Gas properties of Nitrogen and Carbon Monoxide

	Nitrogen	Carbon Monoxide
Formula	*N_2*	*CO*
Molecular Mass (M) [kg/kmol]	*28.013*	*28.011*
Density* (kg/m^3)	*1.165*	*1.165*
Specific Heat at Const. Pressure (Cp) [kJ/kg·K]	*1.039*	*1.04*
Specific Heat at Const. Volume (Cv) [kJ/kg·K]	*0.743*	*0.744*
Ratio of Specific Heats (k)	*1.4*	*1.4*

* Densities defined at normal temperature and pressure (NTP) [20°C, 1 atm]

By mass, density, and ratio of specific heats, these gases are very similar. However, it should be noted that the gas flow through the RGI, is essentially flowing gas through an orifice. The maximum amount of mass, $\dot{m}_{max}$, which can flow through an

orifice, is given by the following relationship in Equation 27 and only holds true if the flow is choked. A choked flow is applicable to compressible mediums and the parameter that becomes “choked” is the velocity. When a gas, at a given pressure, passes through a restriction (in this case, the RGI) and is expelled into a lower pressure then the fluid velocity increases. The conservation of mass requires that the fluids velocity increases as it flows through this small cross-sectional area. At the same time, the Venturi effect causes the static pressure, and therefore the density, to decrease downstream past the restriction. Therefore, choked flow is a limiting condition which occurs when the mass flow rate will not increase with a further decrease in the downstream pressure while upstream pressure is fixed. If the ratio of upstream absolute pressure to downstream absolute pressure is greater than 1.9, then the flow is said to be choked.

$$\begin{aligned} \dot{m}_{max} = \rho^* A^* V^* &= \rho_0 \left(\frac{2}{\gamma+1}\right)^{\frac{1}{\gamma-1}} A^* \left(\frac{2\gamma}{\gamma+1} RT_0\right)^{\frac{1}{2}} \\ &= \gamma^{\frac{1}{2}} \left(\frac{2}{\gamma+1}\right)^{\frac{\frac{1}{2(\gamma+1)}}{(\gamma-1)}} A^* \rho_0 (RT_0)^{\frac{1}{2}} \end{aligned} \tag{27}$$

In the above equation the only “gas specific” property is the ratio of specific heats, γ. Therefore, the maximum amount of mass that can flow through an orifice is a function of the ratio of specific heats (γ), and since the specific heats and thus the ratios are the same for these two gases, one could flow N_2 and measure its flow rate and say

with confidence that when flowing CO we observe very similar mass flow rates. More details on the derivation of Equation 27 can be found in [33].

7.1.2. Mass Flow Calibration Curves. The RGI was run for 100 consecutive cycles at 1800 rpm using the simulated engine within the LabVIEW vi. The injection duration was varied from 0 to 200 CAD. The 200 CAD window is due to the engine fixed valve timing. Intake valve open (IVO) occurs at 705 CAD and intake valves close (IVC) occurs at 227 CAD. Valve timings are referenced at TDC exhaust stroke. This is a window of 242 CAD; however the engine also has 33 degrees of valve overlap. This exhaust valve close (EVC) does not occur until 18 CAD. So from 18 CAD to 227 CAD is a window of 209 CAD, and thus 200 CAD was chosen for maximum injection duration.

It should be noted that in LabVIEW, the duration is in milliseconds (msec) so the CAD had to be converted to time for that given engine speed. Also the RGI has a 7msec liftoff time, which is the time it takes for the injector to actuate. This corresponds to 75 CAD. So the duration of injection does not actually occur until 7msec in to the injection duration. By adding the 200 CAD to the already 75 CAD, the injection timing was varied from 7msec to 26msec. The syn-gas bottle back pressure also influences the amount of mass that is injected during a given duration. A pressure regulator was used to accurately adjust the line pressure upstream of the RGI. This flow test was conducted for a range of back pressures across the entire injection period. The data can be seen in Figures 7.2 and 7.3.

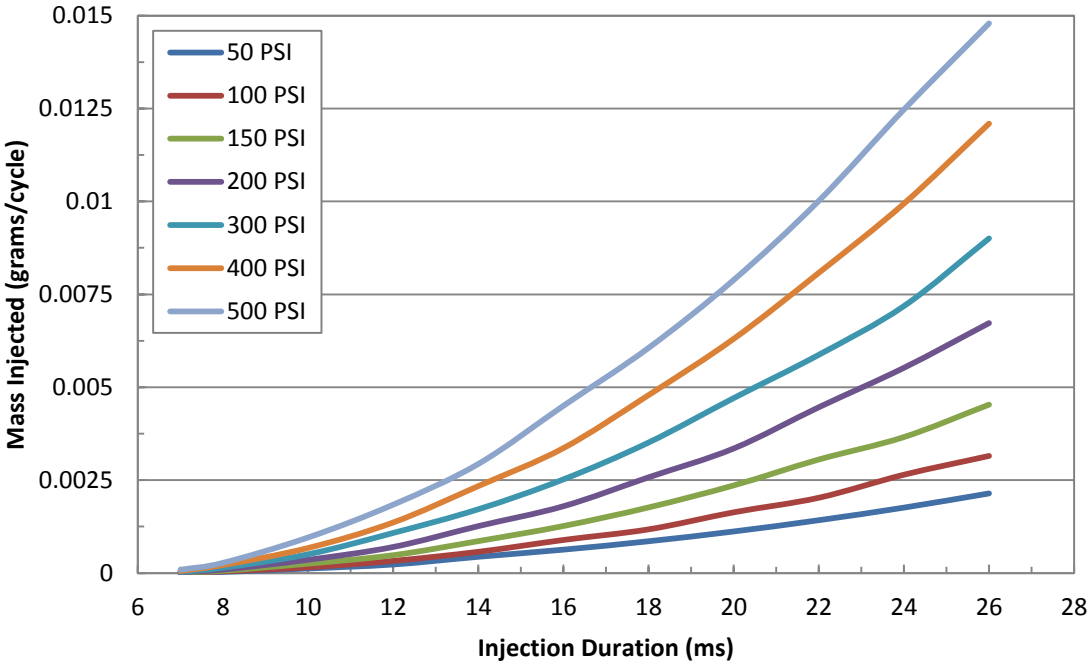

Figure 7.2. Residual gas injector pressure calibration curves, 50-500 psi

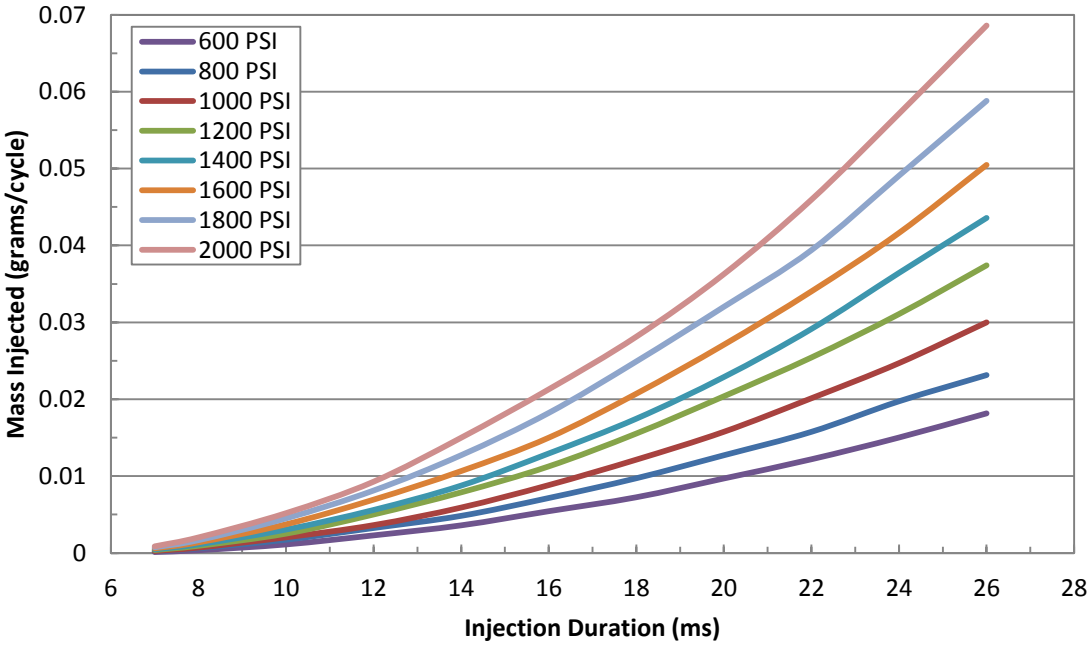

Figure 7.3. Residual gas injector pressure calibration curves, 600-2000 psi

It can be seen that as the line pressure in increased the amount of mass injected increases. With these curves and the fact that CO acts very similarly to N_2, the RGI can be added to the existing engine stand and reactive species addition experiments will be conducted. See section §7.2 for preliminary results from reactive species injection.

7.1.3. Injection Temperature Profiles. As a gas undergoes expansion, the bulk temperature of that gas will decrease. Experiments were conducted to try to quantify that temperature. A fast response thermocouple was mounted at the tip of the injector and CO was injected across the TC junction. These experiments were conducted for both 0.15% mass injection and 0.40% mass injection at 100 and 800 psi. Figure 7.4 shows a single injection event at 800 psi for both the 0.15% and 0.40% mass injection amount.

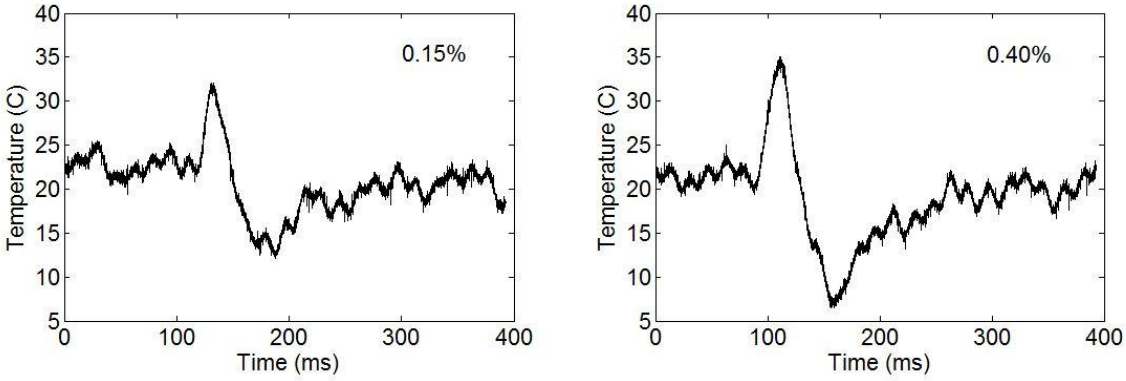

Figure 7.4. Injection temperature for a single injection at 800 psi **a.** 0.15% and **b.** 0.40%

Four hundred milliseconds were collected with one mass injection during that collection period. Figure 7.4 shows an initial increase in injection gas temperature followed by a cool gas temperature. The initial temperature rise is due to the solenoid

coil current heating the valve body and thus heating the CO sitting in the injector body. This gas is then expelled from the body, followed by the cold injected gas. In this case that cold gas is CO. This figure also shows that the greater the mass injected, the cooler the injected gas temperature. If SOC in HCCI was *highly* temperature dependent, then this cool gas would retard combustion upon mixing with the intake charge, however, as it will be shown later that this large mass addition at this cooler temperature advanced SOC, displayed as CA10. Figure 7.5, below, shows 100 consecutive injection events at 800 psi for both the 0.15% and 0.40% mass injection amount.

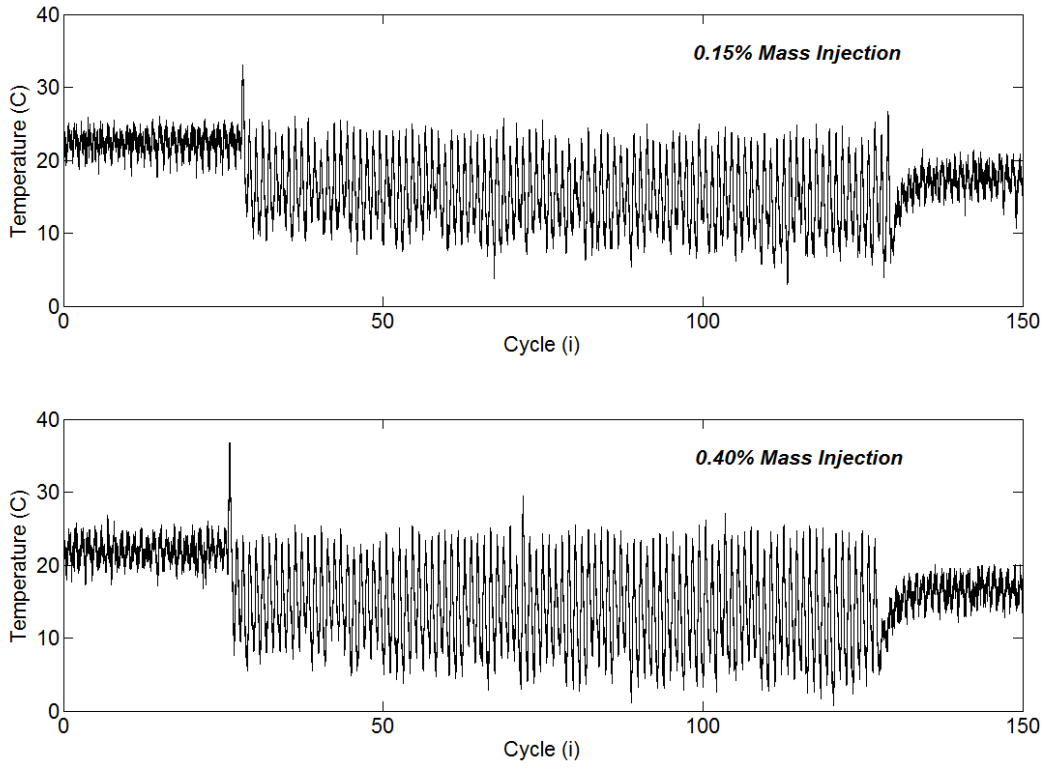

Figure 7.5. Injection temperature for 100 injections at 800 psi **a.** 0.15% and **b.** 0.40%

Again, Figure 7.5 reaffirms that the initial gas within the valve body is being heated by the solenoid and once it is expelled, it is not seen again. The 100 consecutive cycles show that average injected CO gas temperature at 0.15% mass injection is approximately 7°C and the 0.40% mass injection is approximately 4°C. Since the gas is expanding from 800 psi to atmospheric, these injection pressures will result in the coolest gas temperature, therefore the 100 psi injection temperature profiles are not shown here as the temperature of the gas is closer to room temperature than the higher pressure cases. Injecting a cold gas into the cylinder would affect the overall temperature of the bulk gas however in this case only 0.15-0.40% by mass is being injected therefore the overall temperature should not be significantly changed. In fact, by looking at the worst case (0.40% injection at 4°C) scenario by adding CO to 195°C bulk gas temperature of the inlet charge through adiabatic mixing, only reduces the bulk gas temperature to 194.2°C. Therefore the cooling effect on the bulk gas temperature is negligible at these percent mass additions.

7.1.4. Thermochemistry Mass Balance. As mentioned above, the RGI can inject up to 15%, by CO mass, of the inlet charge. Mass fuel flow rate (grams/min) is known from bench testing the low flow metering pump for precise fuel flow rate into the fuel atomizer. Emission gas concentrations of CO_2 (%), CO (%), O_2 (%), uHC (ppm), and NO_X (ppm) are collected using exhaust gas analyzers. The CO_2, CO, and O_2 data are taken from a dry gas analyzer while the remaining species are each collected from wet gas analyzers. The H_2O concentration (%) is not collected during engine tests and thus must

be calculated. This is completed using some of the other collected emissions data and the following equation from [16]:

$$[H_2O] = 0.5\left(\frac{H}{C}\right)\left(\frac{(CO_2)+(CO)}{\frac{(CO)}{[K(CO_2)]}+1}\right) \quad (28)$$

Where [ ] = molar concentration present. In the above equation, K is defined as the water-gas reaction equilibrium constant. A generally accepted empirical determination of K is the constant 3.8. This water-gas reaction is used in conjunction with the atom balances of the global reaction to derive the (H_2O) equation. The thermochemistry balance equation for the oxidation of fuel and air is given by,

$$C_xH_y + a(O_2 + 3.76N_2) \longrightarrow bCO_2 + cH_2O + dCO + eH_2 + fO_2 + gN_2 \quad (29)$$

The amount of fuel consumed in the above reaction can be calculated from a Spindt exhaust gas analysis [16]. The make-up of combustion products, or exhaust gas concentrations, are measured and therefore the amount of fuel consumed can be determined. Previous investigations [35] have concluded that Spindt analyses return values within 0.1 air-to-fuel ratio of the *true value* if the engine is run on gasoline and the sampling location is before an exhaust catalyst. Since these two conditions are met in this experimental setup, the Spindt analyses are deemed appropriate.

The Spindt method calculates the equivalence ratio based on a wet uHC and dry inorganic gas analysis. This is the most accurate for the experimental engine stand due

to the inorganic gas concentrations (CO_2, CO, and O_2) being determined from a dry gas analyzer while the uHC concentration is given in a wet gas analysis. The following formulas were used for this computation [16].

$$\varphi = \frac{2n_{O_2}}{n_P x_{H_2O} + n_P\left(1 - x_{H_2O}\right)\left(x^*_{CO} + 2x^*_{CO_2} + 2x^*_{O_2} + x^*_{NO} + 2x^*_{NO_2}\right)} \tag{30}$$

Where,

$$n_{O_2} = \frac{x + y}{4} \tag{31}$$

(O_2 molecules required for complete combustion of fuel C_xH_y)

$$x_i^* = \text{dry mole fraction of component } i$$

$$x_i = wet \text{ mole fraction of component } i$$

$$x_i = \left(1 - x_{H_2O}\right)x_i^* \tag{32}$$

$$n_P = \frac{x}{x_{uHC} + \left(1 - x_{H_2O}\right)\left(x^*_{CO} + x^*_{CO_2}\right)} \tag{33}$$

(Total moles of exhaust products)

$$x_{H_2O} = \frac{y}{2x}\frac{x^*_{CO} + x^*_{CO_2}}{\left[\frac{1 + x^*_{CO}}{\left(K x^*_{CO_2}\right)} + (y/2x)\left(x^*_{CO} + x^*_{CO_2}\right)\right]} \tag{34}$$

This plus the air-fuel ratio calculated in §3.2 are used in conjunction to determine the amount of mass that is introduced into the cylinder. The inlet mass is determined

using the known fuel flow rate, grams/min, and the air introduced is known from the laminar flow element (LFE) upstream of the intake manifold. The exhaust gas analysis is used to determine the mass of exhaust products for one mole of fuel using thermochemistry and the measured exhaust gas analyzers. Table 7.2 displays experimentally collected exhaust concentrations for 2 different fueling rates. Table 7.3 compares the inlet charge mass to the exhaust products mass for one mole of fuel.

Table 7.2. Emissions data collected from Hatz

		Fuel Flow Rate = 7.5 gpm		Fuel Flow Rate = 9.0 gpm	
		Steady State	Partial Burn	Steady State	Partial Burn
Engine Speed	rpm	1800	1800	1800	1800
CO2 (dry)	%	4.25	3.28	4.81	3.71
CO (dry)	%	0.024	0.16	0.05	0.145
O2 (dry)	%	15	16.1	14.2	15.7
uHC (wet)	ppm C	3280	9440	4280	10000
NOx (wet)	ppm	120.1	5.3	209.2	7.8

Table 7.3. Intake/exhaust mass balance

Thermo-chemistry per one mole of fuel					
Operating Regime	Fuel Flow Rate (grams/min)	Eq. Ratio (φ)	Inlet Charge Mass (grams)	Exhaust Mass (grams)	Percent Error (%)
Steady State	7.5	0.36	4962	4948	-0.29
Partial Burn	7.5	0.34	5129	5213	1.65
Steady State	9.0	0.41	4339	4341	0.03
Partial Burn	9.0	0.40	4687	4771	1.80

More detailed tables on number of moles of products and mass of products can be found in Appendix C. The exhaust mass analysis was conducted on 2 different fuel flows at 7.5 gpm and 9.0 gpm. In order to inject mass percentages, the total mass had to be calculated, given by the procedure above. From here it can be determined what percentages of the total amount need to be injected. From Table 7.4 it can be seen that total average mass of the inlet charge is 0.4147 grams. The percentages (5, 10, and 15%) average 0.020, 0.041, and 0.062 grams respectively. From this, making use of the calibration table for the RGI, the injection duration and line pressure can be determined for preferred mass injection percentage.

Table 7.4. Mass injection percentages

RGI Mass Injection				
Eq. Ratio (φ)	Mass of Inlet Charge (grams/cycle)	5% Mass (grams)	10% Mass (grams)	15% Mass (grams)
0.36	0.39	0.020	0.039	0.059
0.34	0.41	0.020	0.041	0.061
0.41	0.41	0.021	0.041	0.062
0.40	0.45	0.022	0.045	0.067

Moles of fuel per cycle	
	(1800 rpm)
7.5 gpm	7.9E-05
9.0 gpm	9.5E-05

Figures 7.6 and 7.7 show that up to 15% mass injections can be achieved by using the RGI when flowing CO. If a different gas is used then the RGI would have to be calibrated for that gas given it has different molecular weights and specific heats. The

5% mass addition can be achieved by using all of the line pressures except for the 600 psi line pressure. The correct pressure and injection duration can be picked in order to achieve adequate mixing in-cylinder. The RGI will be installed on the engine platform and results can be seen in the next section.

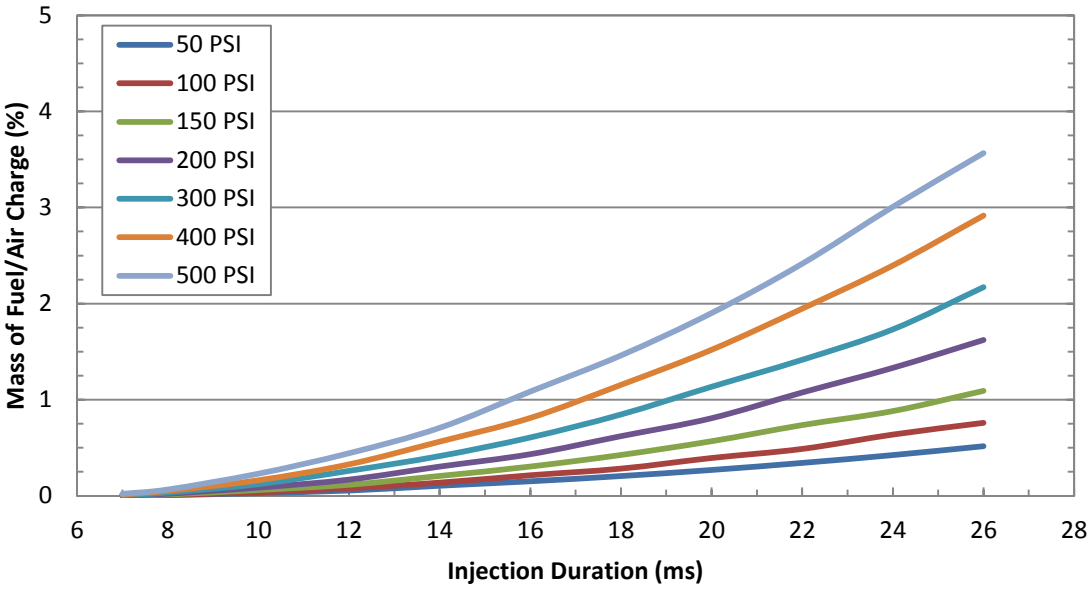

Figure 7.6. Residual gas injector mass percentage calibration curves, 50-500 psi

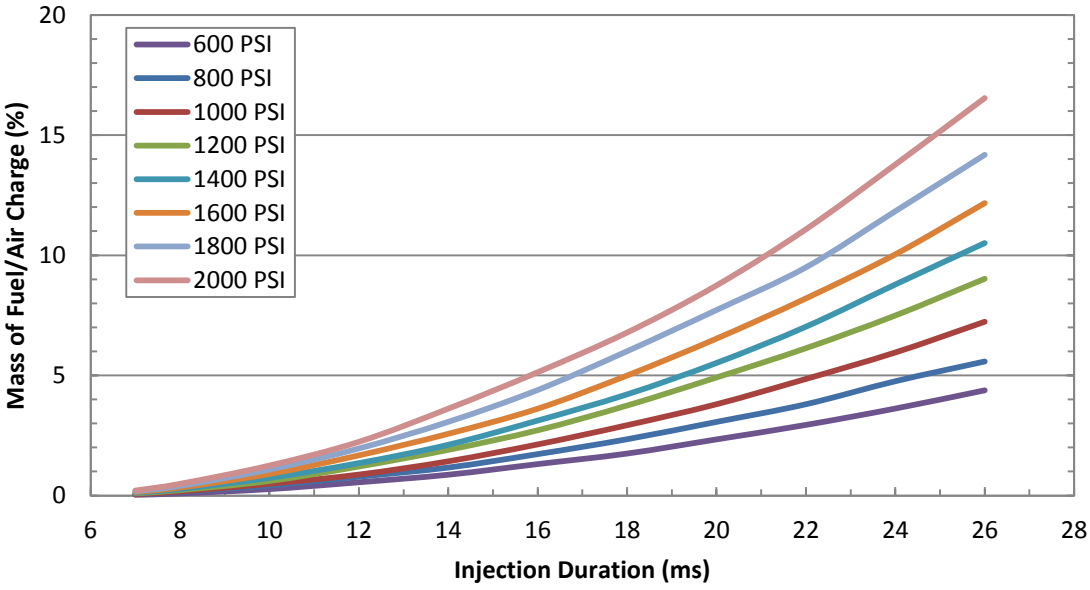

Figure 7.7. Residual gas injector mass percentage calibration curves, 600-2000 psi

7.2. REAL-TIME ENGINE RESULTS

With the injector on the engine running in real-time, it was found that 5% mass injections would significantly affect the engine's combustion development and could lead to damage of the engine/piston/connecting rod structure. Thus the amounts were adjusted and found that mass injections of around 0.1% - 0.5% were acceptable to add cyclically to the inlet charge in order to observe significant changes in the engine's behavior. This section presents the results seen from onboard reactive species mass injection and draws conclusions on these test cases.

7.2.1. Carbon Monoxide Mass Injection Results. CO injections were added at two different injection pressures for the same amount of mass. Mass percent injections of 0.15% and 0.40% were used as these set points affected the engine's performance with respect to a high and low injection amount. The pressures were determined from the calibration tables and found to be 800 psi and 100 psi. The duration of injection was kept under 200 CAD and injected before IVC at 227 CAD. This allowed injections to occur after EVC at 18 CAD. The durations found to fit the criteria were 8ms (800 psi, 0.15% injected), 10ms (800 psi, 0.40% injected), 14ms (100 psi, 0.15% injected), and 20ms (100 psi, 0.40% injected). It should be noted that the valve required 7ms of inherent delay to actuate so start of injection signal (SOI) was triggered 75 degrees (7ms at 1800 rpm) before actual mass SOI occurred. The engine was run at a steady operating speed of 1800 rpm and a fuel flow rate of 7.5 grams/min. Also, the intake temperature was held at a constant 195°C, or 468 K. Table 7.5 lists the averaged data collected from the different test cases.

Table 7.5. Average engine parameters for CO mass additions

Intake Temp (K)	Fueling Rate (grams/min)	Mass Injection (%)	Injection Pressure (psi)	Avg. CA10 (CAD)	Avg. CA50 (CAD)	IMEPg (bar)	Burn Duration (CAD)	Efficiency n_f, (%)
468	*7.5*	*-*	*-*	*363.1*	*370.5*	*4.02*	*10.78*	*56.3*
468	*7.5*	*0.15*	*800*	*363.8*	*369.8*	*4.45*	*9.04*	*55.1*
468	*7.5*	*0.40*	*800*	*362.5*	*364.7*	*4.91*	*3.61*	*56.7*
468	*7.5*	*-*	*-*	*363.1*	*370.5*	*4.02*	*10.78*	*56.3*
468	*7.5*	*0.15*	*100*	*363.5*	*369.1*	*4.22*	*8.59*	*52.3*
468	*7.5*	*0.40*	*100*	*363.3*	*367.63*	*4.43*	*6.82*	*51.1*

This table shows that the set point's SOC, quantified by CA10, does not change due to CO addition; however the location where 50% of heat released occurs does advance a few degrees based on the amount injected. This is interesting as it was thought that since the autoignition event in HCCI is kinetically dependent, the addition of a reactive species would have affected the SOC, by either advancing or retarding when the autoignition event occurs, but perhaps it is affecting more the combustion development than the initiation of combustion. The average IMEPg increases due to the addition of more energy from the mass injection. Also the burn duration significantly decreases as the energy content is increased within the cylinder. The chart above also lists fuel conversion efficiency for these test cases. It can be seen that the addition of CO at 100 psi significantly decreases the fuel efficiency, however it is hard to compare these test cases as the energy within the cylinder is different for each case. Refer to §7.2.2 for further analysis on equivalent energy addition.

Further discussion of the phenomenon experienced by the addition of a reactive species into the cylinder can be seen later in this chapter. This section is here to simply show that mass injection of a reactive species gas, in this case CO, does in fact affect

observed combustion parameters. Figures 7.8 and 7.9 shows the pressure trace for the baseline set point and the 0.15% and 0.40% mass injection of CO at 800 psi and 100 psi, respectively.

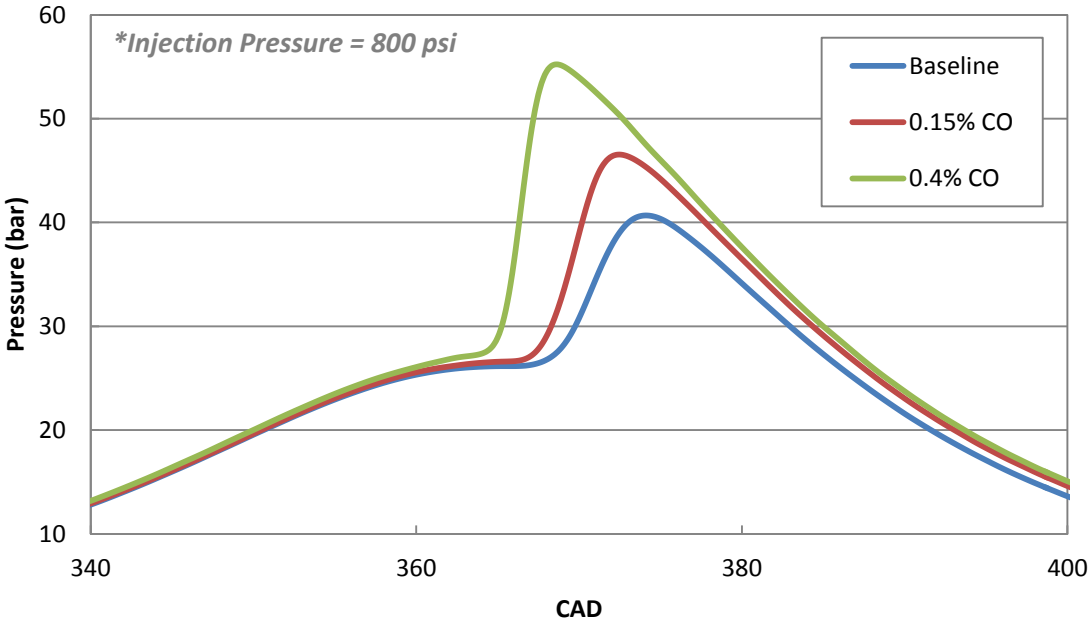

Figure 7.8. Pressure trace comparison of CO mass addition at 800 psi injection pressure

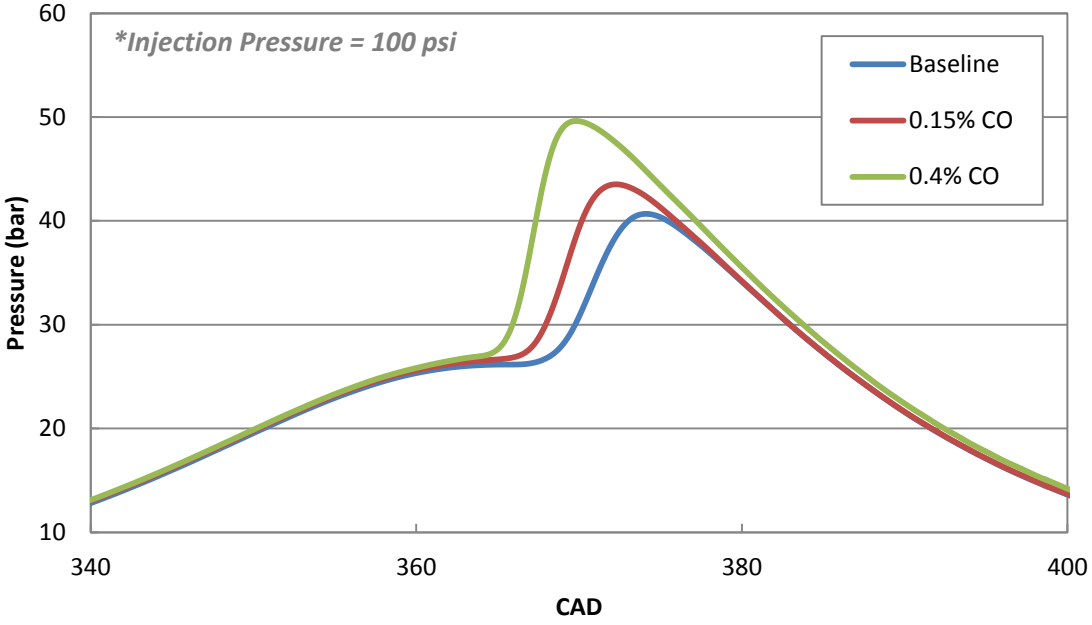

Figure 7.9. Pressure trace comparison of CO mass addition at 100 psi injection pressure

In these figures it can be seen that as higher mass percentages, and thus increased energy content, are added then the pressures in cylinder increase due to increased energy released. This is shown in the higher IMEPg values displayed in Table 7.5. The cumulative heat release curves for these set points are displayed in Figures 7.10 and 7.11. Here it can be seen that the higher injection pressure of 800 psi promotes combustion due to the energy addition and the CA10, CA50, and burn duration values show that above in Table 7.5. The averaged data shows collective trends, however it is beneficial to study temporal data in order to further understand cyclically what is occurring. Figures 7.12 and 7.13 display time-series data for 100 consecutive cycles with a 50 cycle injection time for the 0.4% CO mass addition case at 800 psi.

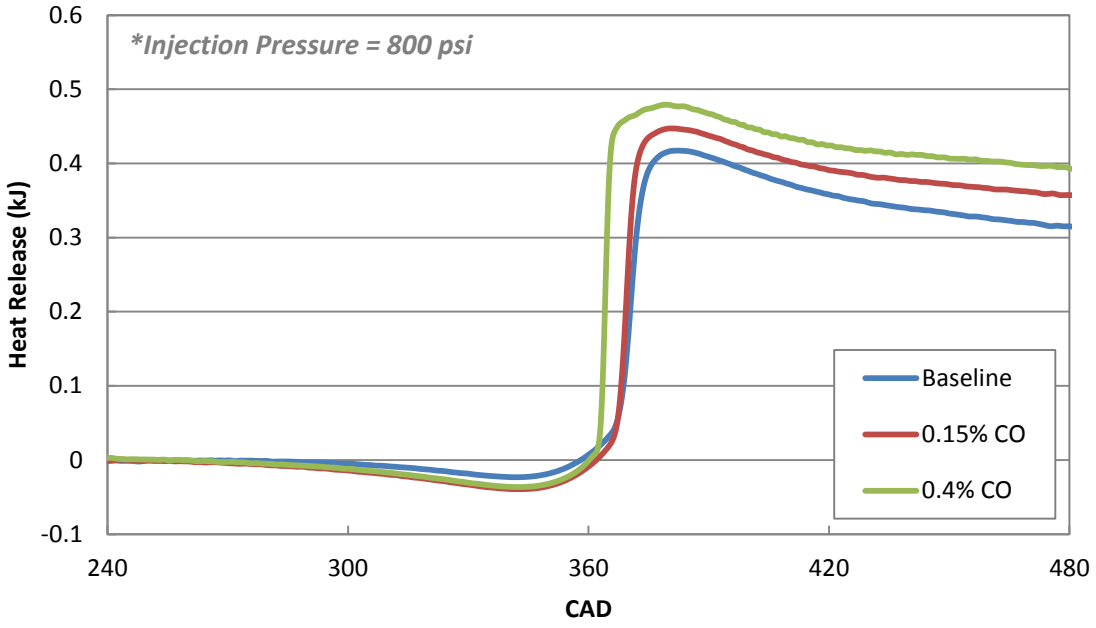

Figure 7.10. Cumulative heat release of CO mass addition at 800 psi injection pressure

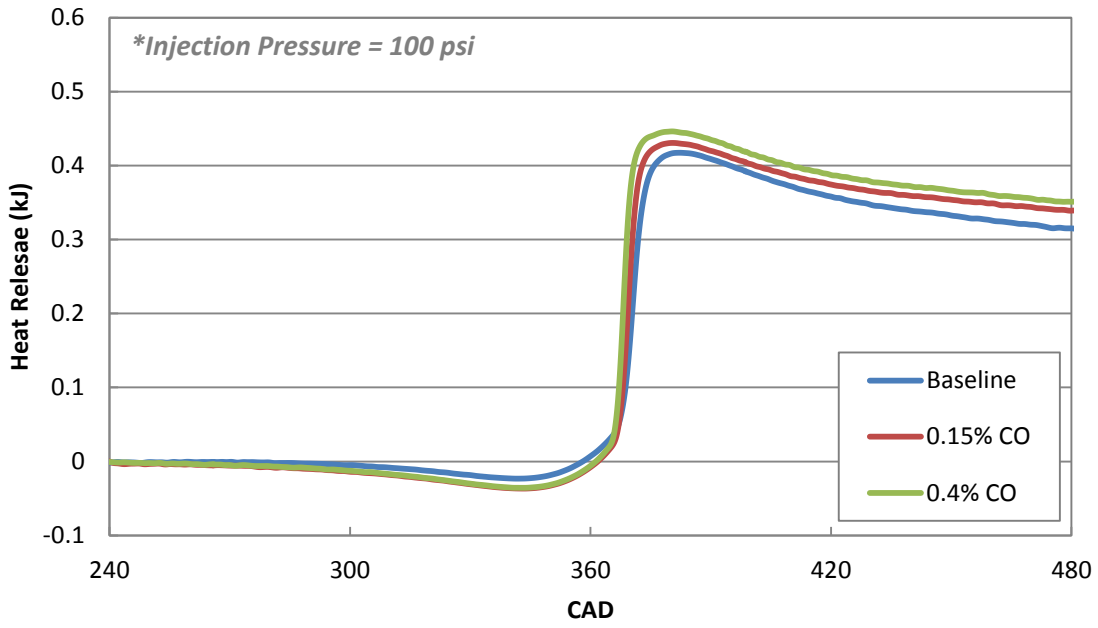

Figure 7.11. Cumulative heat release of CO mass addition at 100 psi injection pressure

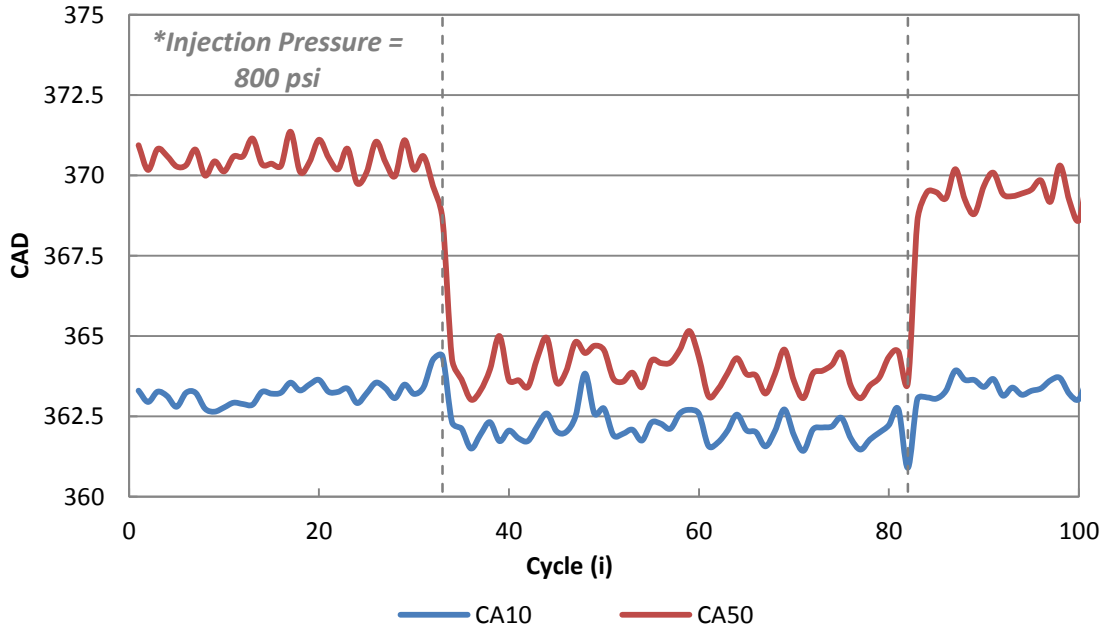

Figure 7.12. Temporal CA10 and CA50 for 0.40% mass injection of 50 cycles, 800 psi

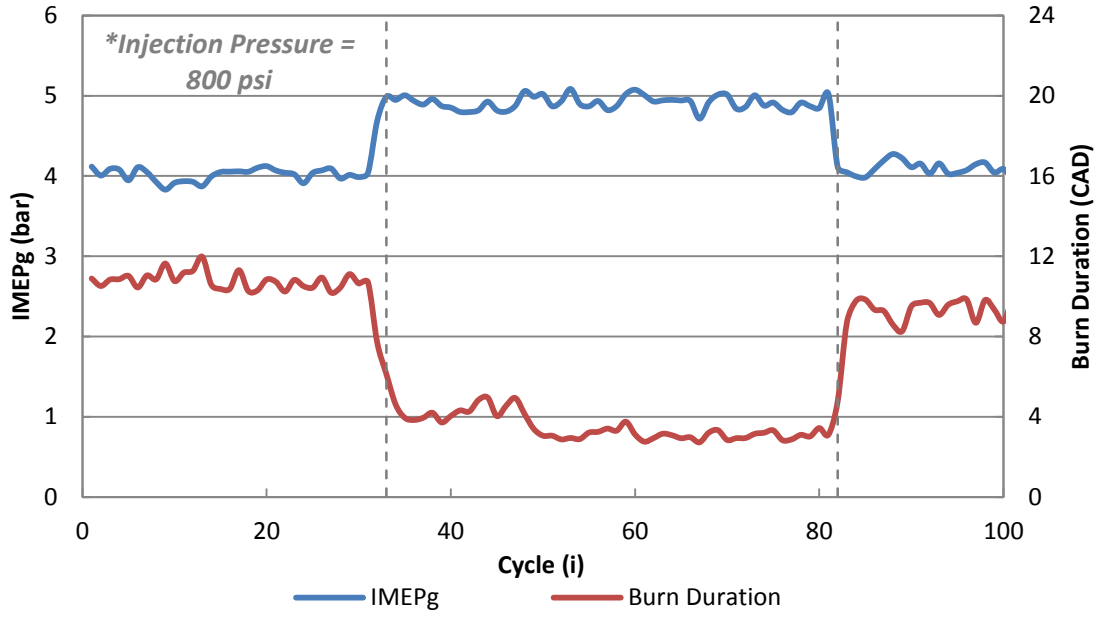

Figure 7.13. Temporal IMEPg and burn duration for 0.40% mass inj. of 50 cycles, 800 psi

Figure 7.12 clearly shows when the first injection cycle occurs and that the extra energy added to the charge mass increased the combustion development shown by the advanced CA50 values. This indicates that the total heat energy in the charge is being released at a faster rate as shown by the burn duration in Figure 7.13. It should also be noted that the CA10, or SOC, is being advanced by approximately a degree during the time of injection.

The significantly higher IMEPg and decreased burn durations seen in Figure 7.13 for the higher mass addition is due to the fact that the energy content in the cylinder is greatly increased during the injection period. The lower mass addition (0.15% at 800 psi) can be seen in Figures 7.14 and 7.15. Figure 7.14 shows that when the mass is injected, the CA50 is nearly unchanged, however the SOC, or CA10, is retarded by approximately a degree, which is not what is seen when 0.40% mass is added as shown by Figure 7.12.

These results are not expected to be similar as different levels of energy are added to the system during 0.15% and 0.40% mass injections. What is interesting is that, by adding energy to the system one would suspect the SOC to occur at an earlier time however there could be a kinetics phenomenon at work causing this slightly retarded SOC. To further this thought, Figure 7.15 shows that during injection of the low mass addition (0.15%), the burn durations are slightly decreased indicating that the increased energy addition along with the fuel/air charge is consumed on a shorter time scale, resulting in slightly higher IMEPg values during injection. Further tests to compare energy addition through fuel amounts can be seen in §7.2.3.

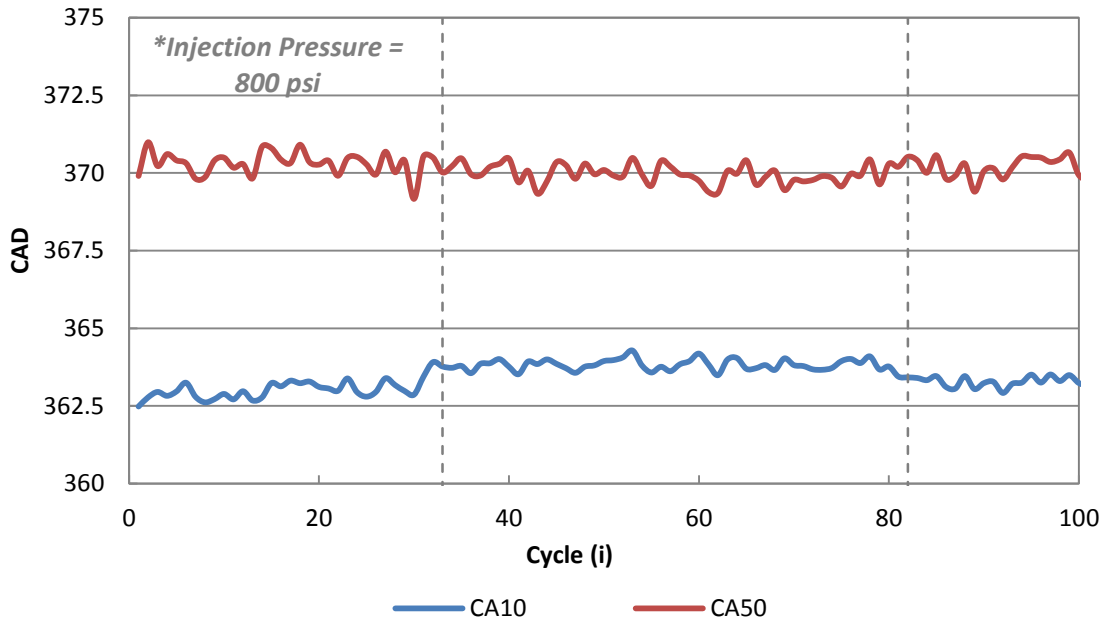

Figure 7.14. Temporal CA10 and CA50 for 0.15% mass injection of 50 cycles, 800 psi

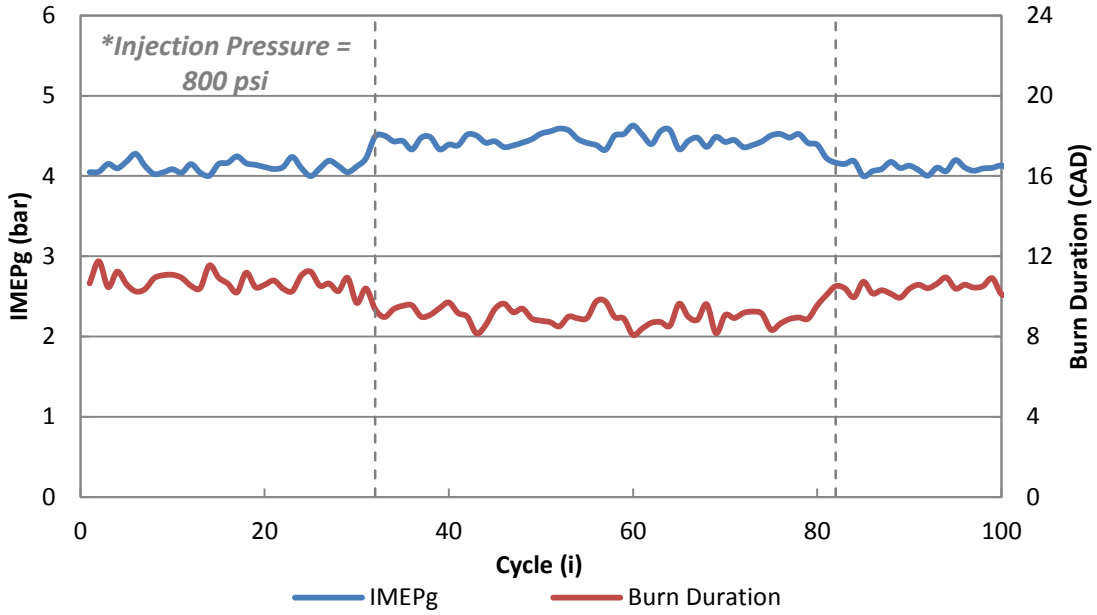

Figure 7.15. Temporal IMEPg and burn duration for 0.15% mass inj. of 50 cycles, 800 psi

Figures 7.16 through 7.19 present the same data as seen above but for the 0.4% and 0.15% CO mass addition cases at 100 psi. This lower injection pressure, but equivalent mass addition of 0.40%, shows relatively the same trends as observed for the 800 psi injection pressure cases but they have a much different level of effect. Figure 7.16 clearly shows when the first injection cycle occurs and that the extra mass, and thus energy, added to the charge mass increased the combustion development shown by the advanced CA50 values. Again, this indicates that the total heat energy in the charge is being released at a faster rate as shown by the burn duration in Figure 7.17. It should be noted that the CA10, or SOC, is not being advanced during the time of injection, unlike the 800 psi injection pressure case.

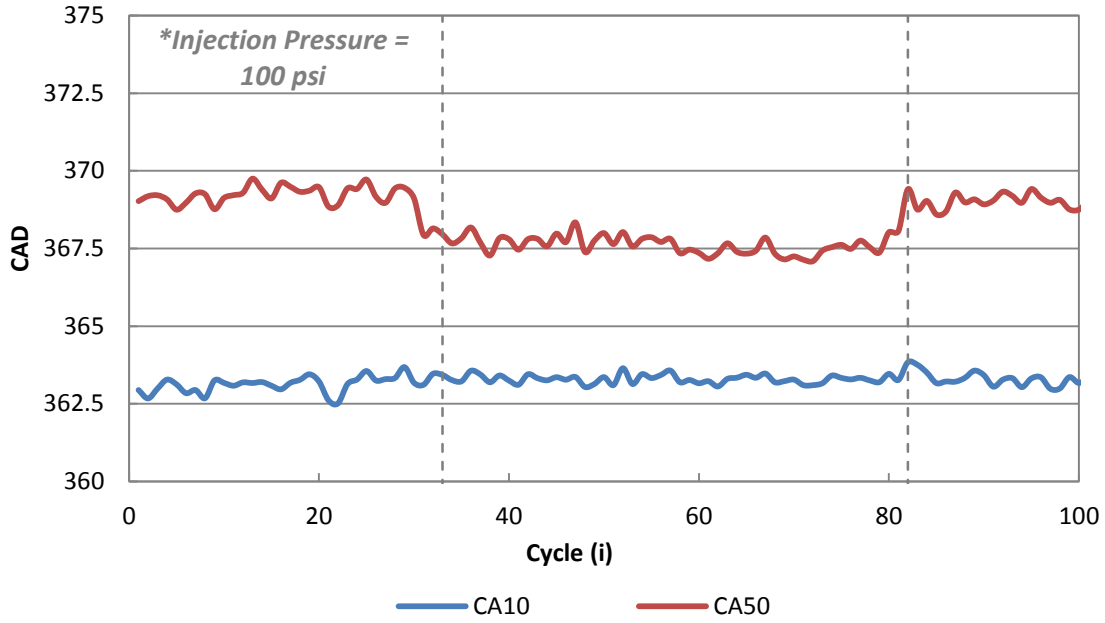

Figure 7.16. Temporal CA10 and CA50 for 0.40% mass injection of 50 cycles, 100 psi

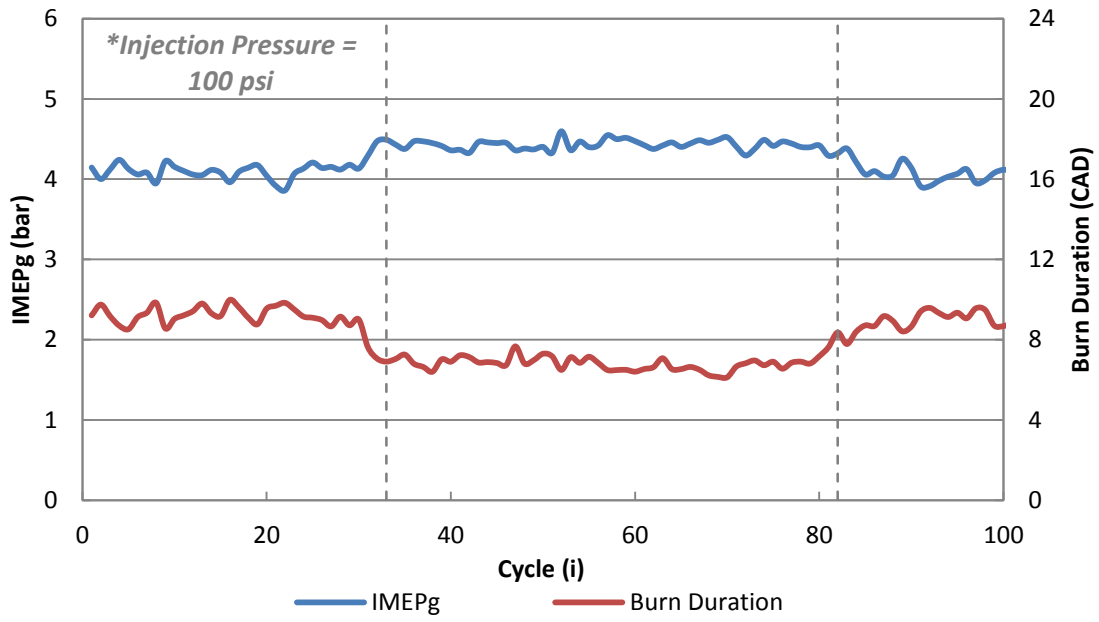

Figure 7.17. Temporal IMEPg and burn duration for 0.40% mass inj. of 50 cycles, 100 psi

Again, it can be seen that the higher mass addition increases IMEPg during injection and decreases the burn duration, increasing the heat released with in the cylinder. Figure 7.18 shows CA10 and CA50 values for the low mass addition (0.15%) at 100 psi injection pressure. Here negligible results can be concluded from the time series data. The averaged data seems to indicate that the CA10 and CA50 values remain unchanged (within 0.5 CAD of the original values) and this is seen on the time series data, from which the averages are taken. Figure 7.19 shows the burn duration and IMEPg values during the mass injection of 0.15% at 100 psi. There is no significant change in the time series data, except for a slight increase in IMEPg that is noted in Table 7.5 and can be seen in the pressure curves displayed in Figure 7.9.

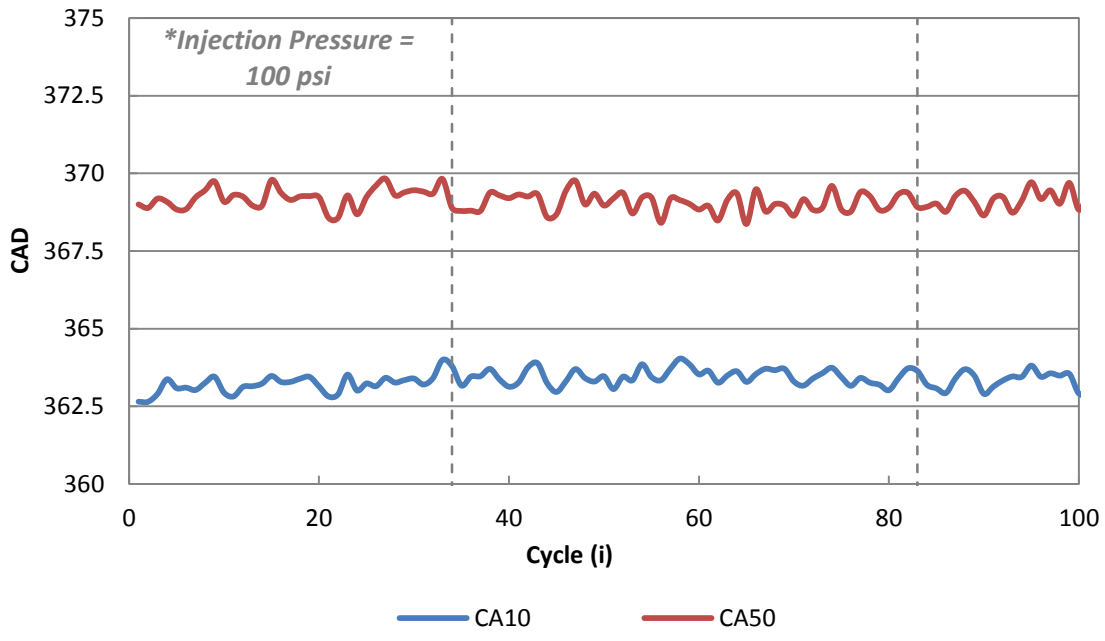

Figure 7.18. Temporal CA10 and CA50 for 0.15% mass injection of 50 cycles, 100 psi

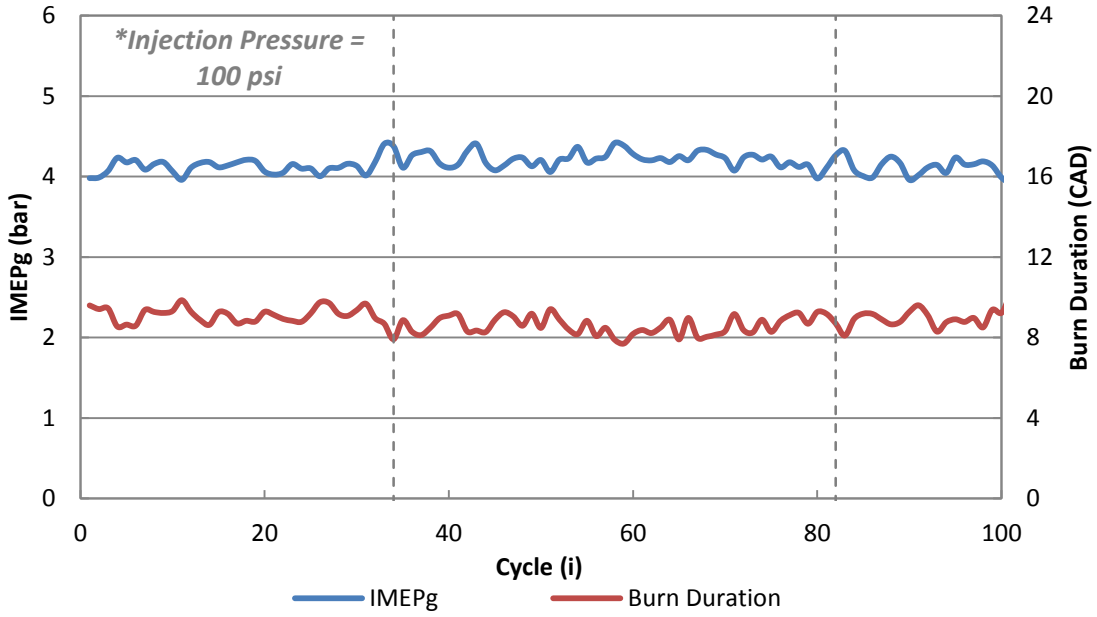

Figure 7.19. Temporal IMEPg and burn duration for 0.15% mass inj. of 50 cycles, 100 psi

In conclusion, injection pressure has an effect on the combustion development for the same amount of energy addition. The mass addition was intriguing because by adding some mass, and thus energy, one could control the development of the autoignition event. This data seems to indicate that mass addition of carbon monoxide has a negligible effect on SOC (CA10) and more of an effect on combustion development as shown by the burn duration and the advanced CA50 values at the 800 psi injection pressure. Further conclusions are made in §7.2.3.

7.2.2. Equivalent Energy Addition Calculations. All of the results shown previously in this chapter are mainly due to the energy that is being added to the system through the mass injection. In order to further our understanding of what is physically happening one must compare test cases where the energy in the cylinder is equivalent.

The energy added by the CO is increasing the overall energy in the system, and needs to be compared to a test case where the energy in fuel content is equivalent without CO addition. Table 7.6 lists the lower heating values (LHV) of iso-octane and CO.

Table 7.6. Lower heating values of CO and fuel

	MJ/kg	kJ/kg	kJ/mol
Carbon monoxide	*10.112*	*10,112*	*283.24*
2-2-4 Trimethylpentane	*44.310*	*44,310*	*5,061.5*

By knowing the amount of mass of CO injected during one cycle, one can determine the mass flow per minute, and thus the energy content added per minute. Using a simple unit balance the amount of extra fuel to be added to the preexisting fuel flow rate can be determined. A sample calculation below shows the 0.40% mass addition test case. The mass injected of CO per one cycle is 0.0016 grams, which is equivalent to 7.0 grams/min mass flow of CO into the engine. From this mass flow and LHV were used to find the energy flow rate to be 70.8 kJ/min. Now that we know the energy flow rate needed, we back calculate fuel flow, in grams/min, using the LHV of the fuel. This yields a value of 1.6 grams/min of fuel flow that needs to be added to the preexisting fuel flow of 7.5 grams/min in order to compare the test cases with 0.40% CO mass injection test cases on equivalent energy content. §7.2.3 expands on the results from these equivalent fuel addition tests.

7.2.3. Equivalent Energy Addition Results. From above it was mentioned that in order to match energy content within the cylinder during each cycle, the fuel flow would have to be increased in order to match the energy content of the CO mass injection cycles. By computing the equivalent energy addition at the 0.40% CO mass injection test case, it was determined that the engine needed an additional energy flow rate of 70.8 kJ/min which corresponds to an additional 1.6 grams/min of fuel to be added on top of the preexisting fuel flow of 7.5 grams/min. This yields a new test case where a fuel flow of 9.1 grams/min needs to be observed at the same intake temperature of 195°C in order to compare results from the engine data. Table 7.7 shows these test cases below.

Table 7.7. Average engine parameters for equivalent energy addition test cases

Intake Temp (K)	Fueling Rate (grams/min)	Mass Injection (%)	Injection Pressure (psi)	Avg. CA10 (CAD)	Avg. CA50 (CAD)	IMEPg (bar)	Burn Duration (CAD)	Efficiency η_f, (%)
468	*9.1*	*-*	*-*	*361.5*	*364.1*	*4.57*	*4.17*	*52.7*
468	*7.5*	*0.40*	*800*	*362.5*	*364.7*	*4.91*	*3.61*	*56.7*
468	*7.5*	*0.40*	*100*	*363.3*	*367.6*	*4.43*	*6.82*	*51.1*

There are several interesting and novel outcomes from this comparison. First, it should be noted that when looking at above averaged engine data, all test cases have the same amount of energy in the cylinder for that cycle. The first case energy content is comprised completely of fuel, while the other two cases use CO mass injection to increase energy content. The two mass injection cases are injected at different pressures, but with the same mass percentage. The 800 psi injection pressure case shows slightly retarded CA10 while maintaining the same CA50 values when compared

to the baseline energy addition case (9.1 grams/min fuel flow). This is explained by the energy within the cylinder being released at a faster rate and within a smaller time scale, as shown by burn duration. The most important point to take away however is the fact that engine power output significantly increases at this test case allowing for a 4% increase in fuel conversion efficiency. Either the mixing effects from the high pressure injection of CO or the chemical kinetics that are interacting between the CO and the fuel/air mixture is allowing for this faster release of energy, causing more of the charge energy to be converted to work instead of heat transfer and hence increase fuel conversion efficiency. This is exciting as IMEPg values of around 5 bar could not have been achieved by purely using fuel energy while keeping a pressure rise rate limit of 10 bar/CAD and these low of intake temperatures. On the other side, when looking at the 100 psi injection case, CA10 is retarded by 2 CAD and the CA50 is pushed later in the cycle. This is also confirmed by the longer burn durations that are seen at this set point. What is interesting to note is that the same amount of fuel energy is introduced into the cylinder as the baseline test, yet by injecting this mass at 100 psi, the burn durations are prolonged giving a longer combustion development, while retarding SOC. It is important to note that the engine's gross power out per displacement volume (IMEPg) is slightly less than the baseline test at 4.43 bar, but maintains this output given longer burn durations. The fuel conversion efficiency suffers by 1.6%. At this test case it is either the kinetics interaction between the CO and fuel/air mixture or the mixing effects that are introduced into the cylinder that are different than the 800 psi case causing combustion

to develop at a slower rate as shown through the burn durations. Figures 7.20 through 7.23 expand on the trends in the data seen above.

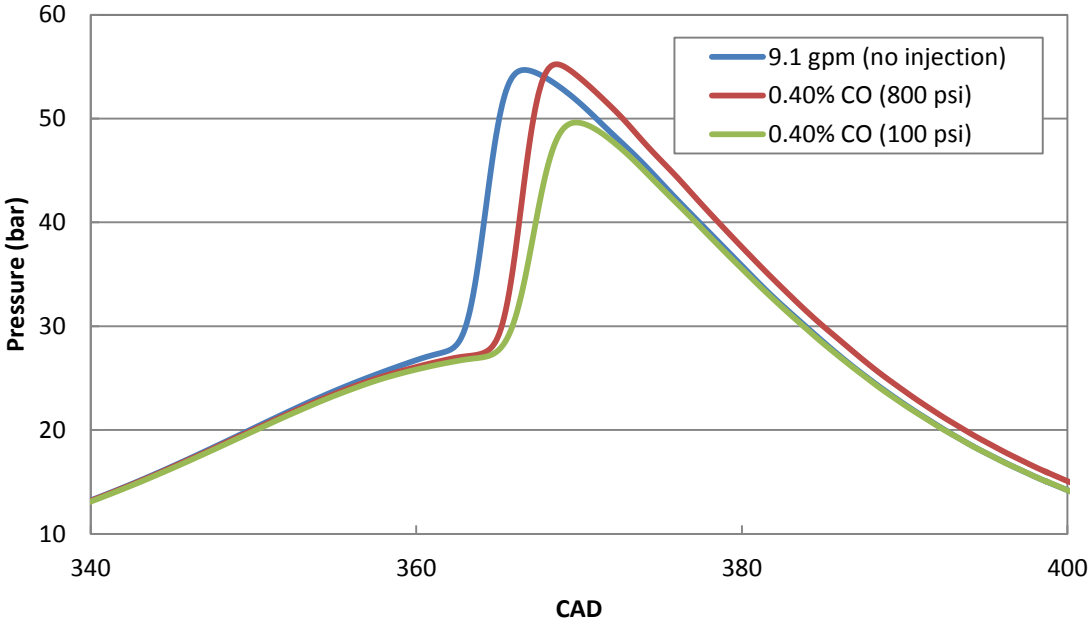

Figure 7.20. Pressure trace comparison of equivalent energy test cases

Figure 7.20 shows the pressure trace for the three equivalent energy test cases. Here it can be seen that the addition of CO slightly retards the combustion process when comparing energy content. Note that in §7.2.1 the CO injections increased CA10, but this was due to adding energy into the system and comparing it to a lower overall energy test case. The peak pressure locations are retarded as the CO addition is injected at different pressures. This could be due to the chemical kinetic reactions as the combustion process develops within the cycle. Further understanding of the CO addition can be had by looking at Figure 7.21 and 7.22.

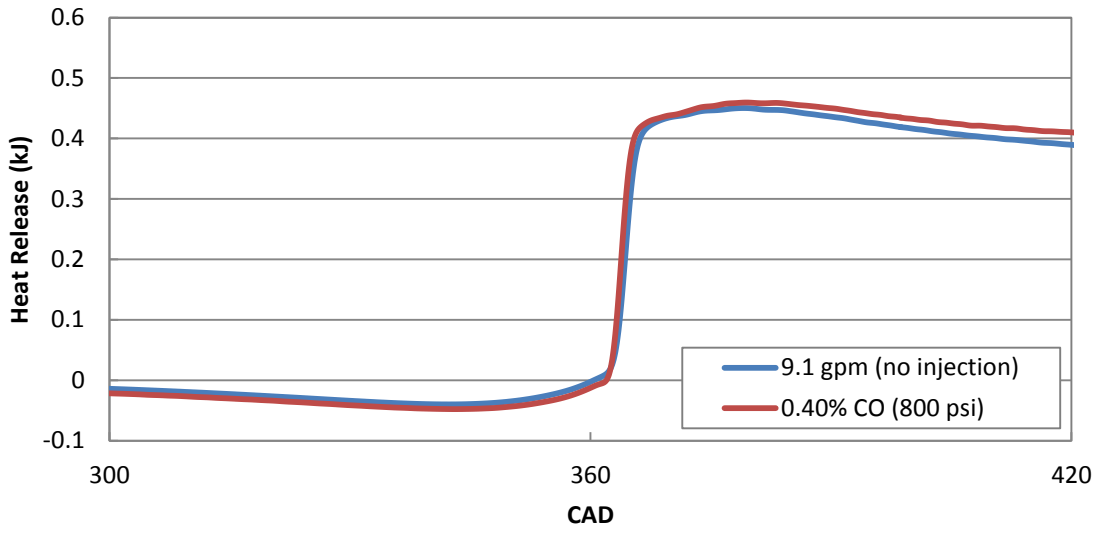

Figure 7.21. Cumulative heat release for 9.1 gpm and 0.40% CO mass injection, 800 psi

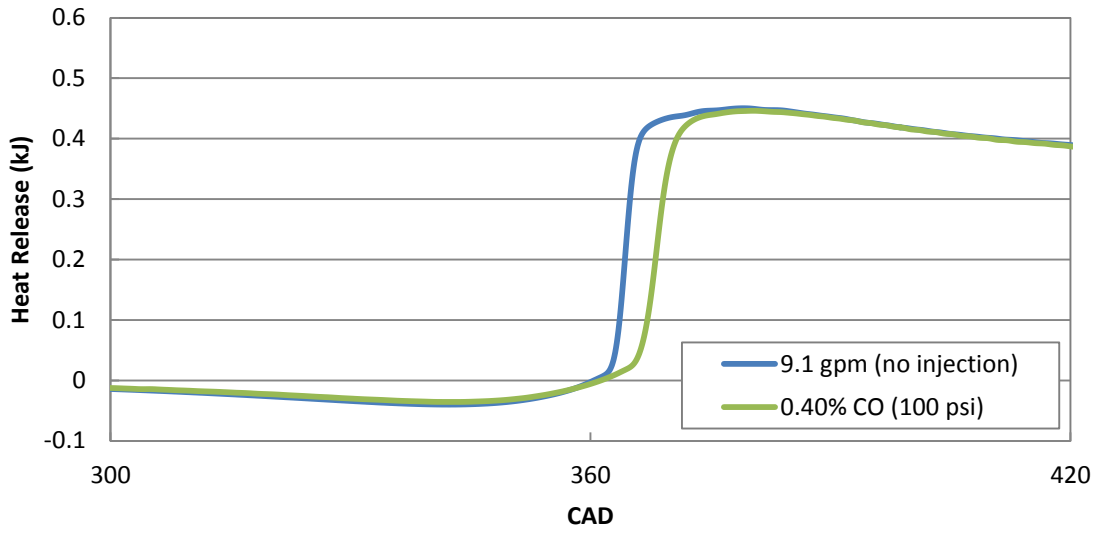

Figure 7.22. Cumulative heat release for 9.1 gpm and 0.40% CO mass injection, 100 psi

The cumulative heat release curves for 800 psi and 100 psi injection pressures are shown in Figures 7.21 and 7.22, respectively. At the 800 psi case it can be seen that heat is released at a slightly higher rate than the baseline case and this is shown through

burn duration. What should be noted is that the red curve (injection case) does not decrease back to the same energy level as quickly as the baseline case. This is due to heat transfer effects in the system. By observing the average exhaust temperatures at EVO, as shown in Table 7.8, it can be seen that the exhaust temperatures at the 0.40% 800 psi injection case are significantly higher than the baseline 9.1 gpm test case.

Table 7.8. Average exhaust temperatures for equivalent energy addition test cases

Intake Temp (K)	Fueling Rate (grams/min)	Percent mass injection (%)	Injection Pressure (psi)	Exhaust Temperature (K)
468	*9.1*	-	-	*707*
468	*7.5*	*0.40*	*800*	*749*
468	*7.5*	*0.40*	*100*	*718*

These higher exhaust temperatures change the heat transfer effects to the cylinder walls, head and valves, and the piston top. This increase in exhaust temperature is either due to the kinetic reactions between the CO and the fuel/air mixture undergoing autoignition or a better mixing process that is introduced from the high pressure injection that is allowing for faster combustion. This shorter burn duration contributes to less time for heat transfer to the walls and head to occur. This is causing a fraction of chemical energy to be converted to work and heat shown by the higher exhaust temperatures. This is only at the 800 psi injection case because this phenomenon is not seen at the 100 psi injection case.

In Figure 7.22, as opposed to the 800 psi injection pressure case, the heat release curve for the 100 psi injection pressure case returned to the same energy level as the 9.1 gpm case. This is shown in the averaged exhaust gas temperature in Table 7.8.

The difference between these two cases is only 11 K and is not as significant as the 42 K temperature difference seen in the 800 psi injection case. It was observed that the addition of CO at 100 psi prolongs combustion and causes a longer burn, drawing out combustion. This is seen in the averaged CA50 values in Table 7.7. What is interesting about this set point is its ability to maintain slightly smaller IMEPg values all while significantly reducing pressure rise rates as seen in Figure 7.23.

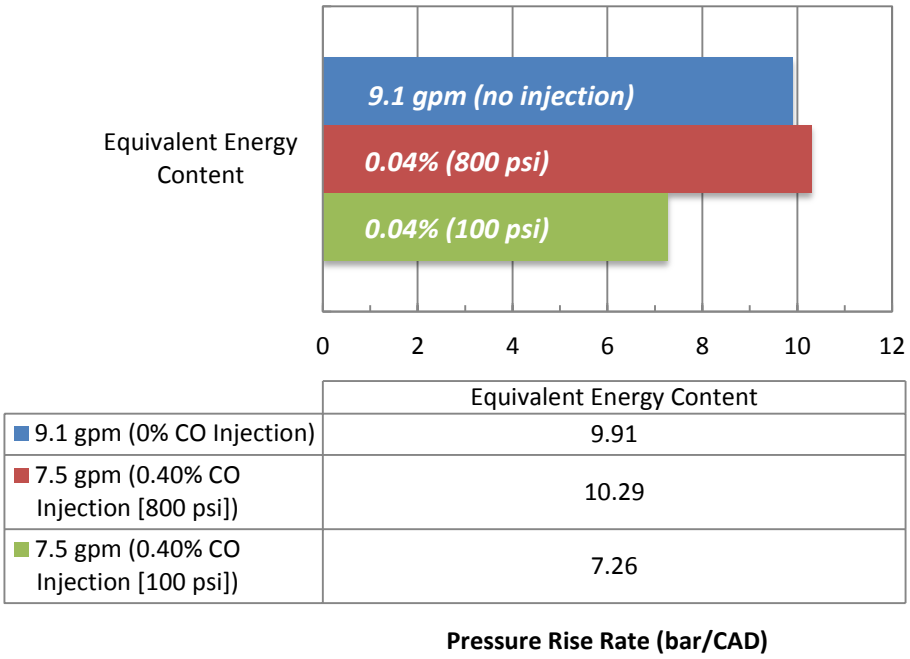

Figure 7.23. Pressure rise rates for equivalent energy test cases

Here it can be seen that the baseline test case has an average pressure rise rate of 9.91 bar/CAD. The 0.40% CO mass injection test case at 800 psi has slightly higher pressure rise rates and this is due to the fact that combustion occurs faster in this set

point than at the baseline as shown by the burn durations. However, this slightly higher pressure rise rate does not account for the fact that IMEPg values saw a 7.5% increase, and the fuel conversion efficiency saw a 4% increase. This means that the addition of CO at 800 psi allows for a more efficient conversion of energy into work due to either the kinetics at work throughout the combustion development, which is near instantaneous or a more complete mixing caused by the high injection pressure of a reactive gas. When looking at the 0.40% CO mass injection test case at 100 psi, it can be seen that the pressure rise rates are significantly reduced from the baseline case. This is interesting as the engine's IMEPg only saw a 3.1% decrease for this test case, and the fuel conversion efficiency was reduced by 1.6%. This work shows that pressure rise rates can be significantly reduced without suffering major losses in power output from the engine. These results indicate that reactive species gas injection could be used for onboard cyclic control of HCCI combustion in order to perturb the system and push the engine away from regions of instability, as seen in the partial burn regime.

8. CONCLUSIONS AND FUTURE WORK

8.1. CONCLUSIONS

Cycle-to-cycle dynamics play a role in HCCI combustion, especially when the engine is operated in the partial burn regime near the misfire limit. This thesis outlines the impact that internally trapped exhaust gas residuals have on the combustion parameters in this operating zone. This work also introduces a simple burned/ unburned residual model into a much larger 5-state physics based thermodynamic control model in order to capture and correctively predict the cycle-to-cycle dynamics regarding the operational regime of an HCCI engine. Lastly, this work explores preliminary data captured that shows the effect of cyclically injecting syn-gas as a possible control scheme in HCCI combustion. This syn-gas has a profound effect based on injection pressure, amount of mass (and thus energy) injected, and species injected.

In conclusion, work presented in this thesis has explored the effect that the internally trapped exhaust gas residual temperature has on the next cycle, through start of combustion represented by CA10. In order to assess the cycle-to-cycle variations in work output, quantified by IMEPg, return maps of 400/1000 consecutive engine cycles at steady state and partial burn operating regimes were plotted and compared. These experimental return maps show that the engine's cyclic variations display stochastic behavior when the combustion phasing is near top dead center and more deterministic behavior near the misfire limit in the partial burn regime. More importantly, it was observed that the measured exhaust gas temperature appears to have limited correlation to the next cycle's start of combustion, quantified by CA10 when considering

simple correlation plots. There appears to be some determinism shown in the return map of CA10 for all three set points.

The exhaust gas residual also affects the composition of the new charge through its composition. From here, the exhaust manifold pressure was increased, and hence more residuals were retained in the cylinder to be carried over to the next cycle. Again, in order to assess the cycle-to-cycle variations in work output, quantified by IMEPg, return maps of the partial burn operating regime were compared. It was observed that with increased exhaust gas residual amounts, the engine could operate longer in the partial burn regime; however this caused a larger dispersion in the IMEPg data collected. The return maps for CA10 at these set points also showed some slight determinism indicating that the current cycle's (i) CA10 is correlated to the next cycle's (i+1) CA10 through some feed forward mechanism. By increasing the residual gas fraction from increased exhaust manifold pressure and hence the thermal effect of these residuals on the fresh charge, one would expect to see a stronger correlation between the current cycle's measured exhaust gas temperature and the next cycle's start of combustion however it was observed that these two parameters once again show a limited correlation. This indicates that the HCCI start of combustion event is not near as dependent on temperature as originally conceived, and even more so at the higher load case which contains hotter exhaust gas temperatures did not display any determinism, despite having these hot residual temperatures. This goes to say that the next cycle's combustion event is more dependent on the chemistry and composition of the residuals than the thermal effect of the residual gas fraction. It was also observed that the

increased residual amount is not affecting SOC; however it is affecting how the combustion develops within the cylinder.

This work has also explored the capability of a five-state thermodynamics non-linear control model to qualitatively capture the cyclic dynamics of an HCCI engine. In order to assess the cycle-to-cycle variations in work output, quantified by IMEPg, return maps of 1000 consecutive engine cycles of experimental and simulated data were plotted and compared. The experimental return maps show the engine's cyclic variations display very stochastic behavior when combustion phasing is near top dead center and more deterministic behavior near the partial burn limit. The simulated results show that the non-linear model is capable of capturing this stochastic and deterministic behavior but only through the inclusion of unburned exhaust residual (i.e. chemical composition) effects. Therefore, it is shown that exhaust residual composition effects through inclusion of an unburned gas residual impacts the ability of the model to predict deterministic behavior at the partial burn limit.

In an attempt to expand on the aforementioned conclusions, a residual gas injector was developed to cyclically inject a reactive species gas, in this case carbon monoxide, in order to perturb the fresh intake charge through its chemical composition. This perturbation allowed the chemical effects to be separated from the thermal effects in order to study the kinetics behind HCCI combustion development. It was observed that injecting CO at the same fueling rate would increase CA50 and IMEPg while decreasing the burn duration. This was an expected result as adding a reactive gas increases energy content of the charge. The interesting result from this experiment was

that CA10 did not change based on energy content added by the injector for the parameters set for these test cases. However, CA50 was advanced significantly. So a comparative test with equal energy content was conducted by increasing fuel flow as the baseline test case. When comparing equivalent energy content it was observed that by injecting CO as a percentage of the inlet charge mass, combustion is slightly retarded in the cycle. The high pressure mass injection increased the fuel conversion efficiency by 4%. The most interesting result from this experiment is that fact that the engine is able to operate in a regime by utilizing the RGI for syn-gas addition that has never been observed before when not utilizing mass injections. At the low pressure mass injection set point, the pressure rise rates were reduced by 26.7% while the fuel conversion efficiency suffered by only 1.6%. This shows that pressure rise rates can be controlled in order to increase engine output quantified by IMEPg all while keeping start of combustion relatively close to the equivalent energy addition set point through fueling rate.

8.2. FUTURE WORK

Results in this thesis have exposed the chemical and thermal effects that residuals have on the next cycle in the partial burn regime of an HCCI engine. More importantly, initial results uncover the complicated chemical kinetics or mixing effects behind the combustion development in controlled autoignition. This section will address future work that would bring further clarity to the results or provide greater applicability of the 5-state thermodynamic model studied.

As found in this work, the cyclic addition of CO significantly affects combustion development. A more complete understanding is sought of the role of reformed gas properties on the next-cycle ignition and heat release through controlled, therefore cyclically resolved, engine experiments could be guided by existing chemical kinetics modeling packages. This would focus on the underlying cycle-by-cycle dynamic impact of carefully controlled in-cylinder injection of perturbation gases using the RGI on an individual cycle basis. It is desired to push instability limits with this added syn-gas and determine the gains/advantages associated with syn-gas addition in the partial burn regime. The fraction of added syn-gas should be varied to determine the "sensitivity", measured by cyclic variability in per cycle output. Time series and conventional statistics can be used to determine the impact on output. The varying sensitivity of the cyclic output to syn-gas addition over a range of internal dilution is important to understanding controlling kinetic mechanisms with inlet conditions, changes in controlling mechanisms, and control opportunities. The variation in syn-gas CO/H2/N2 fraction is critical for understanding changing impact of species at various dilution and inlet temperature conditions. Furthermore, with the RGI, it will be possible to perturb the composition of burned gas by the addition of CO_2/CO/H_2/H_2O/C_XH_Y will help in the understanding of the role of composition of residual gas in feed forward mechanisms at various dilution levels and inlet temperature conditions.

Future work on the 5-state thermodynamic model should be improved to capture the feed forward mechanism of the residual gas, chemical composition and thermal make-up, and their effects on SOC and RHR. Currently the model does not

incorporate a reactive species mass addition in the reactants/products of combustion. The thermochemistry reaction includes a portion of internally trapped residuals; however the carry over or feed forward from the residuals from the last cycle is through the thermodynamic properties and the inclusion of burn/unburned exhaust gas residual effects and not from individual species themselves. The current thermochemistry equation in the model should be changed to incorporate the reactive gas mass fraction addition in the reactants to be mixed through adiabatic mixing during the intake process as well as the chemical make-up and composition of the residual gas fraction. The adaptive neural network controller needs these additions in order to alter the cycle-by-cycle mass additions to push the SOC out of these strong cyclic instabilities that we see when operating in the partial burn regime, toward a stable and efficiency operating location.

APPENDIX A

RESIDUAL GAS INJECTOR DRAWINGS

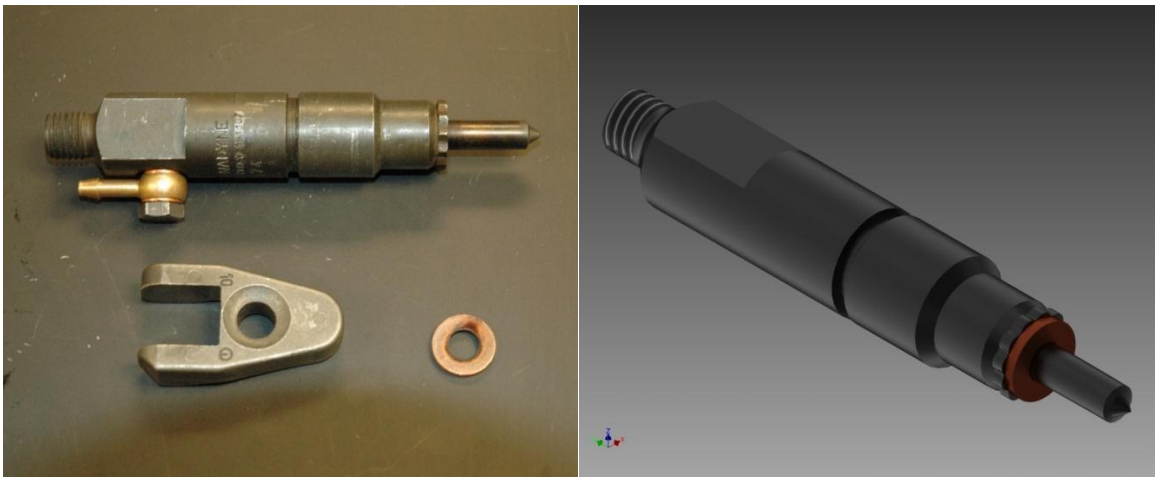

Figure A-1. OEM Diesel Injector a. actual and b. solid model

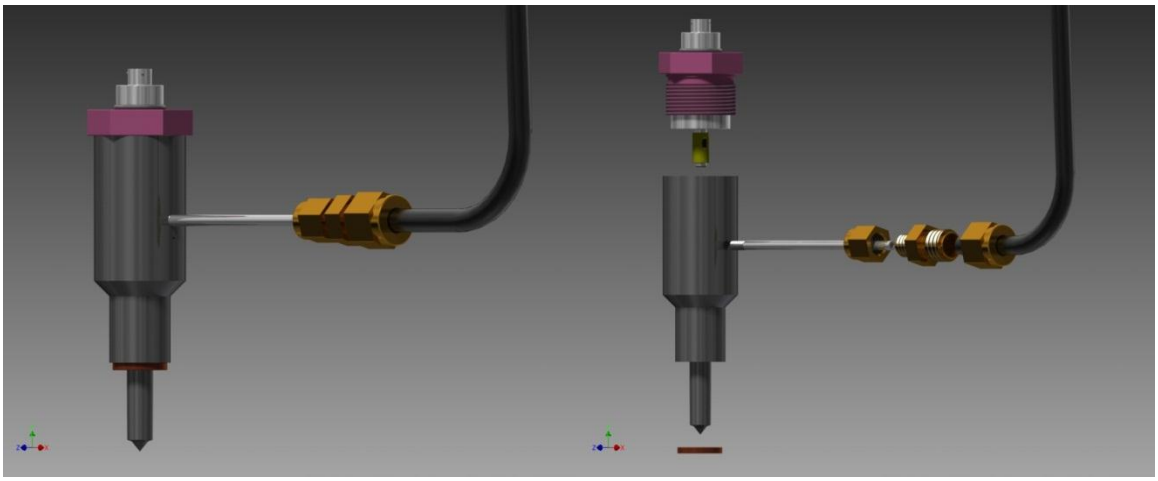

Figure A-2. Residual Gas Injector solid modeled a. assembled view and b. exploded view

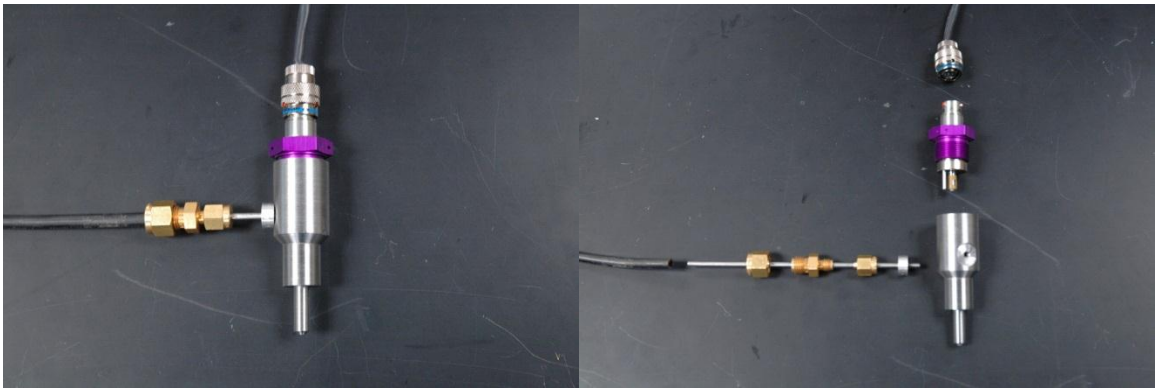

Figure A-3. Residual Gas Injector prototype a. assembled and b. exploded

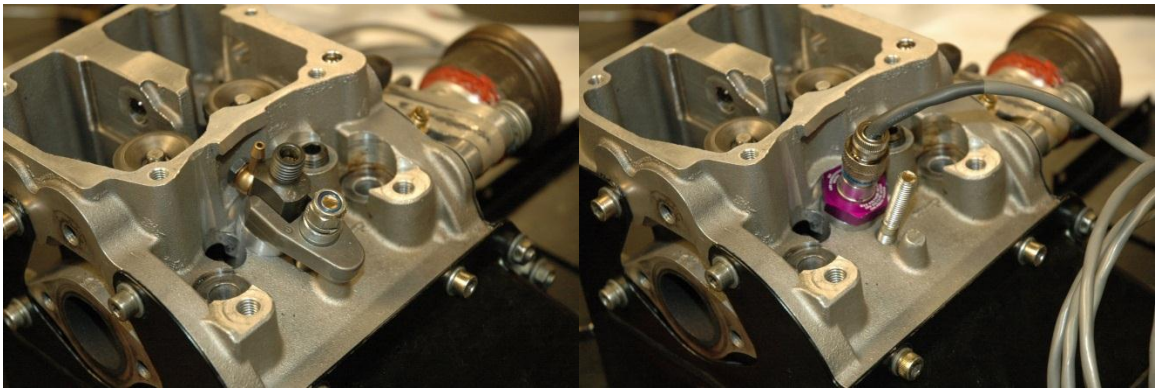

Figure A-4. Head/injector installation a. OEM Diesel Injector and b. RGI

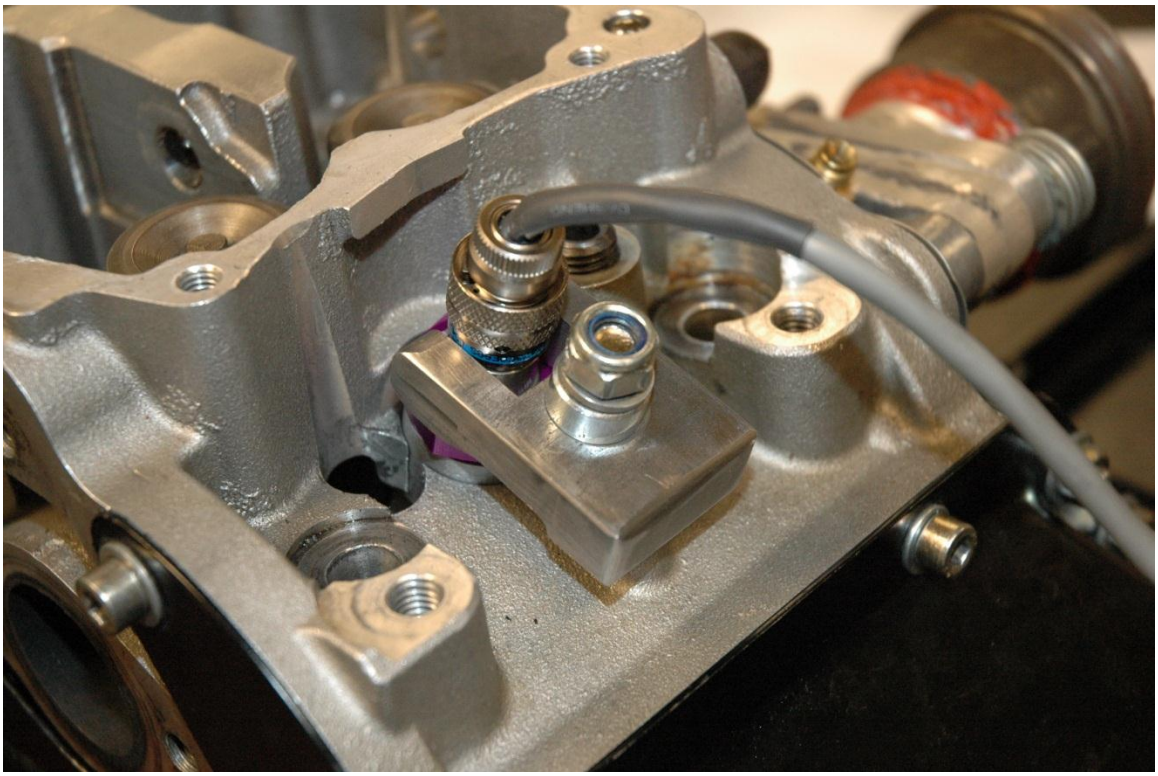

Figure A-5. RGI installed in Hatz engine head with fabricated clamp

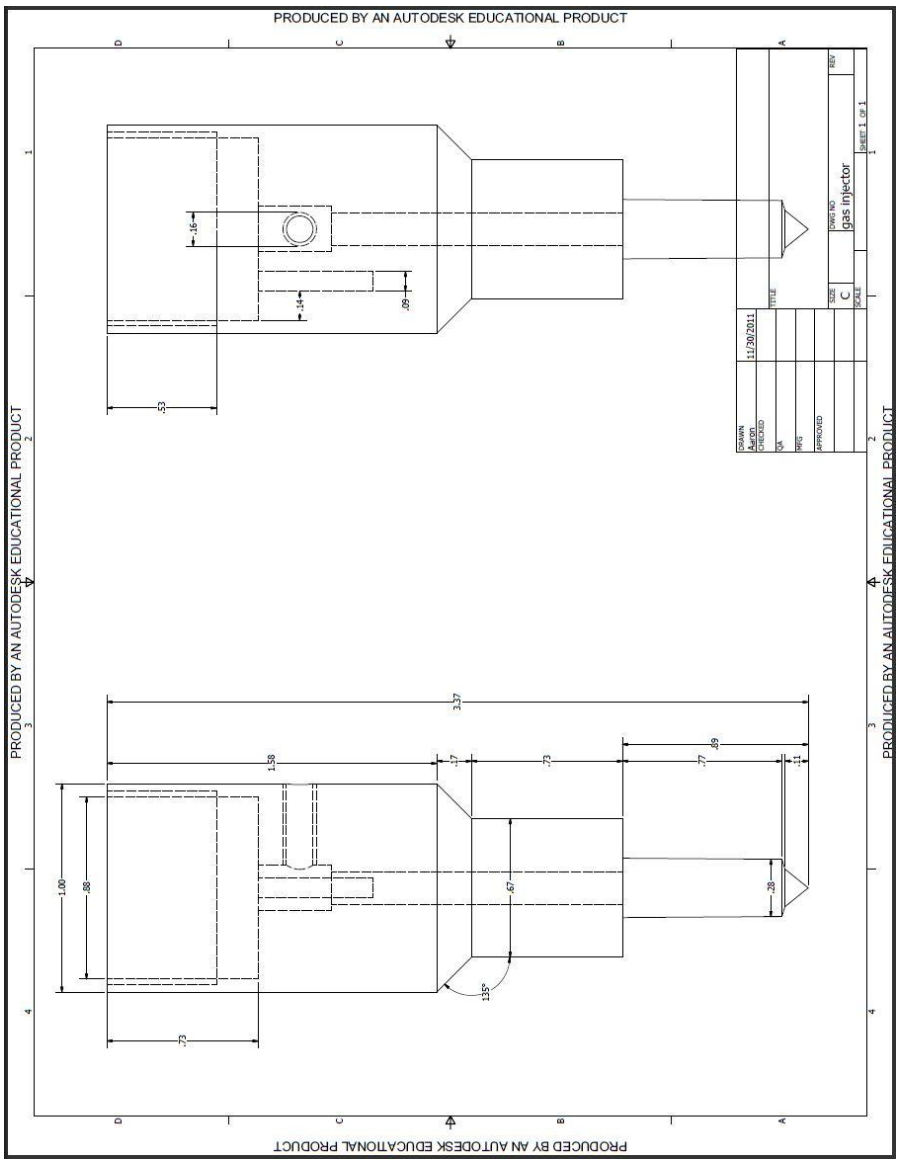

Figure A-6. Solid model spec sheet for RGI fabrication

APPENDIX B

EXPERIMENTAL TESTING MATRICIES

Table B-1. Experimental testing matrix

Operating Regime	Intake Temp (K)	Eq. Ratio (φ)	Fueling Rate (grams/min)	Avg. CA50 (CAD)	IMEPg (bar)	COV (%)
Steady State	*503*	*0.29*	*6.0*	*361.5*	*3.34*	*1.57*
Partial Burn	*466*	*0.28*	*6.0*	*374.9*	*2.47*	*13.00*
Steady State	*495*	*0.36*	*7.5*	*361.3*	*3.79*	*1.58*
Partial Burn	*460*	*0.34*	*7.5*	*377.9*	*3.12*	*10.60*
Steady State	*468*	*0.41*	*9.0*	*364.3*	*4.57*	*1.20*
Partial Burn	*452*	*0.40*	*9.0*	*380.6*	*3.88*	*8.99*
Steady State	*437*	*0.50*	*11.2*	*368.7*	*5.38*	*1.72*
Partial Burn	*442*	*0.50*	*11.2*	*383.7*	*4.96*	*5.96*

Table B-2. Experimental testing matrix with increased exhaust manifold pressure

Operating Regime	Intake Temp (K)	Eq. Ratio (φ)	Fueling Rate (grams/min)	Avg. CA50 (CAD)	IMEPg (bar)	COV (%)
Steady State	*495*	*0.36*	*7.5*	*361.0*	*3.74*	*1.31*
Partial Burn	*459*	*0.34*	*7.5*	*378.1*	*2.70*	*19.07*
Steady State	*475*	*0.42*	*9.0*	*363.2*	*4.27*	*1.44*
Partial Burn	*453*	*0.40*	*9.0*	*381.3*	*3.30*	*17.45*
Steady State	*453*	*0.50*	*11.2*	*366.4*	*4.87*	*1.69*
Partial Burn	*447*	*0.49*	*11.2*	*382.0*	*4.16*	*9.97*

Table B-3. Residual amount experimental testing matrix

Operating Regime	Fueling Rate (grams/min)	Eq. Ratio (φ)	Exhaust Temp (K)	Exhaust Pressure (bar)	Residual Amount (%)
Steady State	*6.0*	*0.29*	*644*	*0.989*	*6.18*
Partial Burn	*6.0*	*0.28*	*584*	*0.987*	*6.32*
Steady State	*7.5*	*0.36*	*673*	*0.988*	*5.82*
Partial Burn	*7.5*	*0.34*	*662*	*0.988*	*5.50*
Steady State	*9.0*	*0.41*	*702*	*1.006*	*5.29*
Partial Burn	*9.0*	*0.40*	*736*	*1.004*	*4.87*
Steady State	*11.2*	*0.50*	*753*	*1.004*	*4.61*
Partial Burn	*11.2*	*0.50*	*844*	*1.009*	*4.18*

Table B-4. Residual amount experimental testing matrix with increased exhaust manifold pressure

Operating Regime	Fueling Rate (grams/min)	Eq. Ratio (φ)	Exhaust Temp (K)	Exhaust Pressure (bar)	Residual Amount (%)
Steady State	*7.5*	*0.36*	*691*	*1.243*	*7.56*
Partial Burn	*7.5*	*0.34*	*647*	*1.247*	*7.21*
Steady State	*9.0*	*0.42*	*706*	*1.251*	*6.86*
Partial Burn	*9.0*	*0.40*	*732*	*1.265*	*6.25*
Steady State	*11.2*	*0.50*	*752*	*1.265*	*6.06*
Partial Burn	*11.2*	*0.49*	*806*	*1.285*	*5.67*

APPENDIX C

THERMOCHEMISTRY INTAKE/EXHAUST MASS CALCULATION TABLES

Table C-1. Emmisions data collected from Hatz

		7.5 gpm		9.0 gpm	
		Steady	Partial	Steady	Partial
Engine Speed	rpm	1800	1800	1800	1800
CO2 (dry)	%	4.25	3.28	4.81	3.71
CO (dry)	%	0.024	0.16	0.05	0.145
O2 (dry)	%	15	16.1	14.2	15.7
uHC (wet)	ppm C	3280	9440	4280	10000
NOx (wet)	ppm	120.1	5.3	209.2	7.8

Table C-2. Chemical Calculations

Property	*Values*				
Mass Fuel Flow	g/s	0.128525	0.128525	0.151294	0.151294
Mass Air Flow	kg/s	0.004968	0.005246	0.006102	0.006603
Ambient Pressure	Pa	97698.65	97698.65	97698.65	97698.65
Ambient Density	kg/m3	1.156643	1.156643	1.156643	1.156643
A/F Ratio		46.2589	47.84621	40.32985	43.64115
a		35.2203	36.42884	30.70608	33.22722
x		7.534019	7.534019	7.534019	7.534019
y		14.49296	14.49296	14.49296	14.49296
gN2		132.8862	137.446	115.4549	124.9343
nO2 (Stoich)		11.15726	11.15726	11.15726	11.15726
xCO2		0.0425	0.0328	0.0481	0.0371
xCO		0.00024	0.0016	0.0005	0.00145
xO2		0.15	0.161	0.142	0.157
xH2O (Wet)		0.039429	0.031634	0.044541	0.035402
xuHC (Wet)		0.00328	0.00944	0.00428	0.01
xNOx (Wet)		0.00012	5.3E-06	0.000209	7.8E-06
np		169.9347	176.227	148.5552	159.6689
xH2 (Wet)		5.86E-05	0.000406	0.000122	0.000364
xN2 (Wet)		0.77265	0.770685	0.770519	0.775848
xCO2 (Wet)		0.040824	0.031762	0.045958	0.035787
xCO (Wet)		0.000231	0.001549	0.000478	0.001399
xO2 (Wet)		0.144086	0.155907	0.135675	0.151442
Phi		0.320587	0.309951	0.367718	0.339817
Sum of mole fractions		1.000678	1.001389	1.001781	1.010249

Table C-3. Moles of exhaust products

Species	*Moles (grams/mole)*			
nN2 (Wet)	131.30	135.82	114.46	123.88
nO2 (Wet)	24.49	27.48	20.16	24.18
nCO2 (Wet)	6.94	5.60	6.83	5.71
nH2O (Wet)	6.70	5.57	6.62	5.65
nuHC (Wet)	0.56	1.66	0.64	1.60
nCO (Wet)	0.04	0.27	0.07	0.22
nNOx (Wet)	0.02	0.00	0.03	0.00
nH2 (Wet)	0.01	0.07	0.02	0.06
Total moles of Products	170.0499	176.4718	148.82	161.31

Table C-4. Mass of exhaust products

Species	*Mass (grams)*			
mN2 (Wet)	3678.11	3804.60	3206.49	3470.22
mO2 (Wet)	783.28	878.93	644.77	773.54
mCO2 (Wet)	305.32	246.34	300.47	251.47
mH2O (Wet)	120.71	100.43	119.20	101.83
muHC (Wet)	58.58	174.84	66.82	167.81
mCO (Wet)	1.10	7.65	1.99	6.26
mNOx (Wet)	0.61	0.03	0.93	0.04
mH2 (Wet)	0.02	0.14	0.04	0.12
Total Mass of Products	4947.723	5212.958	4340.710	4771.281

BIBLIOGRAPHY

[1] Zhao, Fuquan, Thomas N. Asmus, Dennis N. Assanis, James A. Dec, and Paul M. Najt. "Homogeneous Charge Compression Ignition (HCCI) Engines." SAE International, 2003.

[2] Zhao, H., Z. Peng, and N. Ladommatos. "Understanding of controlled autoignition combustion in a four-stroke gasoline engine." *Journal of Automobile Engineering* 215 (2001): 1297-1310.

[3] Dec, John E. "Advanced compression-ignition engines – understanding the in-cylinder processes." *Proc. of the Combustion Institute* 32 (2009): 2727-2742.

[4] Koopmans, Lucien, Ove Backlund, and Ingemar Denbratt. "Cycle to Cycle Variations: Their Influence on Cycle Resolved Gas Temperature and Unburned Hydrocarbons from a Camless Gasoline Compression Ignition Engine." *SAE Paper* 2002-01-0110.

[5] Persson, H., R. Pfeiffer, A. Hultqvist, B. Johansson, and H. Ström. "Cylinder-to-Cylinder and Cycle-toCycle Variations at HCCI Operation With Trapped Residuals." *SAE Paper* 2005-01-0130.

[6] Xingcai, Lu, Ji Libin, Ma Junjun, and Huang Zhen. "Experimental study on the cycle-by-cycle variations of homogeneous charge compression ignition combustion using primary reference fuels and their mixtures." *Journal of Automobile Engineering* (2007): 859-866.

[7] Shahbakhti, Mahdi, Robert Lupul, and Charles Robert Koch. "Cyclic Variations of Ignition Timing in an HCCI Engine." *Proc. of the ASME/IEEE Joint Rail Conference and Internal Combustion Engine Spring Technical Conference* (2007): 405-415.

[8] Shahbakhti, M., and C. R. Koch. "Characterizing the cyclic variability of ignition timing in a homogeneous charge compression ignition engine fuelled with n-heptane/iso-octane blend fuels." *International Journal of Engine Research* 9 (2008): 361-397.

[9] Maurya, Rakesh Kumar, and Avinash Kumar Agarwal. “Experimental investigation on the effect of intake air temperature and air-fuel ratio on cycle-to-cycle variations of HCCI combustion and performance parameters.” *Journal of Applied Energy* 88 (2011): 1153-1163.

[10] Agarwal, Avinash Kumar. “Experimental Investigations on Intake Air Temperature and Air-Fuel Ratio Dependence of Random and Deterministic Cyclic Variability in a Homogeneous Charge Compression Ignition Engine.” *SAE Paper* 2011-01-1183.

[11] Wagner, Robert M., K. Dean Edwards, C. Stuart Daw, Johney B. Green Jr., and Bruce G. Bunting. “On the Nature of Cyclic Dispersion in Spark Assisted HCCI Combustion.” *SAE Paper* 2006-01-0418.

[12] Daw, C. Stuart, Robert M. Wagner, K. Dean Edwards, and Johney B. Green Jr. “Understanding the transition between conventional spark-ignited combustion and HCCI in a gasoline engine.” *Proc. of the Combustion Institute* 31 (2007): 2887-2894.

[13] Daw, C. Stuart, K. Dean Edwards, Robert M. Wagner, and Johney B. Green Jr. “Modeling Cyclic Variability in Spark-Assisted HCCI.” *Journal of Engineering for Gas Turbines and Power* 130 (2008): 052801 1-6.

[14] Sen, A.K., G. Litak, K.D. Edwards, C.E.A. Finney, C.S. Daw, and R.M. Wagner. “Characteristics of cyclic heat release variability in the transition from spark ignition to HCCI in a gasoline engine.” *Journal of Applied Energy* 88 (2011): 1649-1655.

[15] Hyvönen, Jari, Göran Haraldsson, and Bengt Johansson. “Operating Conditions Using Spark Assisted HCCI Combustion During Combustion Mode Transfer to SI in a Multi-Cylinder VCR-HCCI Engnie.” *SAE Paper* 2005-01-0109.

[16] Heywood, J.B. “Internal Combustion Engine Fundamentals.” McGraw-Hill, 1988.

[17] Bettis, Josh B. “Thermodynamic Modeling for Nonlinear Control of Combustion Phasing in HCCI Engines.” Thesis. Missouri University of Science and Technology, 2010.

[18] Waero, Rolf R. “The Effect of Spark Timing on Residual Gas Fraction.” Thesis. Massachusetts Institute of Technology, 2000.

[19] Morey, Francis, Patrice Seers. “Comparison of cycle-by-cycle variation of measured exhaust-gas temperature and in-cylinder pressure measurements.” *Journal of Applied Thermal Engineering* 30 (2010): 487-491.

[20] Chiang, Chia-Jui, Anna Stefanopoulou, and Mrdjan Janković. “Nonlinear Observer-Based Control of Load Transitions in Homogeneous Charge Compression Ignition Engines.” *IEEE Transactions on Control Systems Technology* 15.3 (2007): 438-448.

[21] Chiang, Chia-Jui, and Anna Stefanopoulou. “Sensitivity Analysis of Combustion Timing of Homogeneous Charge Compression Ignition Gasoline Engines.” *Journal of Dynamic Systems, Measurement, and Control* 131 (2009): 014506 1-5.

[22] Shahbakhti, M., A. Ghazimirsaied, and C. R. Koch. "Experimental Study of Exhaust Temperature Variation in an HCCI Engine." *Journal of Automobile Engineering* 224 (2010): 1177-1197.

[23] Fathi, Morteza, R. Khoshbakhti Saray, and M. David Checkel. “The influence of Exhaust Gas Recirculation (EGR) on combustion and emissions of n-heptane/natural gas fueled Homogeneous Charge Compression Ignition (HCCI) engines.” *Journal of Applied Energy* 88 (2011): 4719-4724.

[24] Lee, Donghoon, Anna G. Stefanopoulou, Satheesh Makkapati, and Mrdjan Janković. “Modeling and Control of a Heated Air Intake Homogeneous Charge Compression Ignition (HCCI) Engine.” *Proc. of the American Controls Conference* (2010): 3817-3823.

[25] Yu, X. R., X. S. Bai, A. Vressner, A. Hultqvist, B. Johansson, J. Olofsson, H. Seyfried, J. Sjöholm, M. Richter, and M. Aldén. “Effect of Turbulence on HCCI Combustion.” *SAE Paper* 2007-01-0183.

[26] He, X., M.T. Donovan, B.T. Zigler, T.R. Palmer, S.M. Walton, M.S. Wooldridge, and A. Atreya. “An experimental and modeling study of iso-octane ignition delay times under homogeneous charge compression ignition conditions.” *Journal of Combustion and Flame* 142 (2005): 266-275.

[27] Dubreuil, A., F. Foucher, and C. Mounaïm-Rousselle. “Effect of EGR Chemical Components and Intake Temperature on HCCI Combustion Development.” *SAE Paper* 2006-32-0044.

[28] Subramanian, G., A. Pires Da Cruz, R. Bounaceur, and L. Vervisch. “Chemical Impact of CO and H_2 Addition on the Auto-Ignition Delay of Homogeneous n-Heptane/Air Mixtures.” *Combustion Science and Technology* 179 (2007): 1937-1962

[29] Hosseini, Vahid, and M. David Checkel. “Effect of Reformer Gas on HCCI Combustion – Part 1: High Octane Fuels.” *SAE Paper* 2007-01-0208.

[30] Hosseini, Vahid, and M. David Checkel. “Reformer Gas Composition Effect on HCCI Combustion of n-Heptane, iso-Octane, and Natural Gas.” *SAE Paper* 2008-01-0049.

[31] Hosseini, Vahid, W. Stuart Neill, and M. David Checkel. “Controlling n-Heptane HCCI Combustion with Partial Reforming: Experimental Results and Modeling Analysis.” *Journal of Engineering for Gas Turbines and Power* 131 (2009): 052801 1-11

[32] Ghazimirsaied, Ahmad, and Charles Robert Koch. "Controlling cyclic combustion timing variations using a symbol-statistics predictive approach in an HCCI engine." *Journal of Applied Energy* 92 (2012): 133-146.

[33] White, Frank M. “Fluid Mechanics.” McGraw-Hill, 1979.

[34] Fox, Jonathan W., Wai K. Cheng, and John B. Heywood. “A Model for Predicting Residual Gas Fraction in Spark-Ignition Engines.” *SAE Paper* 931025**.**

[35] Alkidas, A. C. “The Use of Availability and Energy Balances in Diesel Engines.” *SAE Paper* 890822.

VITA

Aaron David Attebery was born in Springdale, Arkansas to David and Sherrie Attebery on August 20, 1988. He graduated from North Callaway High School in Kingdom City, Missouri in May 2006. He worked as an Engineering Technician for the City of Fulton during the summer of 2007. During the summers of 2008, 2009, and 2010 he worked as an Engineering Intern for Ameren UE at Callaway Nuclear Power Plant in Fulton, Missouri. In December 2010, he received his B.S. with Honors in Mechanical Engineering from Missouri University of Science and Technology (formerly known as University of Missouri – Rolla). In April 2012, Aaron was awarded first place in the Chancellor's Fellowship Research Poster Competition. During the summer of 2012, he spent two weeks studying abroad on the topic of Intercultural Communications at the University of Western Cape in Cape Town, South Africa. In December 2012, Aaron received his M.S. degree in Mechanical Engineering from Missouri University of Science and Technology.